MONTANA STATE UNIVERSITY

Structural basis of rhodopsin/G protein coupling : biochemical activity of peptide complexes, photo cross-linking, and mass spectrometric analysis

by Paul Camille Kraft

A dissertation submitted in partial fulfillment of the requirements for the degree Of Doctor of Philosophy In Biochemistry
Montana State University
© Copyright by Paul Camille Kraft (2001)

Abstract:
Physiological and sensory mechanisms are primarily controlled by membrane impermeant signals—which are usually detected by membrane-spanning receptor proteins that ultimately trigger intracellular responses. Similarly, development and repair in multi-cellular organisms are controlled by specific adhesion mechanisms that recognize macromolecular binding sites outside cells and control cytoplasmic responses. Understanding of signaling and adhesion mechanisms could be greatly advanced if the structures of the membrane-spanning receptor proteins and their non-covalent interaction partners could be determined at atomic resolution—but these structures can not typically be deduced by x-ray crystallography or NMR.

Mass spectrometry is able to mass analyze high molecular weight species, however, non-covalent protein-ligand or protein-protein interactions are disrupted by the non-aqueous conditions used in conventional mass spectrometry. This thesis describes new mass spectrometric methodologies to analyze proteins directly from aqueous solutions, which is an important first step in mass spectrometry of non-covalent protein-ligand complexes. Insight is gained into fundamental mechanisms of laser desorption ionization mass spectrometry from aqueous solutions.

This thesis also describes biochemical and mass spectrometric methods to identify non-covalent interactions between the rhodopsin visual receptor and the G protein, transducin. The contacts between rhodopsin and transducin were studied using synthetic peptides derived from transducin that were characterized by their ability to inhibit rhodopsin catalysis of nucleotide binding by transducin. The peptides were also characterized for their ability to inhibit the homologous formyl peptide receptor's catalysis of nucleotide binding by the Gi protein.

Fluorescent photo-activatable analogs of the most potent peptides were synthesized. Non-covalent rhodopsin-peptide interactions were tested for specificity and covalently stabilized by photo-chemical cross-linking. Rhodopsin-peptide complexes (which are about 42,000 Da) must be cleaved into smaller peptides for mass spectrometric analysis of the amino acid sites cross-linked. Cyanogen bromide cleavage of rhodopsin reduced the size of the hydrophobic fragments to facilitate analysis.

Methods are described for mass spectral analysis of all of the cyanogens bromide fragments of rhodopsin at the picomole level, which is an essential first step in identifying the peptide cross-linking sites in rhodopsin. These results represent significant progress in efforts to define the molecular contacts between rhodopsin and transducin and homologous proteins.

STRUCTURAL BASIS OF RHODOPSIN/G PROTEIN COUPLING: BIOCHEMICAL ACTIVITY OF PEPTIDE COMPLEXES, PHOTO CROSS-LINKING, AND MASS SPECTROMETRIC ANALYSIS

By

Paul Camille Kraft

A dissertation submitted in partial fulfillment of the requirements for the degree

Of

Doctor of Philosophy

In

Biochemistry

MONTANA STATE UNIVERSITY
Bozeman, Montana

April 2001

D378
K8557

APPROVAL

Of a dissertation submitted by

Paul Camille Kraft

This dissertation has been read by each member of the dissertation committee and has been found to be satisfactory regarding content, English usage, format, citations, bibliographic style, and consistency, and is ready for submission to the College of Graduate Studies.

Edward A. Dratz _____ (Signature) 4/23/2001 Date

Approved for the Department fo Chemistry and Biochemistry

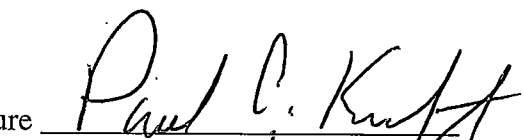
Paul Grieco _____ (Signature) 4/23/01 Date

Approved for the College of Graduate Studies

Bruce McLeod _____ (Signature) 5-2-01 Date

STATEMENT OF PERMISSION TO USE

In presenting this thesis in partial fulfillment of the requirements for a doctoral degree at Montana State University, I agree that the library shall make it available to the borrowers under the rules of the Library. I further agree that copying of this thesis is allowable only for scholarly purposes, consistent with "fair use" as prescribed in the U.S. Copyright Law. Requests for extensive copying or reproduction of this thesis should be referred to Bell & Howell Information and Learning, 300 North Zeeb Road, Ann Arbor Michigan 48106, to whom I have granted "the exclusive right to reproduce and distribute my thesis in and from microform along with the non-exclusive right to reproduce and distribute my abstract in any format in whole or in part".

Signature 

Date 4/23/01

ACKNOWLEDGEMENTS

Thanks to Prof. Edward Dratz, Prof. Jan Sunner, Dr. John Mills, Prof. Sergey Alimpiev, Prof. Heidi Hamm, Dr. Heini Miettinen, Blaine Roberts, and Dr. Joseph Sears.

I would also like to thank my parents, Ken & Anna Kraft, family, friends, and last but certainly not least, Lara Taubner, the love of my life.

TABLE OF CONTENTS

Page

1.INFRARED LASER DESORPTION IONIZATION MASS SPECTROMETRY ON FROZEN AQUEOUS SOLUTIONS OF PROTEINS AND PEPTIDES

Abstract.....1
Introduction.....2
Experimental.....6
Results and Discussion.....14
Cryo-IR-SALDI mass spectra of peptides.....15
Comparison between different SALDI solids for protein Desorption.....18
UV-laser irradiation of cryo-SALDI samples.....20
Laser "drilling" experiments and surface charging.....23
Larger proteins and clustering.....25
Results from aqueous solutions with no cryoprotectant added.....28
Multiple Charging.....30
Ionization processes.....31
Conclusions.....39

2.REVIEW OF LITERATURE AND METHODS USED TO STUDY RHODOPSIN/TRANSDUCIN INTERACTIONS..... 41

Description of Signal Transduction in a Rod Outer Segment Cell.....41
Relationship of Rhodopsin/Transducin System to other GPCR/G Protein Systems..... 43
Rhodopsin dark structure and homology to other GPCRs.....43
Transducin structure and homology to other G proteins.....50
Methods to Study Signal Transduction.....54
Spectral Characteristics of the Rhodopsin/Transducin System.....56
Constitutive Activity of Rhodopsin and Transducin.....59
Role of Retinal in maintaining low basal rhodopsin activity..... 60
Role of rhodopsin residues in maintaining its low basal activity.....61
Role of transducin residues in maintaining its low basal activity.....64
Activation of Rhodopsin and Transducin.....66
Retinal activation of rhodopsin.....66

Role of rhodopsin residues in activation.....68
Role of transducin residues involved in activation/coupling to rhodopsin.....71
Peptides as Probes of GPCR and G Protein Function.....72

3.PROBING NON-COVALENT INTERACTIONS BETWEEN RHODOPSIN AND TRANSDUCIN BY PEPTIDE INHIBITION OF RHODOPSIN-CATALYZED NUCLEOTIDE EXCHANGE, AND CROSS-LINKING PHOTO ACTIVATABLE PEPTIDE ANALOGS TO RHODOPSIN.....78

Abstract.....78
Introduction.....79
Materials and Methods.....81
Results.....84
Discussion.....100

4.MASS SPECTROMETRIC ANALYSIS OF CYANOGEN BROMIDE FRAGMENTS OF INTEGRAL MEMBRANE PROTEINS AT THE PICOMOLE LEVEL: APPLICATION TO RHODOPSIN.....109

Abstract.....109
Introduction.....110
Materials and Methods.....112
Results.....114
Discussion.....127
Conclusion.....130
Acknowledgements.....130

5.CONCLUSIONS AND FUTURE WORK.....131

Preservation of non-covalent complexes in laser desorption Experiments.....131
Defining the amino acid molecular contacts between rhodopsin and Transducin.....135

REFERENCES.....148

LIST OF TABLES

Table Page

1.Summary of cryo-IR-SALDI results for selected solids additives.....21

2. Characteristics of Transducin alpha subunit C-terminal peptide Analogs.....85

3. Peptide masses matched to within 0.05% of the masses expected for the cyanogen bromide digest of rhodopsin.....124

LIST OF FIGURES

Figure Page

1. Cryo-IR-SALDI mass spectrum of 0.9mM angiotensin II in 67% glycerol in water.....17
2. Abundances, as determined by peak heights, of singly protonated nicotinic acid (NH+) and singly protonated angiotensin II (AH+) ions as a function of laser pulse energy using the same experimental conditions as Figure 1.....19
3. Cryo-IR-SALDI mass spectra of equimolar mixture of 0.5mM myoglobin ("M") and cytochrome c ("C")in a 67% glycerol water solution with different SALDI solids added.....22
4. Nicotinic acid cryo-IR-SALDI mass spectrum of 0.05 mM lactic dehydrogenase ("l") adn 0.10 mM cytochrome c ("C") in water:ethanol:glycerol (25:25:50, v:v:v).....27
5. Nicotinic acid cryo-IR-SALDI mass spectrum of 0.34 bovine serum albumin ("B", 66,430 Da) in glycerol/water.....29
6.Thymine cryo-IR-SALDI mass spectrum of 0.1mM myoglobin ("M") in 67% glycerol in water 33
7. The light stimulated signal transduction cascade. Also shown are depictions of the location of rhodopsin in the rod cell, the cis to trans isomerization of retinal, and the hydrolysis of cyclic GMP.....42
8. GPCR Evolution Tree.....44
9. Relationships among mammalian G protein alpha subunits.....45
10. A. Snake Diagram of Rhodopsin 46
10. B. Ribbon model of the crystal structure of dark-adapted rhodopsin.....47
11. Muscarinic receptors M4 & M2 couple to Gi/o, and M5, M3, & M1 couple to Gq. Snake diagram below indicates 24 positions near the cytoplasmic side that Horn et al correlated with G protein selectivity.....49
12. Sequence of the alpha subunit Gi chimera of transducin.....51
13. A. Backbone trace of heterotrimeric transducin Gi chimera that was crystallized by Lambright et al [Nature 1996].....52
13. B. Expanded view of transducin Gi chimeric alpha subunit.....53
14. GTPγS35 filter binding inhibition assay.....57
15. Extra Meta II assay.....58
16. Spectrophotometrically detected intermediates in the Photoisomerization of Rh.....62
17. Structural analysis of A326S Gi alpha-1 (95) 67

18. A summary of 340-350 peptide analogs tested for their abilities to stabilize metarhodopsin II (EC50) and for their abilities to inhibit a340-350 K341R peptide fusion protein (IC50), as measured by ELISA.....75
19. Summary of 340-350 peptide analogs tested for their abilities to stabilize metarhodopsin II (EC50), (149).....76
20A&B. Fluorescent peptide-2 cross-linking experiments.....88
20.C. SDS-PAGE confirmation of cross-linking specificity.....89
21. Circular dichroism analysis of transducin 340-350 peptide.....90
22. Comparison of Unihibited, N-acetyl-VLEDLRSCGLF, and N-acetyl-311-329-amide inhibited GTP-gamma-35S binding in urea washed ROS with exogenous transducin added.....93
23. Ribbon and tube model of Heterotrimer G protein, transducin with expanded view of residues 311-342.....94
24. Sequence alignment of the C-terminus's of Gi1, Gt, and Gs.....95
25. Agonist formyl-MLF stimulated human formyl peptide receptor Catalyzed GTP-γ-S35 binding by transducin.....97
26. Ac311-329NH2 titration of agonist formyl-MLF stimulated human FPR catalyzed GTP-γ-S35 binding by Gi2.....98
27. Peptide inhibition of urea washed (Gt depleted) bovine rhodopsin catalyzed GTP-gamma-S35 binding by exogenous Gi/o.....99
28. Transmembrane topological model of rhodopsin.....115
29. SDS-PAGE analysis of fluoroscein labeled proteins and peptides.....118
30. Delayed extraction and reflected MALDI spectrum spectrum of 2 picomole of reduced and thiol alkylated rhodopsin cyanogen bromide digest in ACHA.....120
31. Unsmoothed (to clearly display monoisotopic resolution of the insets) reflected and delayed extraction MALDI spectrum of 4 picomole of reduced and thiol alkylated rhodopsin cyanogen bromide in ACHA.....122
32. Linear mode, delayed extraction MALDI spectrum of 4 picomole of reduced and thiol alkylated rhodopsin cyanogen bromide digest in 2,5-dihydroxybenzoic acid.....125
33. MALDI post source decay (PSD) spectrum of fragment 310-317.....126
34. Flow chart of cross-link isolation.....137
35A. Fluorescence image of tris/tricine gel of cyanogen bromide digest of peptide-2 cross-linked to rhodopsin.....139
35B. Fluorescence and Coomassie stain image of the same tris/tricine gel of Lys-C digestion of peptide-2 cross-linked to rhodopsin.....142

ABSTRACT

Physiological and sensory mechanisms are primarily controlled by membrane impermeant signals—which are usually detected by membrane-spanning receptor proteins that ultimately trigger intracellular responses. Similarly, development and repair in multi-cellular organisms are controlled by specific adhesion mechanisms that recognize macromolecular binding sites outside cells and control cytoplasmic responses. Understanding of signaling and adhesion mechanisms could be greatly advanced if the structures of the membrane-spanning receptor proteins and their non-covalent interaction partners could be determined at atomic resolution—but these structures can not typically be deduced by x-ray crystallography or NMR.

Mass spectrometry is able to mass analyze high molecular weight species, however, non-covalent protein-ligand or protein-protein interactions are disrupted by the non-aqueous conditions used in conventional mass spectrometry. This thesis describes new mass spectrometric methodologies to analyze proteins directly from aqueous solutions, which is an important first step in mass spectrometry of non-covalent protein-ligand complexes. Insight is gained into fundamental mechanisms of laser desorption ionization mass spectrometry from aqueous solutions.

This thesis also describes biochemical and mass spectrometric methods to identify non-covalent interactions between the rhodopsin visual receptor and the G protein, transducin. The contacts between rhodopsin and transducin were studied using synthetic peptides derived from transducin that were characterized by their ability to inhibit rhodopsin catalysis of nucleotide binding by transducin. The peptides were also characterized for their ability to inhibit the homologous formyl peptide receptor's catalysis of nucleotide binding by the Gi protein.

Fluorescent photo-activatable analogs of the most potent peptides were synthesized. Non-covalent rhodopsin-peptide interactions were tested for specificity and covalently stabilized by photo-chemical cross-linking. Rhodopsin-peptide complexes (which are about 42,000 Da) must be cleaved into smaller peptides for mass spectrometric analysis of the amino acid sites cross-linked. Cyanogen bromide cleavage of rhodopsin reduced the size of the hydrophobic fragments to facilitate analysis. Methods are described for mass spectral analysis of all of the cyanogens bromide fragments of rhodopsin at the picomole level, which is an essential first step in identifying the peptide cross-linking sites in rhodopsin. These results represent significant progress in efforts to define the molecular contacts between rhodopsin and transducin and homologous proteins.

CHAPTER 1

INFRARED LASER DESORPTION IONIZATION MASS SPECTROMETRY ON FROZEN AQUEOUS SOLUTIONS OF PROTEINS AND PEPTIDES

Abstract

Surface-assisted, laser desorption ionization (SALDI) time-of-flight mass spectra of proteins and peptides have been obtained from bulk frozen aqueous solutions by adding solid organic powders to the solutions before freezing. Abundant analyte ions were obtained with a 3.28 μm Nd:YAG/OPO laser. Twenty compounds were evaluated as solid additives, and sixteen yielded protein mass spectra. Successful solids included compounds like pyrene, aspartic acid, and polystyrene. The best results were obtained with nicotinic acid and indole-2-carboxylic acid, which yielded protein mass spectra anywhere on the sample and with every laser shot. Compared with UV-MALDI on the same instrument, cryo-IR-SALDI had a comparable detection limit (≈ 1 μM), a lower mass resolution for peptides, and a higher mass resolution for large proteins. Approximately 2,500 cryo-IR-SALDI mass spectra were obtained from a single spot on a 0.3 mm thick frozen sample before the metal surface was reached. About 0.1 nL of frozen solution was desorbed per laser shot. The extent of protein charging varied between the SALDI solids used. With thymine, myoglobin charge states up to MH_{12}^{+12} were observed. It is tentatively concluded that observed ions are pre-formed in the frozen sample.

Introduction

Matrix-assisted laser desorption ionization mass spectrometry (MALDI-MS) is a powerful and widely used method for the analysis of large biochemical molecules [1,2]. In MALDI, the biomolecules are entrained into crystals of a UV-absorbing matrix by solvent evaporation [3]. Irradiation of the sample with a short pulse from a UV laser results in the desorption and ionization of the biomolecules. Together with electrospray [4], MALDI has revolutionized biochemical mass spectrometry.

The goal of performing laser desorption mass spectrometry of biomolecules directly from water solutions has been pursued over several years for a number of reasons. 1) Aqueous solutions constitute the native environment for most biomolecules, and analysis of biomolecules directly from aqueous solutions would require a minimum of sample manipulations. 2) A sample preparation method that uses a water matrix might work equally well for a wide range of biomolecules. Presently, a number of different matrices are used in MALDI, and finding the best matrix and sample preparation method for a given analyte is partly a matter of trial and error. 3) UV-MALDI is sometimes troubled with a wide range of sensitivities for components in mixtures and widely varying signal intensities at different spots on the sample surface. A desorption method with a more uniform and predictable sensitivity would be extremely useful. 4) An aqueous environment is usually necessary to maintain the structure of, and interactions between, most proteins and other biomolecules (although aqueous glycerol is a fairly mild solvent.) Thus, mass spectra of macromolecules in conformations competent to form native intermolecular complexes, as well as the intact

complexes of these molecules, are best obtained directly from aqueous solutions. In MALDI, analytes are subjected to drying in concentrated, usually acidic, organic matrix solutions and to the formation of matrix crystals. During this process, there will be a strong tendency for most biomolecules to denature, and this may well explain why the dissociated subunits of complex proteins are typically seen in MALDI mass spectra. Suitable freezing protocols are able to maintain the native, functional conformation of most protein systems [5,6]. Progress in desorbing macromolecules from frozen aqueous solutions may lead to methods for the reliable and sensitive detection of intact subunit proteins and other non-covalent complexes by laser desorption mass spectrometry. 5) If laser desorption could be performed directly from frozen aqueous solutions, the localized *in situ* detection of proteins and other biomolecules from intact frozen cells and tissues might become possible.

Considering the perceived desirable desorption properties above, it is unfortunate that it has proven to be extremely difficult to obtain gas-phase ions of biomolecules by laser desorption from frozen water ice solutions [7,8]. This situation also represents a challenge to our understanding of desorption/ionization processes.

Presently, UV lasers are almost exclusively used for MALDI mass spectrometry. Nitrogen lasers at 337 nm and Nd:YAG laser harmonics at 266 or 355 nm are common. Water, glycerol, and most organic solvents do not absorb at these wavelengths. However, water and other hydroxylated solvents have strong absorption bands in the IR, near 3 μm [9]. A number of publications have appeared that deal with IR laser desorption mass spectrometry [10-16] and with laser desorption from water and hydroxylated solvents [10,17]. Glycerol

was used as a matrix in the early work by Tanaka et al. [17] who obtained protein mass spectra by using 300 Å diameter cobalt particles to couple the laser energy into the liquid.

Hillenkamp et al. demonstrated IR-MALDI using a 2.94 μm Q-switched Er:YAG laser with a 150 ns pulse width [10]. Protein mass spectra were obtained from several MALDI matrices. However, a spectrum of lysozyme (14 kDa) using a liquid glycerol matrix was also reported [10]. The authors later obtained very similar results when using a pulsed 10.6 μm CO_2 laser [11]. In a recent paper, Hillenkamp et al. reported mass spectra of a range of proteins using glycerol as the matrix [15]. IR-MALDI was reported to have a higher upper mass limit and a higher mass resolution for large proteins than UV-MALDI on the same samples [12,15,18]. Metastable fragmentation of larger proteins, above about 20 kDa, was found to much less of a problem with IR-MALDI [15]. On the other hand, IR-MALDI consumed much more material than UV-MALDI, and only a few spectra could be obtained from the same spot on the desorption probe in IR-MALDI [11,13,15]. This was explained by a large neutral yield with an ablation depth of 0.1 to 0.5 μm in the thin, dry samples employed. Biemann et al. have also demonstrated applications of IR-MALDI to dry samples [19,20], and the application of a Cr:LiSAF pumped OPO laser to IR-MALDI was recently demonstrated [21].

The characteristics of liquid water ablation, induced by high fluence IR laser pulses have been studied (see [22] and references therein). Several factors, including changes in the absorption coefficient of water during the laser pulse [23], the development of shock waves, and delayed ablation have been shown to be important to the dynamics of laser-induced

ablation of water and biological materials with a high water content [22,24]. Of particular relevance to the present work are previous reports of laser desorption of biomolecules, with and without mass spectrometry, from frozen aqueous solutions. Williams et al. reported successful desorption of nucleic acid oligomers by laser ablation from films of frozen aqueous solutions where the water content had been reduced by sublimation in vacuum, such that the film had a total thickness of a few micrometers [7,25-27]. A visible wavelength laser beam from a tunable dye laser heated the underlying copper substrate surface. The reproducibility of ionization was, however, reported to be a problem in these experiments [27,28]. Becker et al. have demonstrated advantages of adding photoabsorbing substituted phenols to frozen films containing DNA [29].

Recently, Hillenkamp et al. demonstrated IR-MALDI mass spectra of proteins from air-dried films of protein solutions. In order to retain residual water in the films, they were frozen before being introduced into the vacuum [8]. An Er:YAG laser (2.94 μm, 150 ns pulse length) was used for these experiments. A mass spectrum was obtained only with the first laser shot, from any one single sample spot. Protein spectra had a rather high mass resolution, in the 300 to 350 range. The upper mass limit was reported to be 30 kDa, with a higher mass limit of 70 kDa if TrisHCl, a known IR MALDI matrix, was added to the aqueous solution [8]. Protein spectra were also reported from a hen egg lysozyme crystal. The authors emphasized that no protein spectra had been obtained from the bulk frozen, aqueous solutions, despite extensive efforts to vary experimental conditions [8].

Alimpiev at al. have used CO_2 lasers for ablation of frozen aqueous solutions. They used a tunable UV laser to ionize desorbed organic molecules by time-delayed, resonance-enhanced, multi-photon post-ionization [30-32]. The method was successful for ultra-high sensitivity detection of simple organic molecules, such as aromatic amino acids and phenol, dissolved in water. However, the upper mass limit of the method was found to be low and was limited by fragmentation of the analyte molecules by the UV and IR lasers.

Recently, we introduced the use of carbon powder suspensions in liquid glycerol as a matrix for laser desorption ionization at room temperature [33], and we refer to this method as Surface-Assisted Laser Desorption Ionization (SALDI) Mass Spectrometry. Graphite SALDI/MS has been applied also to frozen water solutions, as reported at a recent conference [34]. Using the 3.28 μm Nd:YAG/OPO laser, we found that spectra of organic molecules and peptides were easily and reliably obtained. However, with carbon powders we were not successful in obtaining mass spectra of proteins larger than about 20,000 Da. In the present work, we present a SALDI method that uses suspensions of organic crystals, instead of the carbon powder, in frozen, aqueous solutions for cryo-IR-SALDI. This cryo-IR-SALDI MS method reliably produces intense peptide and protein ion signals.

Experimental

Experiments were performed on a modified VESTEC 2000, 1.35 m linear time-of-flight mass spectrometer (Perceptive Biosystems, Framingham, MA). The acceleration voltage was 20,000 V, and all spectra were obtained in positive ion mode. A guide-wire

along the center of the flight tube was suspended from a point 6" from the beginning of the field-free region to a point 2" in front of the ion detector. The guide wire was normally held at -120 V. Unless otherwise noted, the guide wire was used as a low mass gate by switching the guide-wire voltage to +120 V for 3.0 μs after the laser pulse. Time-of-flight mass spectra were recorded on a Tektronix TDS520 storage oscilloscope and downloaded onto a PC for analysis. Internal mass calibration was used.

The tip of a 1/4" stainless steel insertion probe consisted of a copper rod with a 5.0 mm diameter front sample loading surface. This surface was flush with the "sample electrode" surface during desorption. The insertion probe tip made both thermal and electrical contact with the sample electrode plate, and both were maintained at the full acceleration voltage. Two additional electrodes defined the extraction electric field. The first acceleration electrode had a 1/4" central hole, was positioned 0.5" from the sample electrode, and was maintained at half the full acceleration voltage. A second acceleration electrode had a 1/4" central hole covered with a fine wire mesh, was positioned 1.0" from the sample electrode, and was kept at ground potential. With a 20,000 V acceleration voltage, the ion extraction field was 7.9×10^3 V/cm.

The sample electrode was cooled by means of a cold-finger. An electrically insulating BeO ceramic rod was attached to the sample plate. BeO was used because its heat conductivity at low temperature is significantly higher than that of other common electrical insulators [35]. A copper rod was soldered to a stainless steel vacuum feedthrough. Inside the vacuum chamber, the copper rod was connected to a copper holder of the BeO rod by

means of a flexible, braided copper strap. Outside the vacuum chamber, the copper rod dipped into a liquid-nitrogen-filled Dewar. One end of a 1/4" diameter aluminum garnet rod was also attached to the sample electrode, and a thermocouple was glued to the other end with epoxy. The temperature of the electrode was monitored with a Fluke 52 digital thermometer (John Fluke, Palantine, IL). Approximately 45 minutes after filling the Dewar with liquid nitrogen, the sample electrode temperature stabilized at about -140°C. A TV camera (Watec 902, Edmund Scientific) was aimed through a view-port at the top of the ion source chamber, and the sample surface was viewed with 19x magnification on a TV monitor.

The mass spectrometer was equipped with a Nd:YAG/OPO IR laser with a fixed wavelength of 3.28 μm (Big Sky Laser, Bozeman, MT). A maximum of about 200 mJ of a 1.064 μm laser pulse from the Nd:YAG laser (model CFR 400) was used to pump a double-pass, KTP OPO crystal. The crystal was used in a non-critically phase matched condition (90° phase matching) to give a signal beam at 1.57 μm and an idler beam at 3.28 μm. A dichroic mirror was used to reflect the signal beam out of the idler beam path. The 3.28 μm IR beam had a pulse length of 6 ns, and the divergence of the beam was 26 mrad (86.5% energy content) as determined by a central fraction method (energy through an aperture) in the far field. The pulse energy was monitored by a calorimeter (Scientech MA10, Boulder, CO) and was varied from zero to a maximum of 3.5 mJ, by changing the power to the Nd:YAG flash lamps. A nitrogen UV laser (Laser Science Inc., Newton, MA) operating at 337 nm was used for some experiments.

The IR beam was focussed onto the probe tip using a 180 mm focal length CaF_2 lens positioned outside a CaF_2 viewport window. The diameter of the IR laser beam at the lens was 60 mm. The laser beam passed the window normal to the window surface and hit the sample at a 60° angle relative to the normal of the probe surface. The UV beam was focused onto the sample surface in an identical manner, except that the UV beam entered the ion source from the opposite side, through a silica lens and window.

There was a concern that low intensity laser light at 1.57 μm and 1.064 μm, leaking through the dichroic mirror in the IR laser path, might contribute to the desorption process. In control experiments, a Ge-plate that absorbs at both of these wavelengths, but transmits efficiently at 3.28 μm, was inserted into the beam path. No differences in the mass spectra were observed, with or without the Ge-filter, when compared at the same pulse energy.

The focal spot size on the probe tip was measured by the following procedure. When the probe tip was covered with a fine graphite powder, the luminescence of the irradiated area was easy to distinguish on the TV monitor. The focal spot was seen to be ellipsoidal and, by comparing with the known dimensions of the probe tip, it was determined that the irradiated surface area was 0.5 mm^2. Correcting for the 60° incidence angle, the laser beam cross section is found to be 0.25 mm^2. With a typical pulse energy of 3.0 mJ, and correcting for 10% Fresnel losses in the lens and 10% reflection losses in the chamber window, the energy fluence (perpendicular to the laser beam), I_o, is calculated to be 1.0 J/cm^2 and the irradiance 1.9×10^8 W/cm^2 at the focal point. The energy deposition in the sample closest to the surface (at a depth that is small relative to $1/\varepsilon$, where ε is the absorption coefficient) is $\varepsilon \times I_o$, where

I_o is the energy fluence in the laser pulse. The absorption coefficient for water ice at 3.28 μm is approximately 2.5 x 10^3 cm^{-1} [9]. For frozen glycerol, we have measured an absorption coefficient of 1.5 x 10^3 cm^{-1}. Assuming an actual absorption coefficient in our samples is 2 x 10^3 cm^{-1}, we find that energy is deposited in the outermost surface layer with a density of 2 x 10^3 J/cm^3. The energy absorbed may be further lowered by reflection losses in the sample surface and by a decrease in the water absorption coefficient, at 3.28 μm, during irradiation [22].

The liquid solvent consisted of water and glycerol (33:67 w/w), unless otherwise noted. This is the eutectic composition of water and glycerol, and the mixture is thermodynamically stable as a liquid to -46°C [36]. Proteins or peptide analytes were dissolved directly into the solvent at room temperature at concentrations from 0.5 μM to 1 mM. The sample probe tip was cleaned with ethanol, and about four microliters of analyte solution in glycerol/water were typically deposited on the probe surface. A small amount of solid powder was placed on the liquid surface using a spatula, and after a few seconds, any excess dry powder was blown off the sample. Some solid powders like nicotinic acid had good wetting properties and quickly formed evenly distributed suspensions. Other powders with poor wetting properties, like polystyrene, tended to remain on the liquid surface. In those cases, suspensions were formed on the probe tip by stirring the powder into the solvent with a spatula for up to one minute. Sufficient powder was added to give the suspension a slurry-like appearance. After stirring, the surface of the slurry was seen to gradually become smooth, but this process was relatively slow. If too much solid powder was added, the

fluidity of the suspension was lost, and inferior mass spectra were obtained. If too little powder was added, reproducibility suffered and ion intensities decreased. For nicotinic acid, between 0.3 mg and 0.5 mg powder was added per 1 μL solvent. All chemicals used in this work were obtained commercially.

Samples of bacteriorhodopsin were prepared by adding 4 μL of 2-pentanol to 4 μL of a suspension of purple membranes in the glycerol/water solvent. The nicotinic acid crystals were then added, and the suspension was observed to turn yellow. The yellow color indicated that the protein partially denatured in the presence of the nicotinic acid crystals, possibly because the pH decreased to 3.5.

After preparing a suspension, the probe tip was cooled by immersion into liquid nitrogen. With the eutectic glycerol/water mixture, this cooling resulted in the formation of a vitreous phase, with essentially no ice crystal formation [37]. Immersion of the sample into liquid propane resulted in much faster cooling, but did not change the mass spectra when the glycerol/water eutectic mixture was used. A thin water frost layer was formed on the cold sample surface as the probe was transferred from the Dewar, where it was frozen, to the vacuum lock of the mass spectrometer. Using a 1 Hz laser repetition rate to obtain single shot mass spectra on the oscilloscope, it was found that weak protein ion peaks were observed from the first laser shots. The protein peaks gradually approached their full intensity during the first 50 laser shots at 3 mJ.

To avoid the formation of a frost layer, the room temperature probe tip with the eutectic glycerol/water sample solution could be inserted into the ion source. The sample was

then cooled *in situ* upon contact with the pre-cooled sample electrode. The cooling was still fast enough (about 1 minute to reach -130°C) that the eutectic solution formed a vitreous phase [37]. The protein mass spectra obtained with in-situ cooling were indistinguishable from the ones obtained by fast cooling in liquid nitrogen (after ablation of the frost layer). However, all spectra shown in this paper were obtained by immersion of the sample in liquid nitrogen. Cooling below -100°C did not significantly change the mass spectra. All spectra were obtained at -140±5°C, unless otherwise noted.

About half of the compounds tested in this work as cryo-IR-SALDI solids had a low or negligible solubility in glycerol/water. However, other solids used, such as nicotinic acid and the amino acids, had a significant solubility. If all the added crystals dissolved fully, no mass spectra were obtained from the bulk of the frozen solutions. Some solids, in particular aspartic acid and histidine, dissolved quickly. Additional powder typically had to be added to ensure that some crystals remained. The dissolution of the soluble solids could be arrested by quickly freezing the sample. Essentially no additional dissolution was observed once the suspensions had been cooled to below -40°C. However, fast freezing also tended to result in an uneven distribution of solid particles in the suspension, and this made it more difficult to obtain high quality mass spectra. A better alternative was to slow the rate of dissolution by pre-cooling the probe and the liquid sample solution to about 0 °C prior to adding the soluble powder. There was then enough time to distribute the solid evenly throughout the suspension.

Control experiments were performed in which either the organic solid or the glycerol was eliminated from the sample. In the absence of organic solids, mass spectra (of peptides) were only occasionally obtained from the bulk of the frozen phase, and these rare events may well have been due to contamination of the sample by solid particles. In experiments where the glycerol cryoprotectant was not present, it was necessary to freeze the sample prior to inserting the probe into the ion source because the high vapor pressure of water near room temperature led to severe loss of the water solvent in the vacuum. Mass spectra were obtained in the absence of glycerol, as described in the Results and Discussion section.

It is well known that laser desorption mass spectra can be obtained from metal surfaces [8,25,28]. For this work, it was necessary to verify that the mass spectra were obtained from the bulk of the frozen suspensions without involvement of the underlying metal surface. "Laser drilling" experiments were performed where 4 μL of the glycerol/water nicotinic acid suspension was first deposited on the probe, and series of laser pulses were delivered to the same spot close to the center of the sample where the sample thickness was approximately 0.30 mm. The copper surface was reached after about 2,500 laser pulses (about 4 minutes at 10 Hz) with a 3 mJ laser pulse energy. That the copper surface was indeed reached at this point was clearly revealed by bursts of intense ion signals due to Na^+, K^+, and Cu^+ that were not seen from the bulk suspension. Thus, the ablation yield was approximately 0.1 μm per 3.0 mJ laser pulse, and the volume of frozen solution desorbed per laser shot was less than 0.1 nL. Unless otherwise noted, the sample size used in this work was 4 μL, the laser was focussed close to the center of the frozen sample, and all spectra

reported were obtained prior to 2 minutes irradiation time (at each spot) at 10 Hz. Under these conditions, the maximum depth of ablation should be less than 25% of the sample thickness.

Results and Discussion

The goal of this work was to obtain mass spectra of biomolecules directly from bulk frozen aqueous solutions. In initial experiments, no solid crystals were added to the analyte solutions in glycerol/water. It was found that the Nd:YAG/OPO laser beam at 3.28 μm was efficiently absorbed by frozen water and glycerol/water solutions, and sample drilling experiments showed that the ablation yield was about 0.3 μm per 3 mJ laser shot [38]. However, we had little success in obtaining mass spectra from the bulk of frozen water or glycerol/water solutions, although peptide mass spectra were occasionally obtained [38]. This is in general agreement with results of Williams et al. [26,27,39] and Hillenkamp et al. [8].

Because useful analyte mass spectra were not obtained from bulk, frozen aqueous solutions, we explored the use of Surface-Assisted Laser Desorption Ionization (SALDI) mass spectrometry [33] to obtain spectra from frozen water solutions. Suspensions of graphite (or activated carbon) particles in aqueous solutions were frozen and irradiated with the 3.28 μm Nd:YAG/OPO laser. It was found that mass spectra of organic molecules and peptides were easily and reliably obtained [34]; however, we were not successful in obtaining mass spectra of proteins larger than myoglobin. In an effort to overcome this limitation, we

explored the use of organic crystals, instead of carbon powder, for cryo-IR-SALDI in frozen, aqueous solutions.

Cryo-IR-SALDI mass spectra of peptides

We first present typical cryo-IR-SALDI results for peptides, before discussing results for proteins. For the mass spectrum of angiotensin II in Figure 1, a suspension of nicotinic acid crystals was prepared and frozen as described in the Experimental section. It is seen that the mass spectrum is dominated by the protonated peptide peak at m/z=1047 and by peaks due to the SALDI solid. Low-intensity clusters of glycerol with Na^+ and K^+ are also sometimes observed.

The mass resolution, ($m/\Delta m$, FWHM), for the peptide peak in Figure 1 is approximately 80. The intensity of the angiotensin peak is low relative to the matrix peaks in the spectrum in Figure 1. This spectrum was obtained at a 1.25 mJ laser pulse energy, and the intensity of the peptide peak was found to increase by about a factor of 10 when the laser pulse energy was increased to the maximum of 3.5 mJ. However, the mass resolution decreased somewhat at higher laser pulse energies. By decreasing the pulse energy below 1 mJ, a mass resolution of 250 (FWHM) could be achieved. This is similar to the mass resolution obtained with UV-MALDI on the same instrument. Using the maximum laser pulse energy, the detection limit (S/N = 3) for angiotensin II was approximately 0.5 μM, or 0.5 pmole for a 1 μL sample.

A 0.5 μM detection limit corresponds to 0.5 pmole of peptide in a 1 μL sample size. However, it is easy to use smaller sample sizes. In room temperature, activated carbon-UV-SALDI, we found that the minimum amount of analyte required was lowered by more than two orders of magnitude by introducing a solvent concentration step on the probe (similar to solvent evaporation in MALDI) and by using smaller sample sizes. These strategies should be possible to use also in cryo-IR-SALDI. The peptide sample consumption during the 100 laser shots used for the spectrum in Figure 2 was about 10 pmole. However, single shot mass spectra were obtained with a peptide consumption of approximately 1 fmole.

Figure 2 shows the abundance of protonated nicotinic acid and protonated angiotensin II, as a function of laser pulse energy in a double logarithmic plot. As the laser pulse energy is increased, the ratio of the abundances of these two ions remains nearly constant up to 1.5 mJ pulse energy, after which the peptide ion abundance is seen to level off more quickly than that of protonated nicotinic acid. The slope of the straight lines at lower laser pulse energy in Figure 2 is approximately 9 for both the nicotinic acid and the peptide which shows that the ion yields increase as the 9th power of the laser pulse energy. This is similar to the slope observed for matrix ions in MALDI [40]. The amount of nicotinic acid in the sample used for Figure 2 was approximately 3,600 times the amount of the peptide, whereas the signal abundance ratio is seen to be about 20. Thus, the relative response for the peptide is much higher than for the SALDI solid.

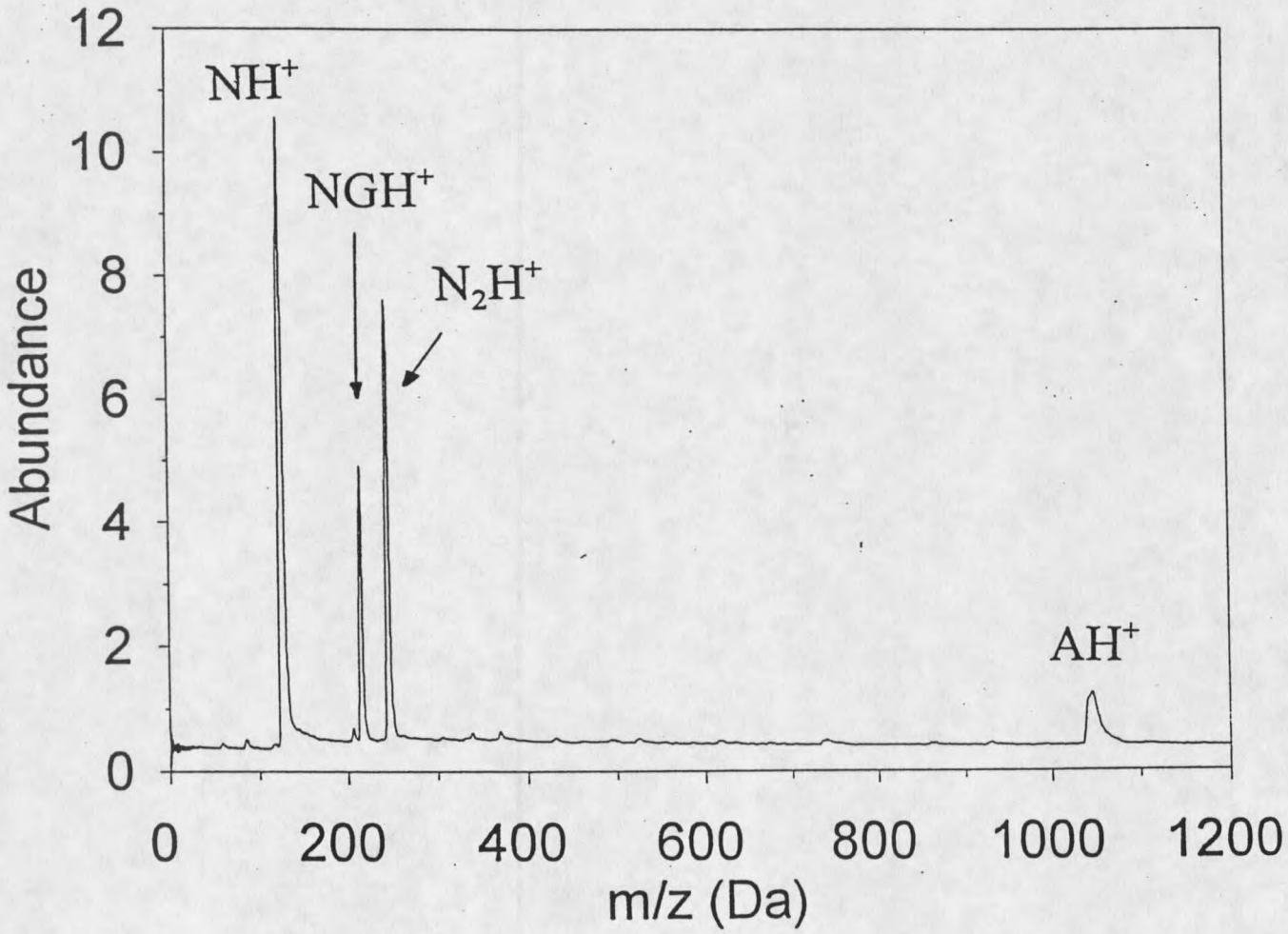


Figure 1. Cryo-IR-SALDI mass spectrum of 0.9 mM angiotensin II in 67% glycerol in water. Nicotinic acid (1.6 mg) was added to 4 μL of the glycerol/ water solution before freezing by immersion of the copper sample tip in liquid nitrogen. Laser pulse energy 1.25 mJ, average of 100 single shot spectra, and low mass gate off. "N" = nicotinic acid, "A" = angiotensin II, and "G" = glycerol.

Comparison between different SALDI solids for protein desorption

We evaluated 20 different organic compounds as SALDI solids using a 0.5 mM equimolar mixture of myoglobin and cytochrome c in the eutectic glycerol/water solution, and the results are summarized in Table 1. Starting at the top of Table 1, the solids evaluated are ordered from the "best" to the "worst" SALDI solids. The approximate signal intensities for the protein peaks are given in the Table, as well as comments on sample preparation. With practice, protein mass spectra were obtained with 16 of the 20 solids. We were unsuccessful with only four of the compounds tested: sodium chloride, cellulose, carboxy-methyl cellulose, and tryptophan. Figure 3 shows a selection of cryo-IR-SALDI protein mass spectra, obtained using (a) nicotinic acid, (b) histidine, © xanthine, and (d) polystyrene as the SALDI solids. The spectra illustrate similarities and differences observed among cryo-IR-SALDI mass spectra using different solids. Singly and multiply charged protein peaks dominate the mass spectra. Several protein/heme and protein/protein clusters, with masses up to 50,000 Da, are resolved in the nicotinic acid and histidine-assisted mass spectra. The extent of multiple charging, and of clustering, is seen to vary between the SALDI solids.

The majority of SALDI solids tested were aromatic compounds, see Table 1. Aromaticity may well contribute to a compound being a successful SALDI solid, but it is not an absolute requirement. For example, aspartic acid crystals gave cryo-IR-SALDI mass spectra of myoglobin and cytochrome c, though the spectra were of lower quality (results not shown). Also, SALDI solids do not have to be volatile or have a low molecular

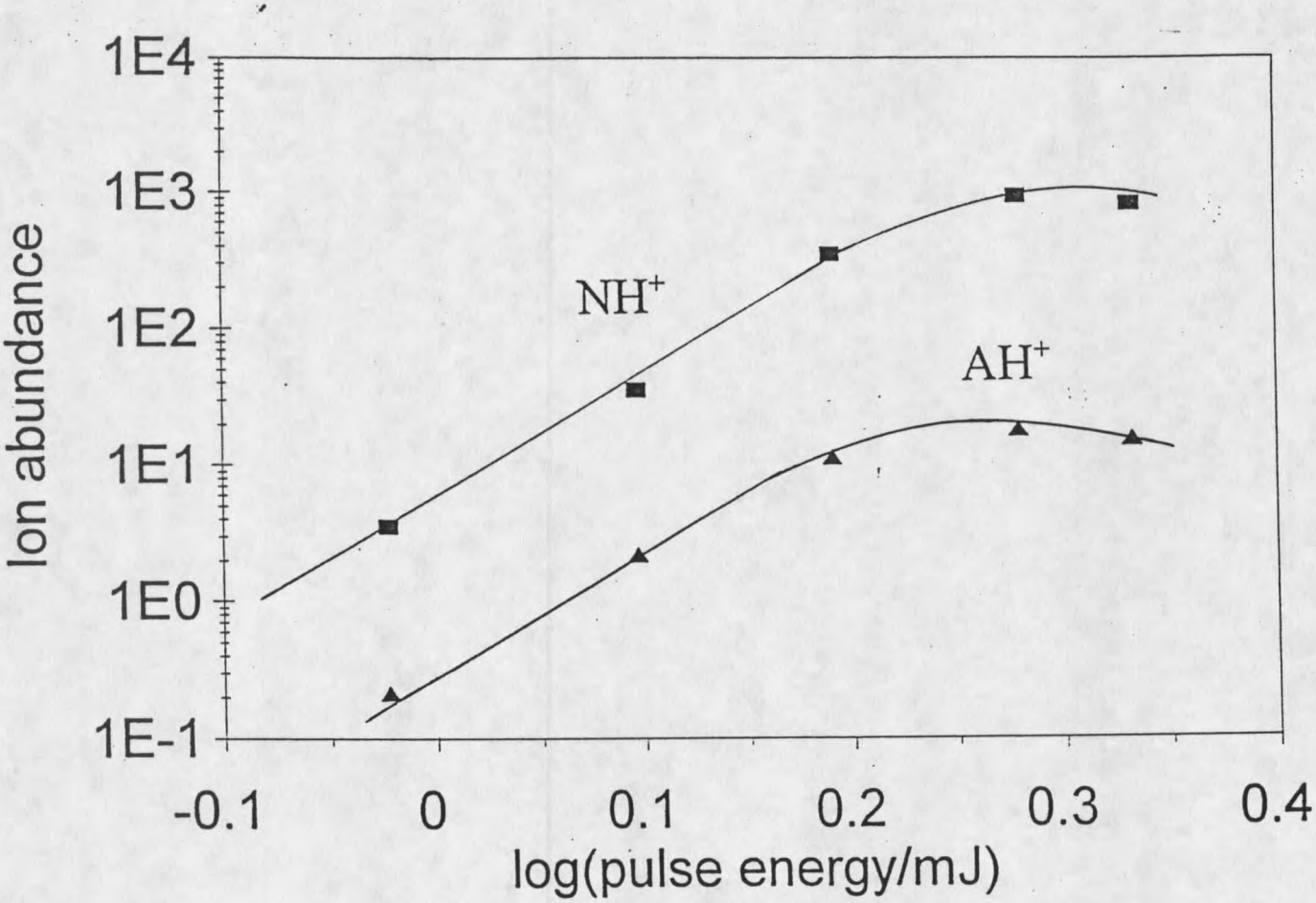


Figure 2 Abundances, as determined by peak heights, of singly protonated nicotinic acid (NH^+) and singly protonated angiotensin II (AH^+) ions as a function of laser pulse energy using the same experimental conditions as in Figure 1.

weight, as illustrated by the fact that polystyrene gave cryo-IR-SALDI mass spectra of proteins, Figure 3d.

The best protein mass spectra with respect to sensitivity and mass resolution were obtained with nicotinic acid, indole-2-carboxylic acid, thymine, and histidine. The mass resolution, m/Δm (FWHM), of the singly charged protein peaks at 15-20 kDa was typically about 50, with somewhat higher resolution obtained at the lowest laser pulse energies. The limit of detection for myoglobin and cytochrome c was about 5-10 μM, compared to about 0.5 μM for peptides, at a signal-to-noise ratio of three. The higher detection limit for proteins as compared to peptides is mainly due to the wider mass peaks for proteins. When peak areas in mass spectra (plotted versus flight time) were compared, it was found that the response for the proteins was close to that for the peptides.

Nicotinic acid was the SALDI solid of choice in this work. Mass resolution and sensitivity were as good as, or better than, those obtained with any of the other solids evaluated. Nicotinic acid, together with indole-2-carboxylic acid, was unique in that it reliably yielded protein mass spectra anywhere on the sample and with every laser shot. In addition, the nicotinic acid powder wets easily, and the suspensions were easy and quick to prepare.

UV-laser irradiation of cryo-SALDI samples

All solids in Table 1 were also tested for their ability to yield cryo-SALDI mass spectra with the 337 nm nitrogen UV laser. In most cases, no ions were observed when the UV laser was first focussed onto a freshly frozen SALDI suspension, but weak signals due

Table 1. Summary of cryo-IR-SALDI results for selected solids additives.

Compound	Protein Mass Spectra Typical Intensity*	Comments
nicotinic acid	5	wets well, fine uniform crystalline powder, rather soluble, low protein charge states
indole-2-carboxylic acid	5	wets well, insoluble, high protein charge, lower mass resolution than nicotinic acid
histidine	4	wets well, very soluble, reliability of analyte signal improved by pre-cooling the glycerol/water solvent before adding crystals
thymine	3-4	poor wetting, required stirring, slightly soluble, dendritic crystals, produces high protein charge states
alpha cyano-4-hydroxy cinnamic acid	2	wets well, almost insoluble, produces high protein charge states
pyrene	1	insoluble, large crystals
6-dimethylaminopurine	1	wets well, slightly soluble
guanine	1	wets well, almost insoluble
xanthine	1	wets well, slightly soluble, tendency to produce high protein charge states
adenine	1	wets well, slightly soluble
2,3-dihydroxybenzoic acid	1	poor wetting, required stirring
sinapinic acid	1	poor wetting, required stirring, insoluble
polystyrene powder (typical m.w. 4,000)	0.5	polystyrene powder was ground by mortar and pestle to remove trapped air, insoluble, required extensive stirring
terepthalic acid	0.5	extensive stirring required, fine powder, insoluble
diphenylamine	0.5	extensive stirring required, large planar crystals do not wet, insoluble
aspartic acid	.5	wets well, very soluble, reliability of analyte signals improved by pre-cooling the glycerol/water solvent before adding crystals
tryptophan	none	slightly soluble
sodium chloride	none	very soluble
cellulose	none	19 μm particle size, wets well, insoluble
carboxy-methyl cellulose	none	insoluble, wets well

*All 20 compounds were tested with a solution of 0.5 mM cytochrome C and 0.5 mM myoglobin in 67% glycerol in water, at ~3.0 mJ per laser shot. Other conditions were as described in the Experimental section. Typical intensities represent the average of one hundred spectra and are quoted in arbitrary units.

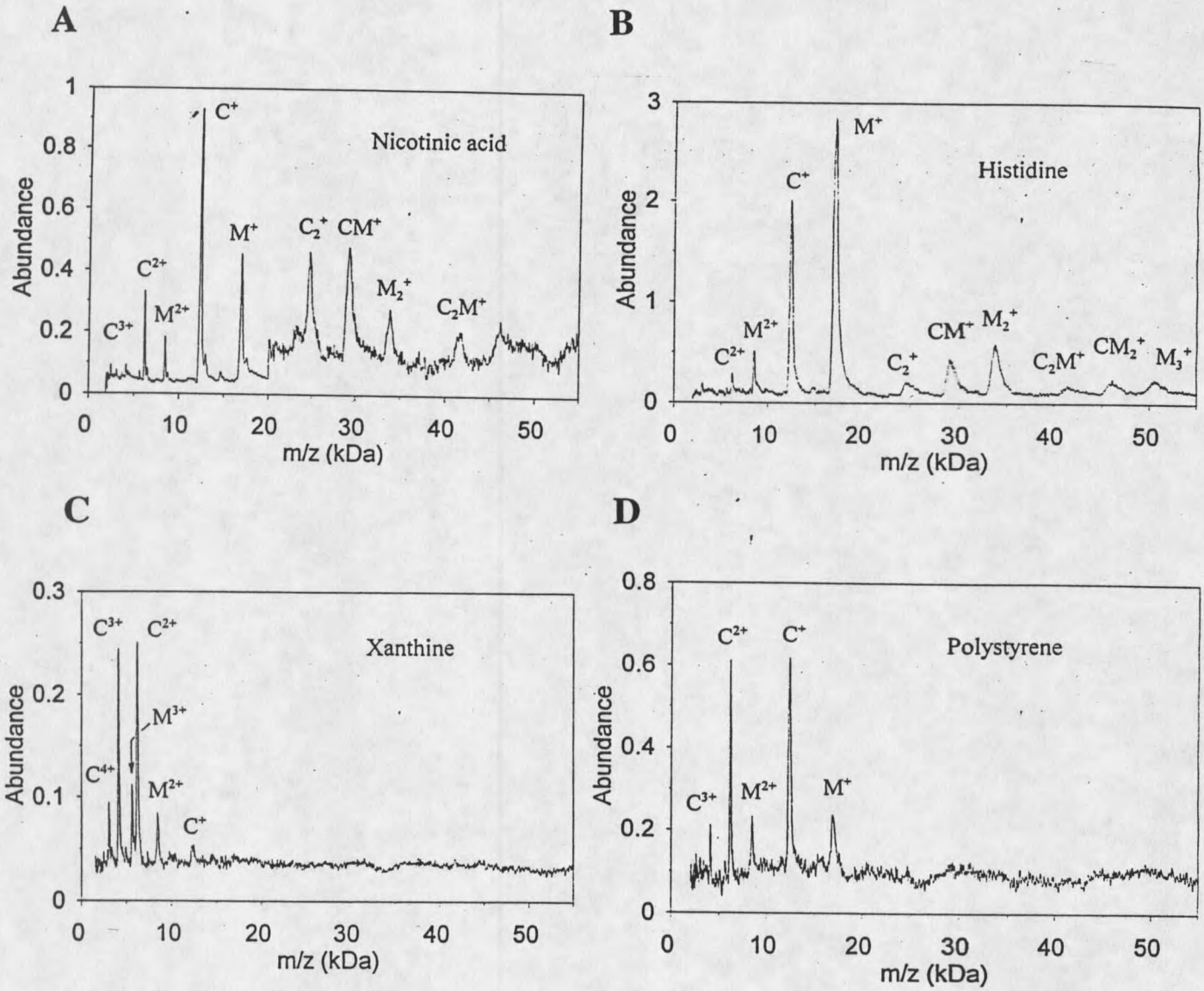


Figure 3 Cryo-IR-SALDI mass spectra of an equimolar mixture of 0.5 mM myoglobin ("M") and cytochrome c ("C") in a 67% glycerol in water solution with different SALDI solids added. a) Nicotinic acid, b) histidine, c) xanthine, and d) polystyrene. Each spectrum is an average of 100 single-shot spectra, and the laser pulse energy was 3.0 mJ.

to ions from the SALDI solid appeared after a few hundred laser shots. For a few solids with unusually large crystals, such as pyrene, as well as for suspensions with a concentration of solid that was high enough that the fluidity of the sample was lost prior to freezing, abundant ions from the SALDI solid were observed from the beginning of UV irradiation. In these samples, it seems likely that crystals protruded out of the sample surface. In additional experiments, samples were first exposed to about 200 IR laser shots of 3 mJ each, during which time protein mass spectra were observed. The shallow "crater" that resulted from the IR laser ablation could be clearly seen on the TV monitor. When the nitrogen UV laser was focussed onto this area, ions from the SALDI solid were observed from the first UV laser shot. These results indicate that the organic crystals must be exposed on the surface of the sample in order to obtain ions from cryo-SALDI samples with the UV laser. Peptide mass peaks were observed in the UV-induced spectra from the cryo-SALDI samples, but only for one solid (indole-2-carboxylic acid) was a (very weak) protein peak obtained and then only at maximum UV laser power.

Laser "drilling" experiments and surface charging

Insights into the analytical potential of cryo-IR-SALDI, and into the mechanisms of ion formation, were obtained from laser "drilling" experiments on nicotinic acid and thymine suspensions in frozen glycerol/water. In these experiments, the IR laser was focussed onto the same sample spot for an extended time. As described in the Experimental section, the copper substrate was reached after about 2,500 laser shots with 3 mJ of 3.28 μm laser energy

in each pulse when a 4 μL sample was used. Protein ion signals were obtained during the entire drilling time. (Remarkably, protein ion signals were obtained from the bottom of the drilled crater for more than 30,000 laser shots. These results, that required the presence of the organic crystals on the metal surface, will be published elsewhere).

During the drilling process, it was observed that the flight time for the ions drifted significantly. For example, with an acceleration voltage of 20,000 V, the flight time for singly charged apomyoglobin ions (16,953 Da) was 95 to 98 μs at the beginning of drilling. The flight time gradually decreased during drilling and was 93 μs as the metal surface was reached. The flight time calculated from the known length of the flight tube was also close to 93 μs. The longer ion flight times observed from the surface of a frozen sample did not vary significantly with laser power. However, there was a correlation with the thickness of the sample - the thicker the original sample, the longer the initial flight time. These observations can not be explained by changes in desorption characteristics, such as a "drying" of the sample during drilling. We therefore concluded that the unexpectedly long initial flight times must be due to the sample surface being at potential lower than that of the metal. This implies that the frozen surface carried a negative charge. In our experiments, the potential of the copper probe was 20 kV. The observed flight times show that the potential of the surface of the frozen sample, at the onset of drilling, was in the range of 18 to 19 kV. It is of interest to note that the charge required to achieve this surface potential is only about 200 singly charged ions per $(\mu m)^2$. With a sample thickness of 0.2 to 0.3 mm, the electric field strength in the frozen sample is found to be approximately $5*10^4$ V/cm. The upper limit for

the electric field strength may well be determined by the leakage of charge carriers between the metal surface and the sample surface.

It is not unreasonable that the sample surface would become negatively charged early in the laser irradiation since positive, but not negative, ions leave the surface during the desorption process. It is also possible that the ionization gauge, or low-current discharges along insulator surfaces in the high-voltage source, supplies the gas-phase ions required to charge the frozen sample surface.

Larger proteins and clustering

Mass spectra of small proteins, such as myoglobin and cytochrome c, are sometimes obtained with methods that will not yield spectra of larger proteins. Room temperature carbon-UV-SALDI, for example, was found to have an upper mass limit of about 20,000 Da [33]. Thus, the question of what size range of proteins can be studied using cryo-IR-SALDI is of considerable interest. Figure 4 shows a nicotinic acid-SALDI mass spectrum obtained from a solution containing lactic dehydrogenase (LDH, 0.05 mM) and cytochrome C (at 0.10 mM). LDH is a tetrameric protein with four identical subunits and a total molecular weight of 146,256 Da. The highest-intensity peak in Figure 4 is that of the LDH monomer, but complexes containing 2, 3, and 4 subunits are also seen. The question arises whether the multimeric complexes could be "surviving" fragments of the intact LDH protein and thus reflect specific subunit associations. However, the gradual decrease in the intensity of the LDH subunit complexes with increasing size and the presence of several low-intensity peaks

that are due to mixed complexes between LDH subunits and cytochrome C make it more likely that non-specific clustering occurred. Other systems likewise showed extensive molecular complex formation. For example, series of peaks in nicotinic acid-SALDI mass spectra of a mixture of 0.5 mM lysozyme (m.w. 14,300 Da) and 1.1 mM angiotensin in glycerol/water were due to clusters with up to five lysozyme and several angiotensin molecules (results not shown). Proteins larger than the LDH subunit can be analyzed by cryo-IR-SALDI. The nicotinic acid-SALDI mass spectrum of bovine serum albumin (BSA) in Figure 5 shows an intense molecular ion mass peak with a mass resolution of about 50. Smaller peaks are due to doubly charged BSA and to singly and triply charged BSA dimers. The weak peak at m/z=99.6 kDa is due to a doubly charged BSA trimer (199 kDa).

For some protein samples, we have observed very broad peaks due to unresolved distributions of complexes or clusters. For example, in experiments where SDS was added to an aqueous solution of lysozyme, a very broad, nearly symmetric peak was observed (results not shown). The apex of the peak corresponded to about four SDS molecules per lysozyme molecule. Dissociation of SDS-protein complexes in the ion acceleration region would explain why peaks due to the protein with different numbers of SDS molecules were not resolved. This result is in sharp contrast to room temperature graphite-SALDI where peaks due to protein molecules, without SDS, were obtained even when 5 to 10 % SDS had been added to the sample. In another series of experiments in this work, cryo-IR-SALDI mass spectra of the integral membrane protein bacteriorhodopsin were obtained directly from a suspension of purple membrane from *Halobacterium Salarium* in glycerol/water. Native

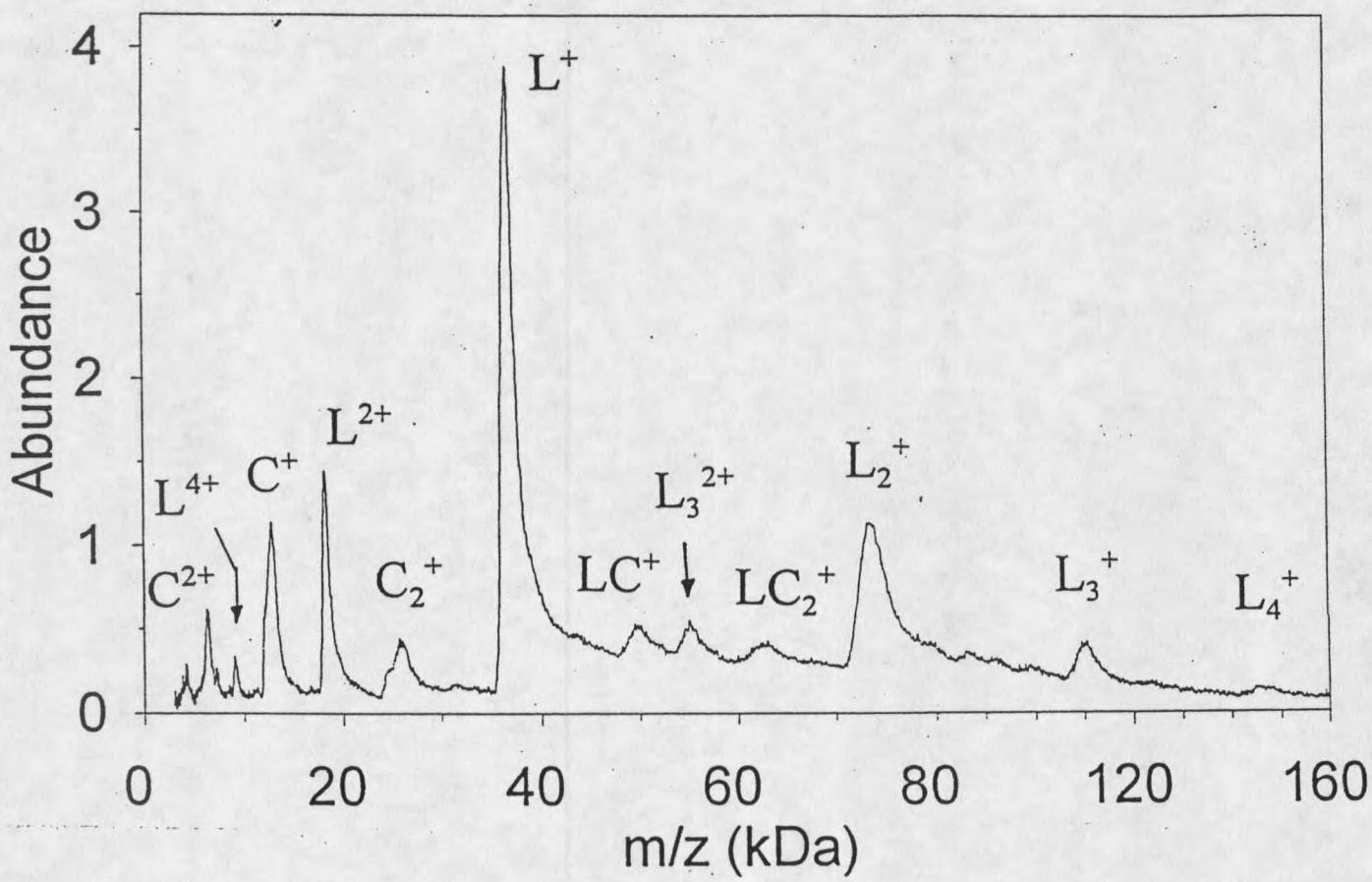


Figure 4 Nicotinic acid cryo-IR-SALDI mass spectrum of 0.05 mM lactic dehydrogenase ("L") and 0.10 mM cytochrome c ("C") in water:ethanol:glycerol (25:25:50, v:v:v). The average of 100 single shot spectra is shown. Essentially the same spectrum was obtained in the absence of ethanol. Note change in mass scale at 80 kDa.

purple membranes contain a high concentration of bacteriorhodopsin embedded in a lipid bilayer with about 11-13 lipids per bacteriorhodopsin dimer. In the mass spectra (not shown), the protein peak was observed to be very broad, and the width of the peak showed that individual bacteriorhodopsin molecules were associated with up to 12 lipid molecules. However, a distinct peak (m/Δm=65) superimposed on the leading edge of the broad distribution allowed for accurate mass determination of the protein, free of any lipid. Clearly, cryo-IR-SALDI is able to desorb proteins from a wide range of physical environments, but it is not always possible to fully dissociate proteins from neighboring molecules using current approaches. There is a need to better understand the factors that determine internal energy deposition, such that the extent of cluster dissociation and the quality of the mass spectra can be optimized for different types of samples.

Results from aqueous solutions with no cryoprotectant added

In this work, we have mainly used the eutectic mixture of 67% glycerol in water as the SALDI solvent. As described in the Experimental section, this mixture forms a vitreous (amorphous) phase, even when using the relatively slow cooling method of immersion of the sample holder into liquid nitrogen [41]. The eutectic mixture was used because we initially believed that suppressing water ice crystal formation was essential. However, it was found that lower concentrations of the glycerol cryoprotectant could easily be used. Even with pure water solvent, the mass spectra were very similar to those obtained with 67% glycerol in

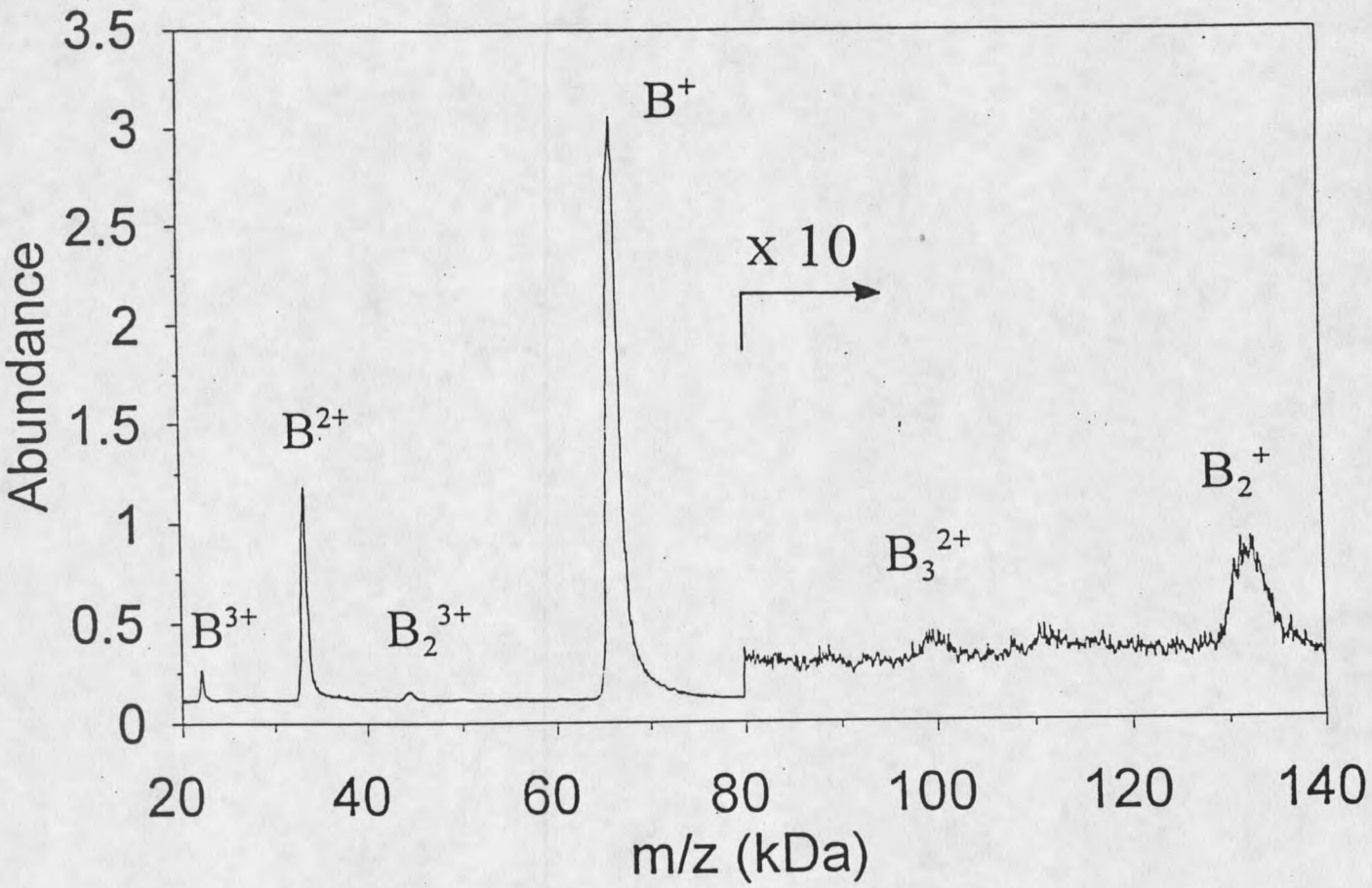


Figure 5 Nicotinic acid cryo-IR-SALDI mass spectrum of 0.34 mM bovine serum albumin ("B", 66,430 Da) in glycerol/water; average of 100 single-shot spectra.

water. Though not required, the addition of glycerol was very beneficial to suppress sweet-spot formation and to achieve a uniform sensitivity over the whole sample surface. When an aqueous sample is cooled in the absence of cryo-protectant, analytes concentrate in the void-volumes ("freeze concentrate") between the growing crystals of water ice [42]. The resulting concentrated solution of proteins or other analytes are, in effect, dried by the formation of pure water crystals. The water content in the protein concentrate can vary from a few to about 40 percent by weight [42]. The "freeze concentrate" would seem to be similar to the protein films, air-dried on metal surfaces, from which laser desorption mass spectra of proteins have previously been obtained [7,8,26,27]. It is possible that the desorption processes are similar, except that metal surfaces were involved in the previous work and solid organic surfaces are used in the present work.

Multiple charging

Multiple charging of proteins is observed in most cryo-IR-SALDI mass spectra, as illustrated in Figures 3 and 4-6. It was found that the extent of multiple charging varied significantly between different SALDI solids but, for a given solid, the extent of multiple charging did not depend on the laser power. For the majority of SALDI solids tested, singly and doubly charged protein ions dominated the mass spectra. However, many solids yielded intense peaks corresponding to protein charge states of three to five, see for example Figure 3c. Of the twenty SALDI solids in Table 1, thymine, α-cyano-4-hydroxy-cinnamic acid, indole-2-carboxylic acid, and xanthine yielded protein mass spectra with the highest charge

states. Figure 6 shows a thymine-SALDI mass spectrum of myoglobin with a charge distribution from MH^+ to MH_{12}^{12+}. The solution had been acidified to pH 4 by adding HCl. The charge distribution shifted from a maximum of 8 charges without acid addition to 12 charges with added acid.

High protein charge states have previously been reported in IR-MALDI. For example, a 150 kDa monoclonal antibody was observed with up to 13 charges [10]. In room temperature, carbon-SALDI, we have observed myoglobin with up to 6 charges. However, the high charge states observed here for a small 17 kDa protein seems unprecedented in laser desorption. Indeed, the high charge states in Figure 6 is approaching those observed for the native protein in electrospray, when using an aqueous solution [43], though even higher charge states, up to 23+, are observed in electrospray when the protein is denatured.

Ionization Processes

Tentative conclusions can be made regarding the ionization processes in cryo-IR-SALDI. Since the SALDI solid is essential in order to produce gas-phase ions, it might seem reasonable to assume that the high-abundance "SALDI solid ions" (i.e. ions originating from the SALDI solid) are reagent ions that ionize neutral analyte molecules in ion/molecule reactions. However, this does not seem to be the case.

In considering the ionization processes in cryo-IR-SALDI, it is useful to compare with a better understood desorption ionization method such as FAB. In FAB, the analyte is homogeneously mixed with a matrix in a solution. Ionization transfer occurs from matrix ions

to neutral analyte molecules and, as a result, protonated matrix ions in FAB are significantly suppressed by the presence of only 1-2 mole percent of a higher proton affinity analyte [39]. In SALDI, the experimental observations are different: Between two analytes that are both present in the liquid phase in room-temperature graphite SALDI, ion suppression effects are significantly stronger than in FAB [33]. In contrast, we have found that suppression effects in cryo-IR-SALDI, between ions derived from the solid compound and ions derived from the frozen solution, are small. For example, when 20% of the high proton-affinity compound diethanolamine was added to the glycerol/water phase, in a suspension with nicotinic acid, it was found that the nicotinic acid ion signal was suppressed by only about 50%. This shows that most nicotinic acid ions experience few collision in the desorption plume with molecules from the frozen phase. Otherwise, few nicotinic acid ions would have survived proton transfer to diethanolamine. Thus, there is only limited mixing between the SALDI solid and the frozen phase, either in the sample or in the desorption plume.

There is good evidence that analyte ions in cryo-IR-SALDI are preformed, i.e. already present in the frozen phase prior to the desorption event. First, the only possible reagent ions present in the mass spectra are the ions derived from the SALDI solid. Because of limited mixing with molecules from the frozen phase, as explained above, it seems unlikely that these are reagent ions. Second, in comparing IR- and UV-induced cryo-IR-SALDI mass spectra, large variations were observed for the abundances of the SALDI solid ions. For example, nicotinic acid ion abundances were two to three orders of magnitude higher with the IR than with the UV laser, whereas the abundances of indole-2-carboxylic acid ions were a factor of

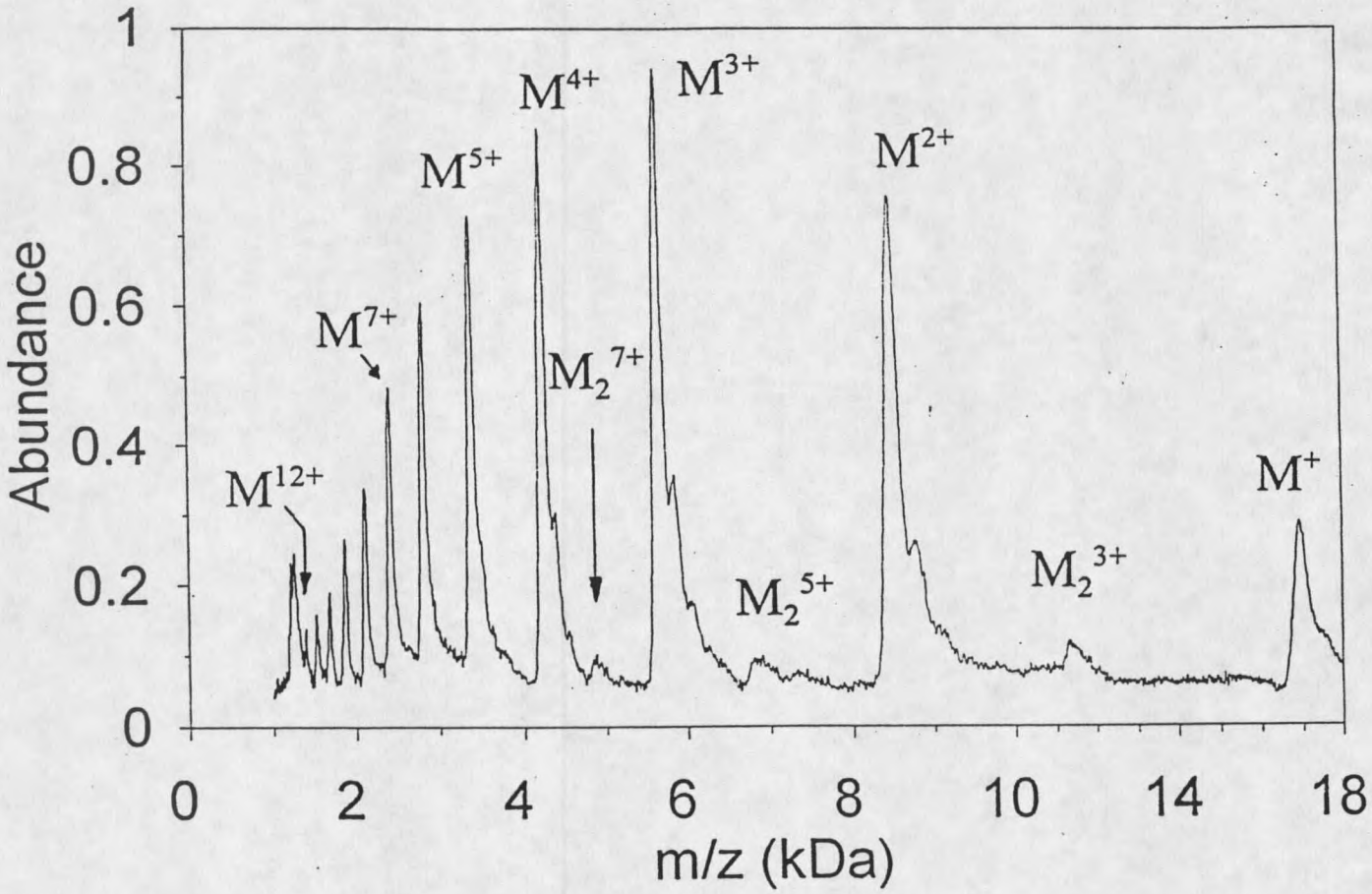


Figure 6 Thymine cryo-IR-SALDI mass spectrum of 0.1 mM myoglobin ("M") in 67% glycerol in water; HCl was added to give a pH of 3.5 in the final suspension. Average of 100 spectra. Note change in mass scale at 10 kDa.

2-3 higher with the UV laser. These large intensity variations were not reflected in the abundances of analyte and glycerol ions, as would have been expected had the SALDI solid ions been the precursors of the ions from the frozen phase. Third, the most convincing evidence for analyte ions being preformed in cryo-IR-SALDI comes from the observation of extensive multiple charging of protein ions. It is extremely difficult to form ions in charge states higher than one by gas-phase ion-molecule reactions because of the strong electrostatic repulsion between a singly charged ion and a reagent ion of the same charge. Thus, multiply protonated ions must have been present in the condensed phase prior to the laser pulse (i.e. "preformed").

The discussion above leads to a picture of the cryo-IR-SALDI desorption ionization process where 1) ions originate **both** from the SALDI solid phase and from the frozen phase; 2) there is limited mixing, in the sample and in the desorption plume, between the molecules of these two phases; and 3) most analyte ions are **preformed**.

The conclusion that analyte ions, observed in cryo-IR-SALDI mass spectra, are preformed in the frozen phase does not answer the question of why the SALDI solid is required to observe analyte ions. The crucial function of the solid may well be to facilitate charge separation. The observation of highly charged protein ions in cryo-IR-SALDI requires that the multiply charged ions, present in solution, be separated from their counter ions. To see why this represents a problem, we may consider the minimum distance by which a counterion must be separated from a charged protein, in order for the applied electric (extraction) field to overcome the electrostatic, attractive force between the ions. For the

8,000 V/cm ion extraction field, used in this work, and for a singly charged ion and a singly charged counter-ion, the required separation distance in vacuum is calculated to be 42 nm in the direction of the extraction field. This minimum distance increases approximately with the square root of the number of charges on the protein, and exceeds 100 nm for a protein with six charges. (In the dense plume, the dielectric constant is larger than one. However, the calculation of the minimum separation distance is only weakly dependent on the dielectric constant, since both ion/ion attractive forces and the extraction field are attenuated to nearly the same degree). Should more than one multiply charged protein be present nearby in space, the calculated minimum distances become larger, approaching 1 μm. It is important to note that the calculated minimum separation distances are comparable to the thickness of the sample layer ablated per laser shot, 0.1 to 0.3 μm [38]. This calculation shows that achieving charge separation in the laser-generated desorption plume must be expected to be a significant barrier to successful ion desorption, particularly for multiply charged ions. The problem of extracting positive ions from the frozen sample surface in the present cryo-IR-SALDI experiments seems even more daunting when it is considered that the surface carries a significant net charge of opposite sign (here negative), as concluded above. An attractive solution to this problem would be that the counter-ions are "immobilized", i.e. they would remain in that part of the sample that is not ejected into the vacuum. Minimum separation distances in the sample, prior to laser desorption, could then be significantly shorter because the expanding dense plume will exert a viscous force on the positive charges and this will facilitate charge separation.

One possibility for achieving charge separation in the sample is that the counter-charges are associated with the SALDI solid surfaces. To explore this possibility, we will consider thymine and α-cyano-4-hydroxy-cinnamic acid. Exposed amino groups on thymine crystal surfaces are expected to be partially protonated at the low pH employed, giving the surfaces a net positive charge. In contrast, exposed carboxylic groups in α-cyano-4-hydroxy-cinnamic acid should be partially deprotonated giving these surfaces a net negative charge. However, both these solids yielded cryo-IR-SALDI mass spectra with protein ions in high, positive charge states. Indeed, we have found no correlation between pK_a-values for the SALDI solids and their tendency to produce protein ions. Also, experiments using ion exchange chromatography beads as the SALDI solids were unsuccessful. For these reasons, we have tentatively concluded that crystal surface charging is not important to the formation of (multiply charged) analyte ions.

A second possible explanation for successful charge separation in the cryo-IR-SALDI sample is that the crystals might create local electric fields that are significantly higher than the 8,000 V/cm extraction field applied in our laser desorption ion source. Only charge separation needs to be accomplished because the desorption process considered here is induced by the laser pulse and not by the electric field. Therefore, the electric field strength required is lower than that experienced by ions desorbed in electrospray ($\approx 10^9$ V/cm). Strong, local electric fields would be created by edges or needle-like structures in the surface of the frozen suspensions. Scanning electron photomicrographs were obtained of nicotinic acid, α-cyano-4-hydroxy-cinnamic acid, and thymine. The micrographs of nicotinic acid (that

yields low charge state mass spectra) were dominated by rounded shapes, with smallest structural features having dimensions of about 1 μm. The images of the thymine and α-cyano-4-hydroxy-cinnamic acid samples, solids known to yield high charge state mass spectra, were very different. Both samples had surfaces with complicated morphology that included extensive structural features such as tips and edges with characteristic dimensions smaller than 100 nm.

To achieve charge separation in local, high electric fields in the SALDI sample surface, it is not sufficient that structural features are small. It is also required that a sharp edge or a fine tip of the solid is protruding out of the sample surface. We were not able to study frozen samples with the scanning electron microscope; however, it seems likely that such protrusions are formed on the surface of a frozen SALDI suspension as the aqueous phase between SALDI crystals is efficiently ablated by the IR laser. Charge separation would be achieved also on larger structures with characteristic radii of the order of 1 μm or larger, such as those seen in nicotinic acid. However, the calculated charge density on a protruding tip varies inversely with the radius of the tip. The significance of the sharper structural features in the solid is then that the charge density that can be maintained is large enough to support multiply charged protein ions.

In cryo-IR-SALDI, singly charged analyte ions are likely to be produced by the same process as multiply charged analyte ions. The reason is that if singly charged analyte (protein) ions were formed by a different process, one should find two intensity maxima in the protein

charge distributions, one for singly charged ions and one for multiply charged ions. Instead, a single maximum was always observed, see for example Figure 6

The only conditions that altered the protein charge distribution was the elimination of water from the sample by drying, or simultaneous exposure of the laser beam to the frozen analyte and the copper substrate surface. If the protein is dried in a ACHA saturated aqueous solution (as is done in conventional MALDI), lower charge states are observed. When ACHA is used as a cyro-solid in protein aqueous suspension, high charge states are observed if the laser is focused on the bulk of the sample. If the laser is focused on the interface of the copper substrate and the same frozen ACHA protein suspension, a shift to lower charge state ions is observed.

Following the discussion above, we propose that the formation of singly as well as multiply charged analyte ions in cryo-IR-SALDI involves charge separation, prior to desorption, in high, local electric fields on the points or edges of the organic crystals, followed by IR-induced desorption of the preformed ions. Sharp tips on the SALDI solid may be required for observation of high charge states. The presence of water also seems required for the preservation of high charge states. In Cryo-IR SALDI, water may shield electron protein recombination in the plume during desorption.

Following the discussion above, we propose that the formation of singly as well as multiply charged analyte ions in cryo-IR-SALDI involves charge separation, prior to desorption, in high, local electric fields on the points or edges of the organic crystals, followed by IR-induced desorption of the preformed ions. These desorption conditions are reminiscent of those in laser-enhanced field desorption. Buttrill et al. [44] reported pulsed

laser desorption experiments using the Nd:YAG laser fundamental at 1.06 μm and a time-of-flight mass spectrometer. However, mass spectra were obtained only of small ions [44].

As discussed in the Introduction, efforts to obtain ions of biomolecules from frozen water solutions (in the absence of solid surfaces) have largely been unsuccessful. If cryo-IR-SALDI analyte ions are preformed in the frozen solvent phase, as argued above, the question arises as to why the solid organic surfaces are required in order to observe them. The reason may be that the organic crystals are required to achieve charge separation, as discussed above. However, it may well be that ion desorption from bulk water ice is prevented also by very fast evaporative cooling or by the difficulty of depositing a sufficient energy density to achieve disintegration into mainly monomolecular species [45]. The presence of the organic crystals can have an effect on either of these potential problems.

Conclusions

This work demonstrates a technique that reliably produces laser desorption mass spectra of proteins and peptides from frozen aqueous solutions using an IR laser. Desorption/ionization from the aqueous phase is made possible by the presence of organic crystals, added prior to freezing the solution. The analytical figures of merit for the new technique, referred to as cryo-IR-SALDI, are promising: A uniform sample preparation method can be used, and the upper mass limit is high; ions with masses beyond 10^5 Da were observed in this work. Mass spectra have been obtained with a sample consumption of about 1femtomole of peptide or 10 fmole of protein. Compared with UV-MALDI on the same instrument, the mass

resolution for peptides was lower, and the mass resolution for proteins slightly higher. Significant future improvements to cryo-IR-SALDI seem possible. Higher mass resolution should be obtained on time-of-flight mass spectrometers with a more modern design, for example incorporating reflectrons and delayed ion extraction [46,47] and by solving the problem of surface charging in frozen samples. Improved mass resolution should also further increase sensitivity. Future investigations to more fully characterize matrix effects, such as the sensitivity towards electrolytes and detergents, and to determine typical minimum amounts of "real-world" samples will better define the analytical utility of cryo-IR-SALDI.

Cryo-IR-SALDI points to novel approaches in laser desorption ionization. There is extensive contact between the organic crystal surfaces and protein analytes in the suspensions used in the present work. This will tend to denature proteins and make it impossible the detect intact sub-unit proteins and non-covalent complexes. However, it may well be possible to "engineer" the cryo-IR-SALDI surfaces in order to optimize the desorption/ionization process. One can envisage, for example, maneuverable probes that have tips with such "designed" SALDI surfaces. Such probes would allow for the aqueous solution, before and after freezing, to be physically separated from the SALDI surfaces until the point of desorption. The chances of being able to reliably detect non-covalent complexes of biomolecules, that pre-exist in solution, would thus be maximized. Such probes would also allow for the interaction between the SALDI surfaces and the frozen aqueous phase to be spatially controlled. This, in turn, might allow for new types of ion microscopy, as well as in-situ detection of biomolecules in tissues.

CHAPTER 2

REVIEW OF THE LITERATURE AND METHODS USED TO STUDY RHODOPSIN/TRANSDUCIN INTERACTIONS

Description of Signal Transduction in a Rod Outer Segment Cell

Figure 7 shows a pictorial schematic of the visual signal transduction cascade. Absorption of a photon and isomerization of rhodopsin's chromophore retinal, intitiates the first amplification step of the light signal ---- rhodopsin/transducin binding. Each excited rhodopsin catalyzes activation of 600 transducin molecules/second at 22 degrees celcius (49) by catalyzing GDP release from the alpha subunit of transducin. The nucleotide free transducin then binds the much more cellularly abundant GTP. The transducin alpha subunit (Gt alpha) with GTP bound dissociates from the two other transducin subunits (beta and gamma), and goes on to activate a 3',5'-cyclic-GMP phosphodiesterase, which each catalyze the formation of several thousand 5'GMP/second from cyclic GMP. The decrease of cyclic GMP concentration which leads to the closure of Na^{+}/Ca^{+2} channels in the outer plasma membrane of the retinal roud outer segment, hyperpolarizes the rod cell membrane. The several stages of amplification leads to exclusion of ~10^{7} Na^{+} ions/photon, and is the reason one photon can produce a physiologically measurable change in cellular current.

The rhodopsin-transducin coupling is an archetype for the large superfamily of GPCR-G protein systems in biology. Understanding the mechanisms of rhodopsin-

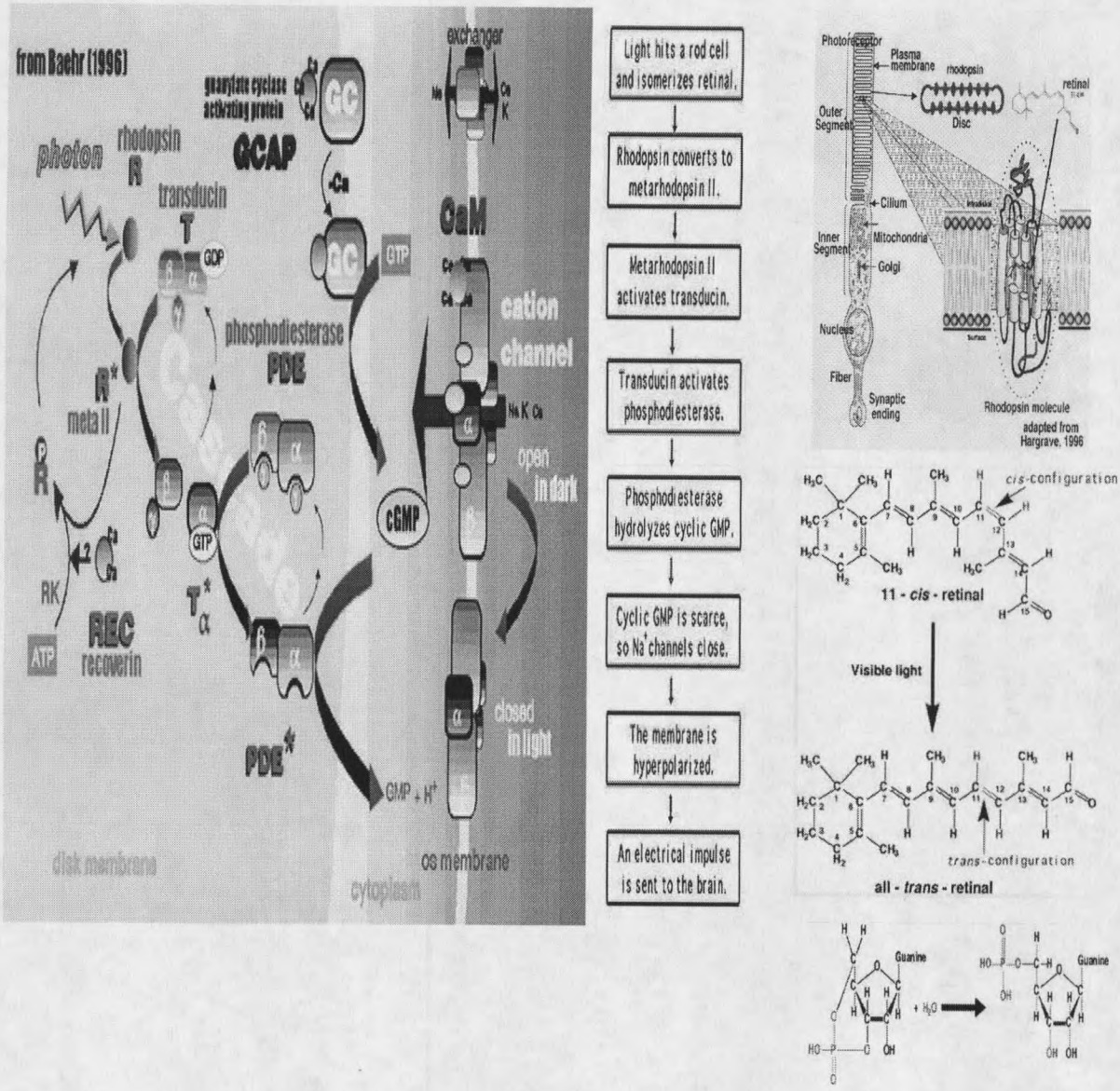


Figure 7. The light stimulated signal transduction cascade. Also shown are depictions of the location of rhodopsin in the rod cell, the cis to trans isomerization of retinal, and the hydrolysis of cyclic GMP.

transducin coupling is expected to also be valuable for understanding the coupling mechanism in a vast number of homologous systems.

Relationship of Rhodopsin/Transducin System to other GPCR/G protein Systems

Rhodopsin dark structure and homology to other GPCRs

Homology predictions of the rhodopsin transducin interface concur with many of the mutagenesis studies. Figure 8 shows the evolutionary relationships of GPCR's based on sequence homology (50). Rhodopsin is a member of the Class A Rhodopsin like, family of seven transmembrane G protein coupled receptors (GPCR's). It shares approximately 30% sequence homology with other members of it's class. Figure 9, from Strathmann et al (51), shows the evolutionary relationship of G protein sequences. Transducin,the G protein (Gt) that binds to light excited rhodopsin binds, is most homologous (68%) to the Gi proteins which inhibit adenyl cyclase. A snake diagram of rhodopsin in Figure 10A highlights mutational analyses of functional importance to rhodopsin activation of transducin. Recently, the crystal structure of dark-adapted rhodopsin has been solved to 2.8 angstrom resolution, and Figure 10B shows a backbone trace of the approximate dark adapted transmembrane disposition (52). Proteins with greater than 30% sequence homology typically have structures within 1 Angstrom RMSD (53). While both the dark structure of rhodopsin and the structure of Gt is known, neither the light adapted rhodopsin structure, nor the rhodopsing/Gt complex

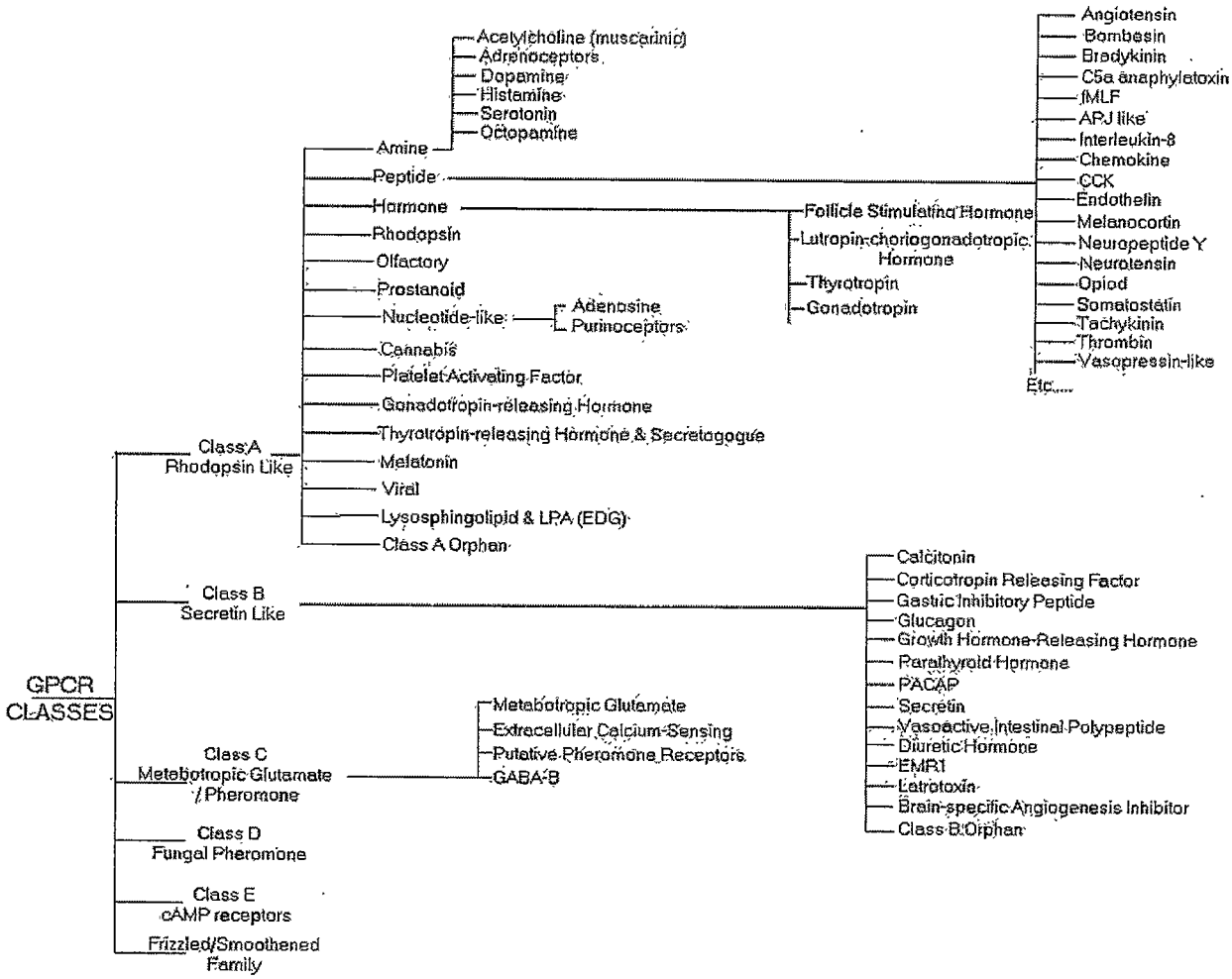


Figure 8. GPCR Evolution Tree

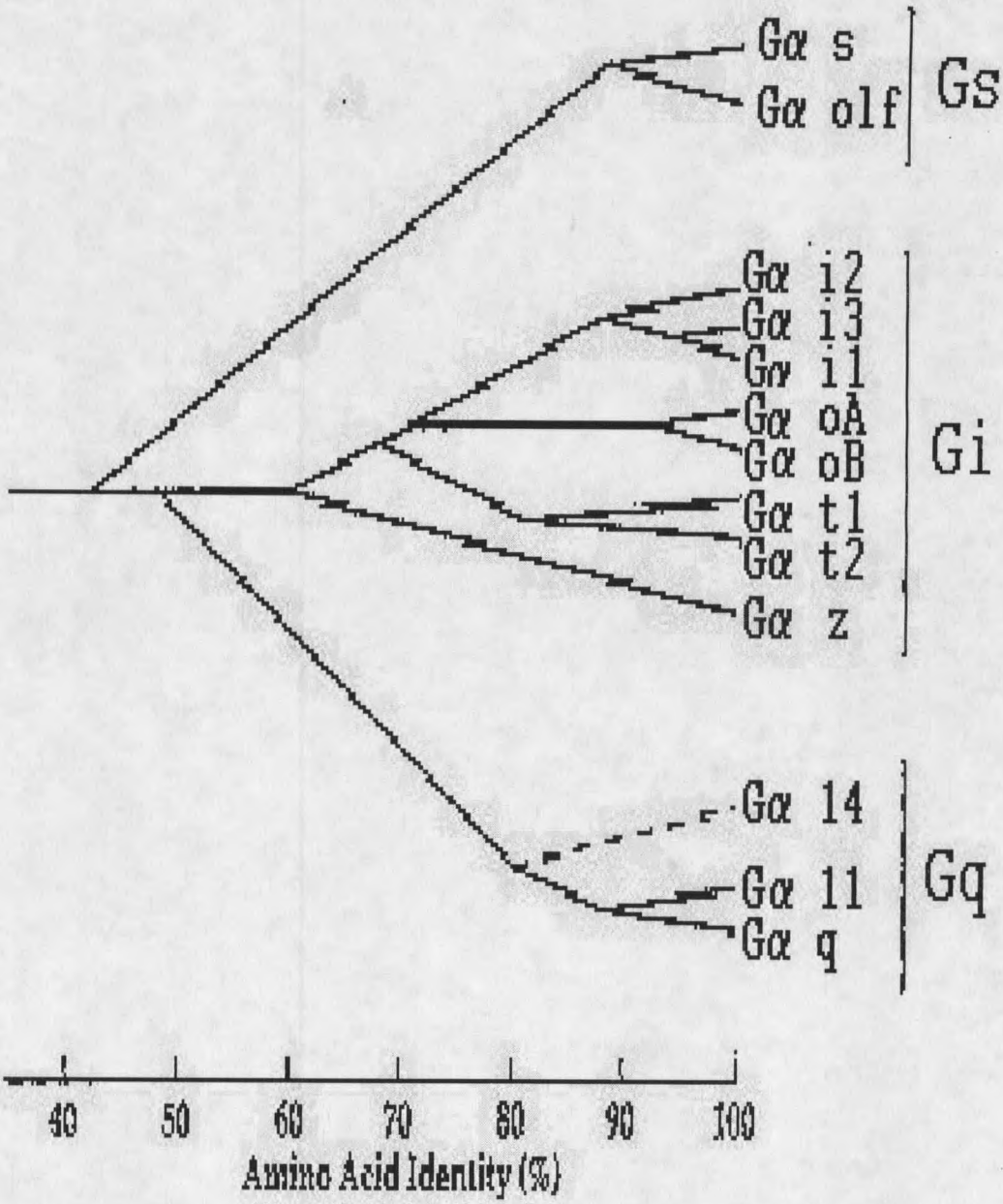


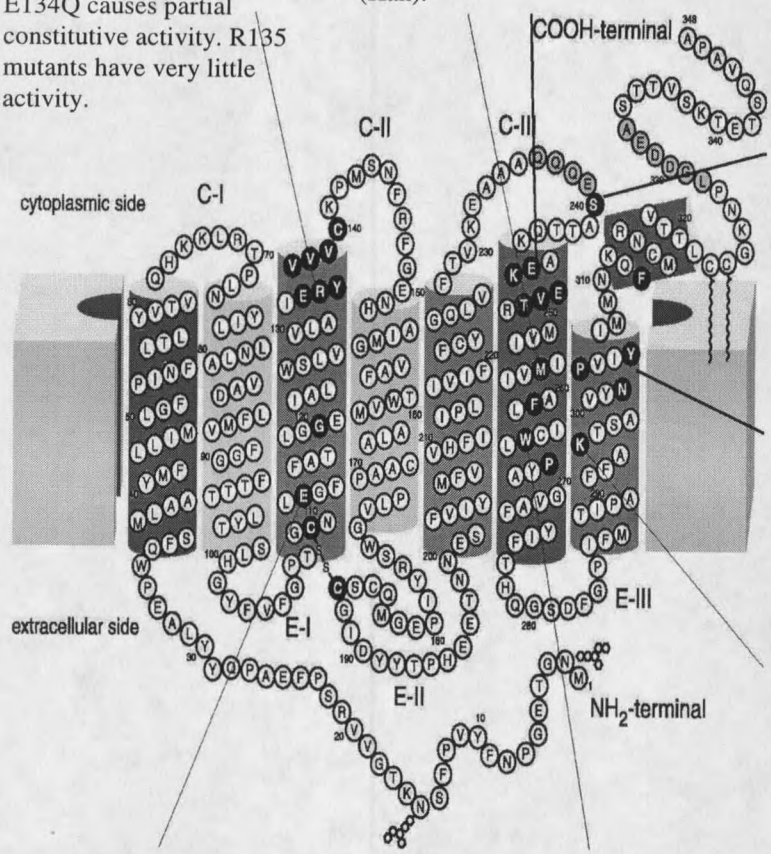
Figure 9. Relationships among mammalian G protein alpha subunits.

ERY is highly conserved in rhodopsin family. Evidence presented that YVVV interacts with EKEVT of H-VI (Acharya). V138, E134, C140 are critical for full activation (Yamashita). E134Q causes partial constitutive activity. R135 mutants have very little activity.

M257Y opsin has 33% of WT rhodopsin activity (Han).

A spin label attached to V250C indicates Environment change upon Meta II formation (Dunham)

S240C + photo probe cross-Links to Gt alpha (Resek). Swapping C-III loop of Go Switches specificity (Yamashita)



NPXXY is highly conserved In all GPCR's. H-VIII above Was previously thought to be C-IV. N310S reduces activity to 39% of wild type (Marin).

K296 site of retinal Schiff's base attachment

G121 is the steric trigger of the 9-methyl of retinal. E113 is thought to be the counter ion to K296. E113Q opsin has 23% of WTrhodopsin activity (Han).

Beta-ione ring of photo-activatable retinal cross-links to W265 in dark state (Nakayama, Zhang, Borhan)

Figure 10A Snake diagram of rhodopsin (4). Grey scale residues were not located in the crystal structure.

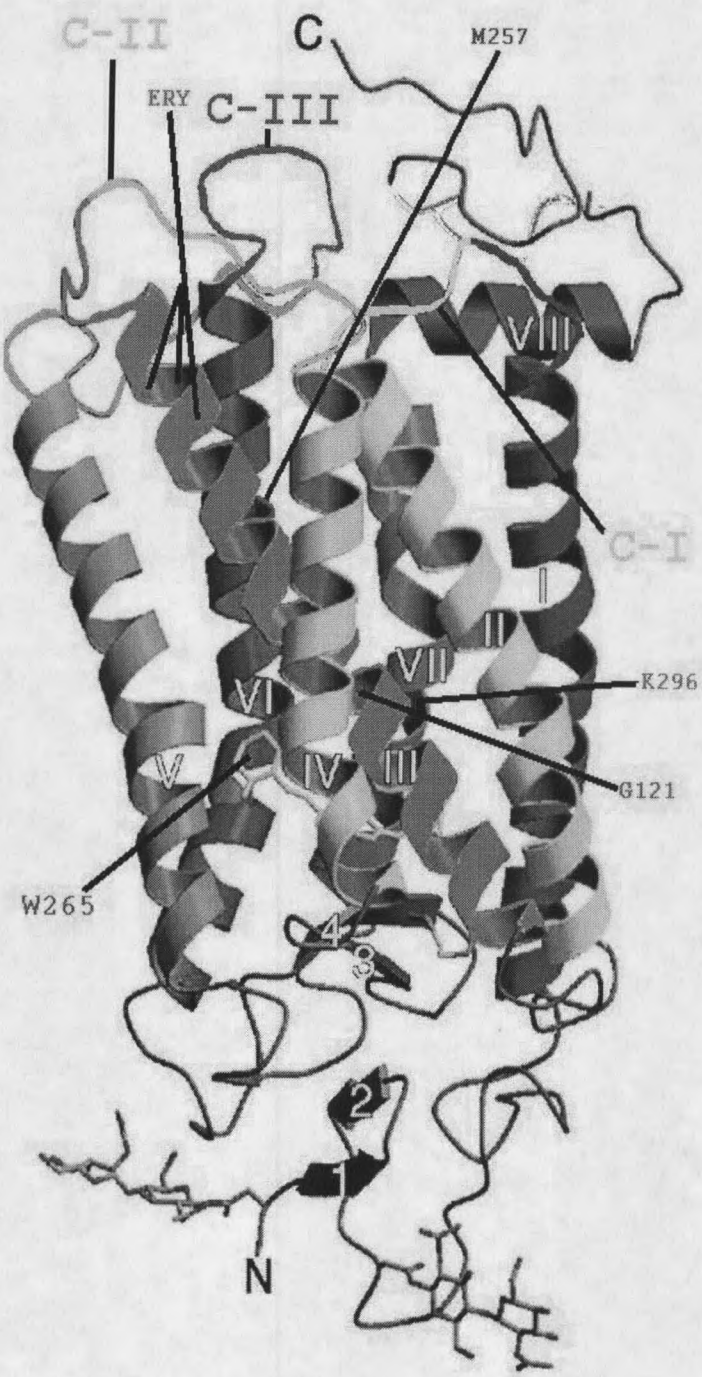


Figure 10B. Ribbon model of the crystal structure of dark-adapted rhodopsin.

has been solved. Using cDNA derived protein sequences of many GPCRs' and G proteins, Oliveria et al (54), Lithtarge et al (55), and Horn et al (56) attempted to define the residues that correlated with functional variation. Oliveira et al emphasized the importance of the conserved DRY motif (which is ERY in rhodopsin) near the cytoplasmic side of H-III in G protein binding. The authors proposed an "arginine switch" in which agonist binding favors movement of the arginine, conserved in H-III of all Class A rhodopsin like GPCRs, moves from a polar pocket in the transmembrane region to the cytosol to favor coupling to the G protein. Horn et al compared several GPCR sub-families within the Rhodopsin like, A Class. By looking at particular highly homologous families that all bound the same ligand, but bound different G proteins, they sought to see which amino acid residues that correlated with G protein selectivity. For example, Figure 11 (from Horn et al (56)) shows that Muscarinic m1, m3, and m5 receptors couple to Gq subtype, whereas, m2 and m4 couple to Gi/o. 24 positions correlated 100% with G protein coupling in muscarinic receptors. 18 are located in or close to the intracellular loops, mostly in the N- and C-terminal parts of the long third loop. 6 positions were considered false positives because they are located far from the intracellular compartment. Ten were confirmed by experimental data, 8 are putative candidates that have not yet been validated by mutational studies. Similar analyses were performed with the other Class A rhodopsin GPCR families, but with much less convincing results perhaps because there were fewer sequences to compare.

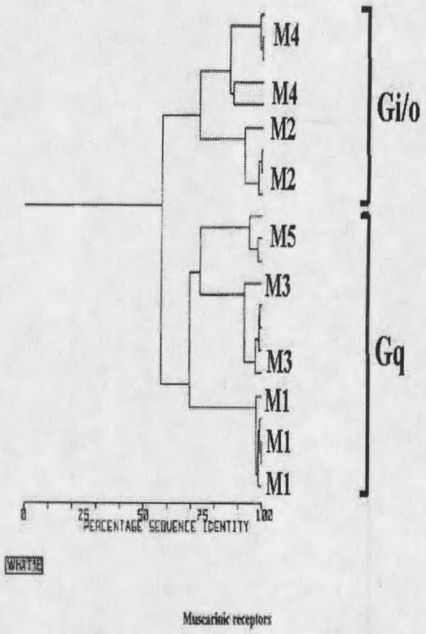
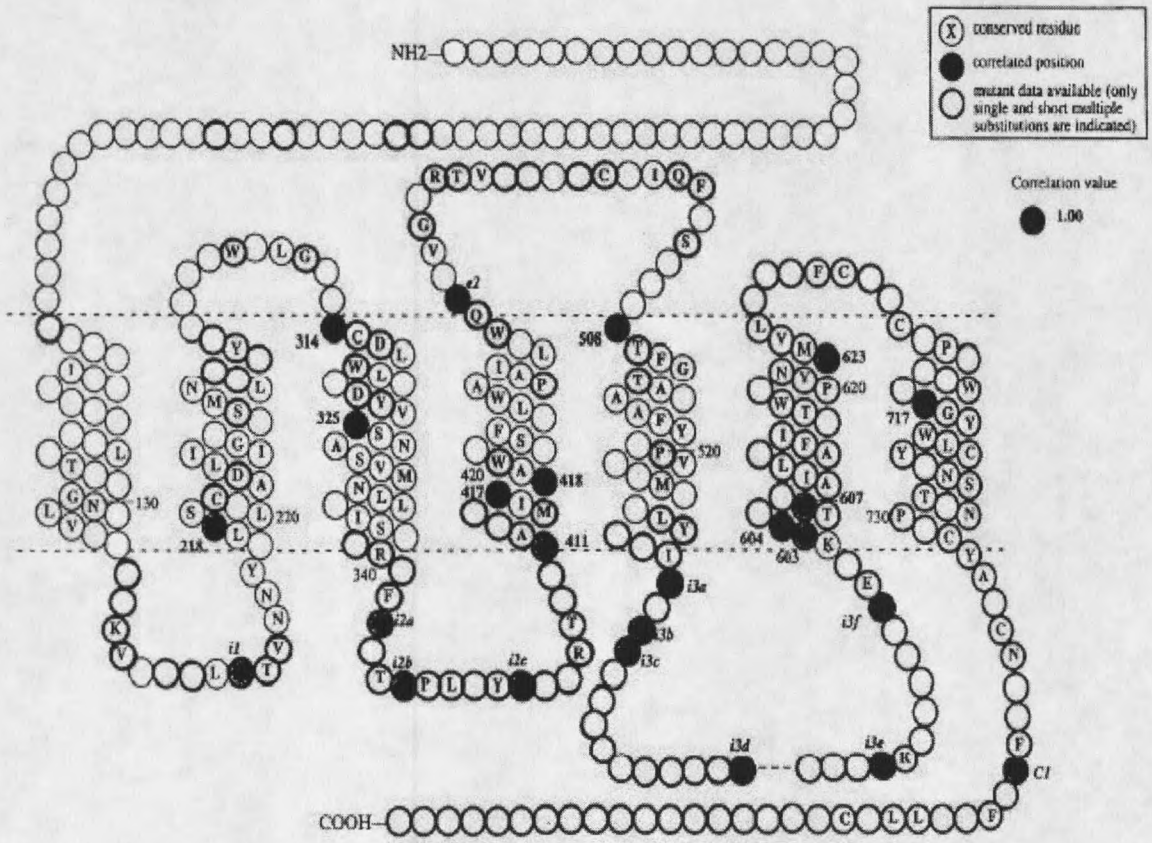


Figure 11. Muscarinic receptors M4 & M2Couple to Gi/o, and M5, M3, & M1 couple to Gq. Snake diagram below indicates the 24 positions near the cytoplasmic side (bottom side) that Horn et al [Proteins 2000] correlated with G protein selectivity.



Transducin structure and homology to other G proteins

Figure 12 shows the sequence of the alpha subunit of transducin with structural and mutational points of interest. Figure 13A shows a backbone trace of transducin with its beta-gamma subunits in back, and the alpha subunit in front. Figure 13B shows and expanded view of the alpha subunit. As highlighted in Figure 13B, the alpha subunit is composed of an alpha helical domain, and a GTPase domain, and the nucleotide issandwiched between them in the interdomain cleft. Mutational studies have focused on the alpha subunit, since it is the site of nucleotide binding, although nucleotide exchange on the alpha subunit will not occur unless it is bound to the beta-gamma subunits (57-61). Lichtarge et al (55) used what they call Evolutionary Trace Analysis of 112 G alpha, 20 G beta, and 16 G gamma sequences to identify functional sequence variations in G proteins. They identified two surface clusters, A1 and A2 in the alpha subunit, that they attributed to sites of interaction with the receptor and effector. Cluster A1 consists of 17 residues stretching form the membrane face to the interdomain cleft. They include regions of the distal two thirds of helix alpha 5, the sixth beta-strand, the alpha 4/beta 6 loop, the N-terminal ends of beta 4, and beta 5, and the C-terminal tail. 9 of the 17 residues are GPCR class specific. The A1 cluster is thought to be the probable contact region for the GPCR. Cluster A2 of G alpha, comprising 32 residues (14 of which are class specific) interacts with G beta/gamma and probably with effectors as well. This prediction is confirmed by the published G protein holoenzyme structure. The interface of alpha to beta-gamma , defined as the set of residues in G alpha that lie within 4 angstroms of G beta-gamma comprise 16 of the 32 residues in cluster A2.

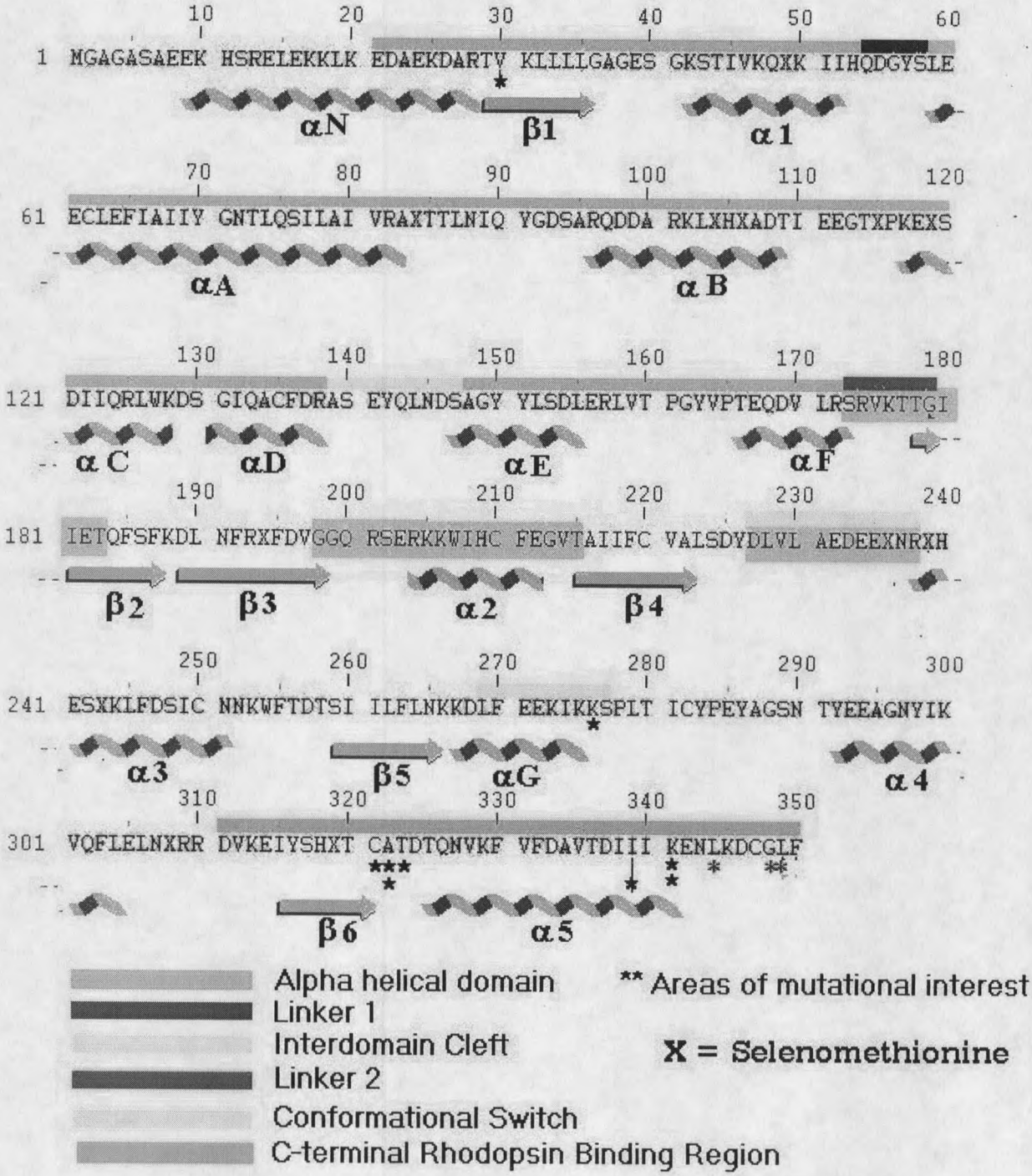


Figure 12. Sequence of the alpha subunit Gi chimera of transducin.

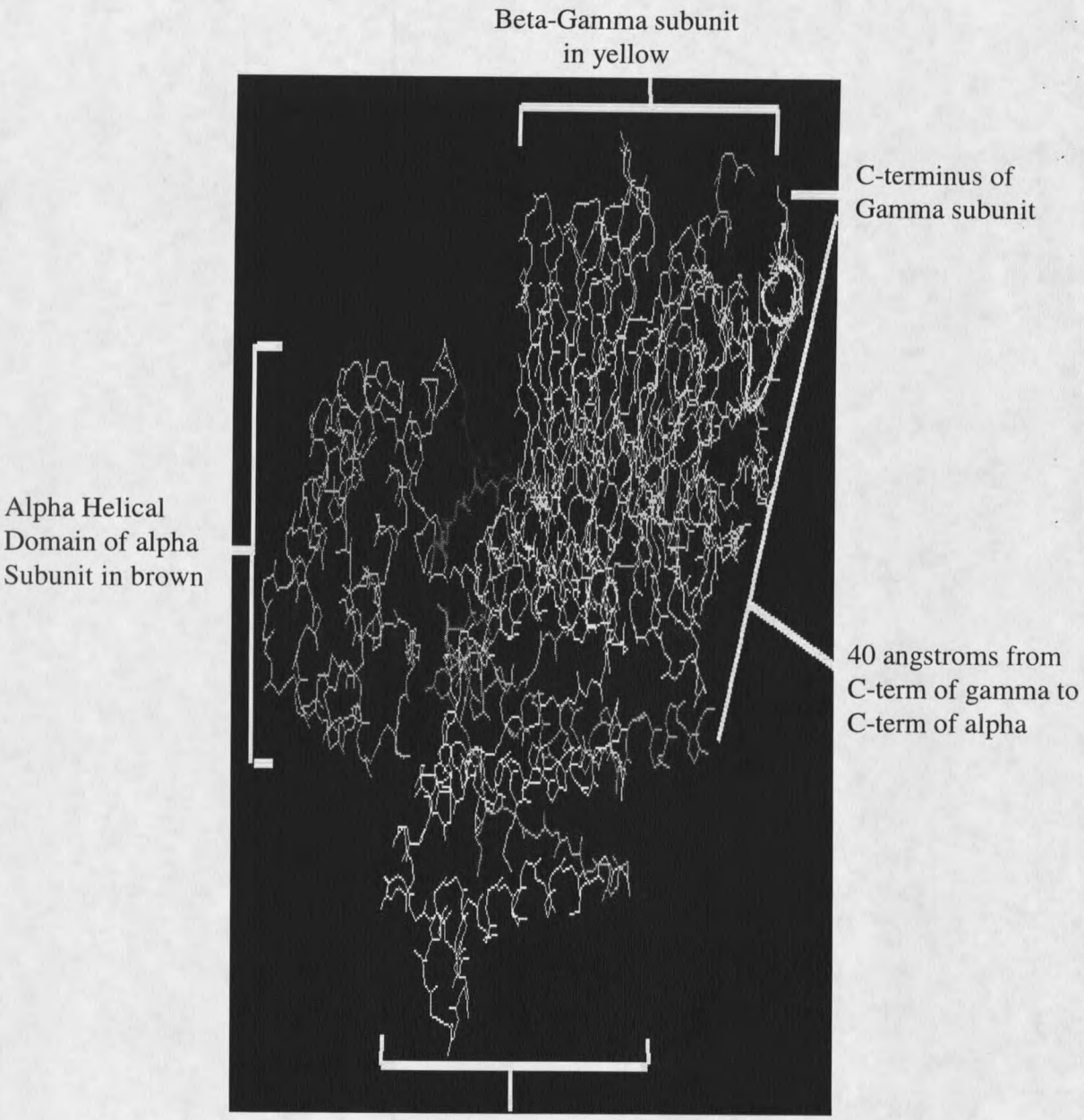
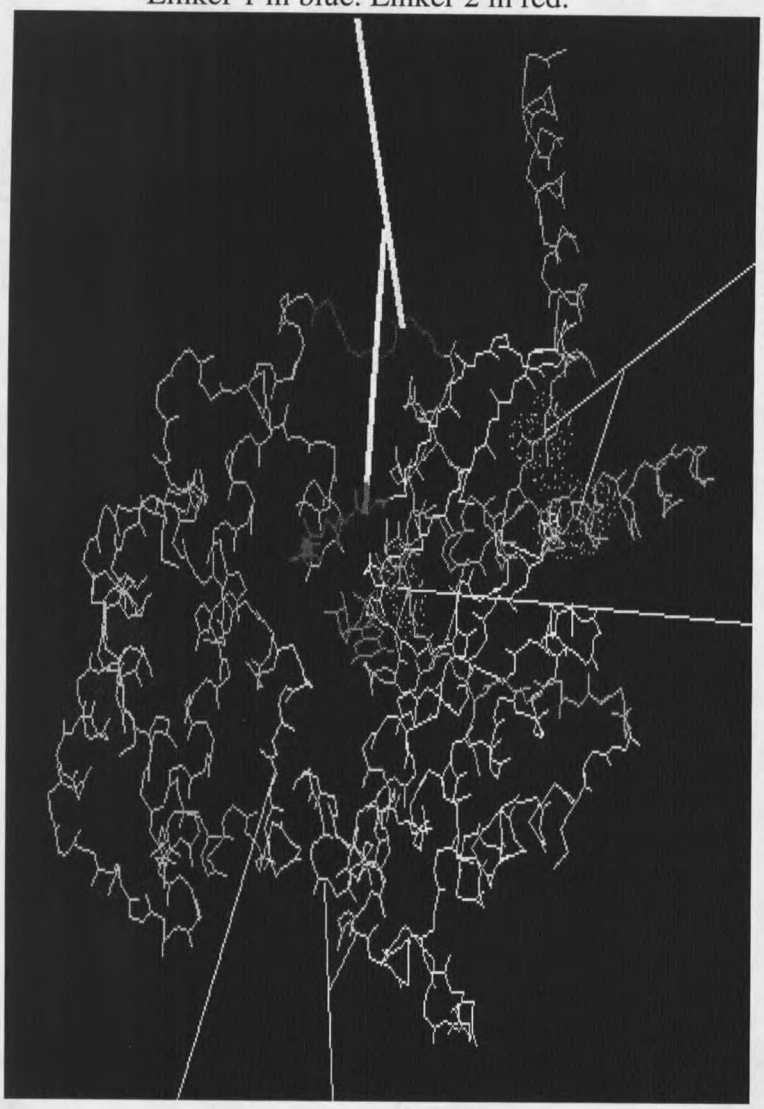


Figure 13A. Backbone trace of heterotrimeric transducin Gi chimera that was crystallized by Lambright et al [Nature 1996].

Linker 1 in blue. Linker 2 in red.



Mutations of V30 of N-term and I339 of C-term increase basal nucleotide exchange rate [Muradov].

Residues 311-350 in green are part of GTPase domain . C321, A322, and T323 contact the guanine ring (in pink). The white line points to A322, which is analogous to A326 of Gi1. The A326S mutant of Gi1 has a 250X increase in basal GDP nucleotide dissociation rate [Posner]. Peptides Ac311-329NH2 and Ac340-350 stabilize Metarhodopsin II [Hamm] and block rhodopsin catalyzed nucleotide exchange [Kraft, Chapter 3].

Residues 139-147 of interdomain cleft of helical domain in yellow

Residues 227-238 and 269-277 of interdomain cleft of GTPase domain in yellow. K276E mutant has 10X increase in basal nucleotide exchange rate (Marin).

Figure 13B. Expanded view of transducin Gi chimeric alpha subunit.

Methods to Study Signal Transduction

The ability to obtain an X-ray or NMR structure depends for the most part on obtaining significantly large milligram quantities of very pure folded protein from its native tissue, or recombinantly from bacteria or insect cells. For structures of mutant proteins, to study correlations between sequence variations and function, this requires recombinant expression. Wild type transducin has proven impossible to express recombinantly in bacteria, whereas the 68% homologous Gi1 alpha is readily expressed in great quantities as a soluble folded protein. Skiba et al (62) used this as a strategy to get recombinant transducin to fold by systematic replacement of transducin regions, which inhibit proper folding, with Gi1 alpha , which are permissive for folding. Doing this were able to express large quantities of a Gt/Gi chimera that retained the functional characteristics of transducin ---- low basal guanine nucleotide exchange, and a high amplification (780X) in nuceotide exchange in the presence of light adapted rhodopsin. The structure depicted in Figures 6, and 7A & B is of this transducin chimera. Gt alpha residues 344-350 and Gt gamma residues 66-71 do not appear in the crystal structure, but were added to yield a more complete model. Crystal structures of wild type transducin alpha (purified from its natural abundant source in bovine retinas) with GTP-gamma-S, GDP, GDP and Mg++, GDP and AlF have also been solved, but a nucleotide free G alpha structure has yet to be reported.

The dark adapted structure of rhodopsin has only very recently been solved, ---- despite a large quantities of pure source of rhodopsin obtainable from bovine retinae. The

light adapted structure has not been solved presumable because of the difficulty in obtaining a single conformation of the light state. Expression of rhodopsin recombinantly has so far only produced quantities too small to make crystallization studies feasible. Rhodopsin mutants are usually expressed in COS cells where they are usually correctly folded, but are not expressed in high purity of in high quantities necessary for obtaining good crystals. Mutational studies of rhodopsin can be difficult to interpret because most of them have been designed without the aid of any GPCR crystal structures. Without crystal structures of the mutants, or at least of the wild type light adapted rhodopsin, an observer does not know if the mutation is "making or reporting the news". The dark adapted rhodopsin crystal structure is bound to lead to more focused design of mutational experiments. Despite the inability to obtain structures of mutants, mutational analysis has played a critical role in deriving the mechanisms of GPCR and G protein activation.

Biochemical and spectroscopic methods used on wild type protein or on mutants has provided the bulk of our present knowledge of the interactions responsible for the coupling of rhodopsin to transducin. These efforts can be categorized into four strategies. 1) Spectroscopic assessment of GPCR activation of the G protein using UV/VIS, light scattering, fluorescence, FTIR, and radioligand detection of binding. 2) Mutagenesis of select amino acid residues in the GPCR, and/or the G protein to determine their effect on G protein activation. 3) Chemical modification and/or cross-linking of the GPCR and/or G protein. 4) The use of peptides as probes of GPCR and G Protein function. Peptides derived from the G protein or GPCR can affect GPCR ligand binding, and GPCR catalysis of G protein radionucleotide binding, and therefore they also affect proteins

downstream of G protein activation. Examples of the strategies one and four are described in Figures 14 & 15 respectively.

Spectral Characteristics of the Rhodopsin/Transducin System

Rhodopsin makes up 90% of the protein content of washed rod outer segment membranes (63). Multiple conformational states of rhodopsin were first characterized spectroscopically by changes in the visible/UV absorption spectrum (reviewed by (64; 65)) resulting from chemical tuning of the environment of its chromophore in the protein (11-cis retinal in the dark state absorbance max at 498nm, Ext Coef = 42,000 M-1cm-1). Retinal is formed from a vitamin A by oxidation of the alcohol to an aldehyde that attaches to lysine 296 in rhodopsin via a Schiffs' base linkage. The purity of dark adapted rhodopsin is often assessed as the 280nm /496nm absorbance ratio. Protein impurities contribute to the 280 absorbance, but not the 498nm absorbance. Washed membranes typically have a ratio of 2 – 2.5, while the purest preparations have a ratio of about 1.6-1.65 (63). Productive rhodopsin/transducin interaction was first characterized (as depicted in Figure 14) by the radionucleotide ([^{3}H]GDP and [^{32}P]GTP) binding studies of ROS membranes by Godchaux & Zimmerman(66), and Fung & Stryer (67). Emies et al (68) confirmed the transducin binding by rhodopsin using a visible spectrum "extra Meta II" assay (as depicted in Figure 15. The Meta I state (Abs max 478) is in equilibrium with the Meta II state (Abs max 380nm).Binding of transducin

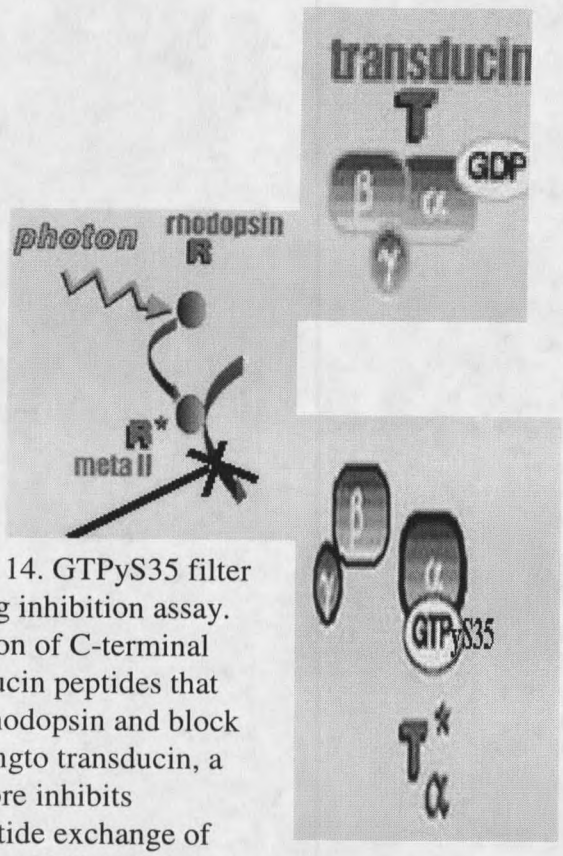
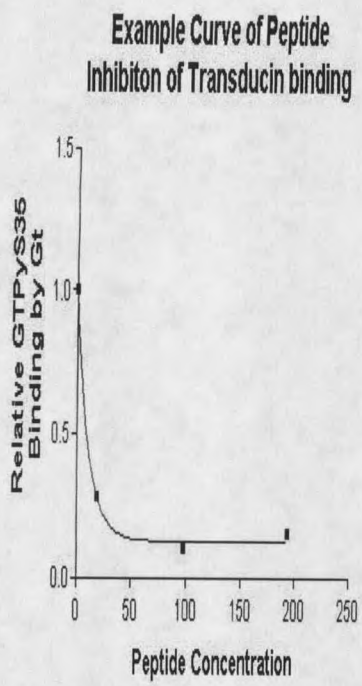
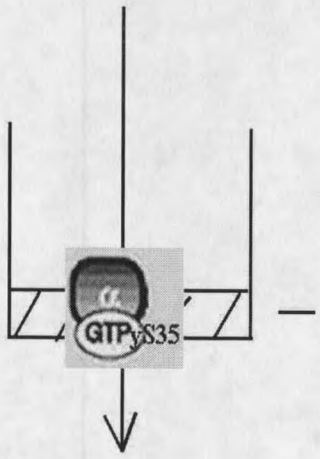


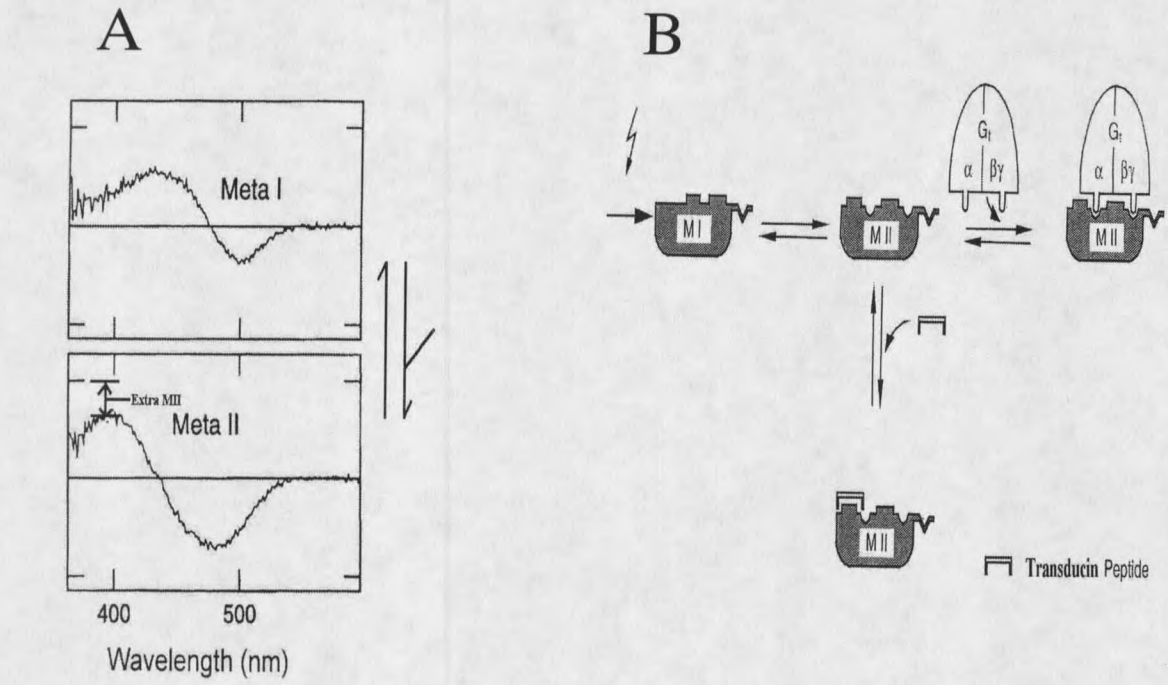
Figure 14. GTPyS35 filter binding inhibition assay. Addition of C-terminal transducin peptides that bind rhodopsin and block couplingto transducin, a therefore inhibits nucleotide exchange of GDP for GTPyS35 (non-hydrolyzable GTP analog) on transducin.

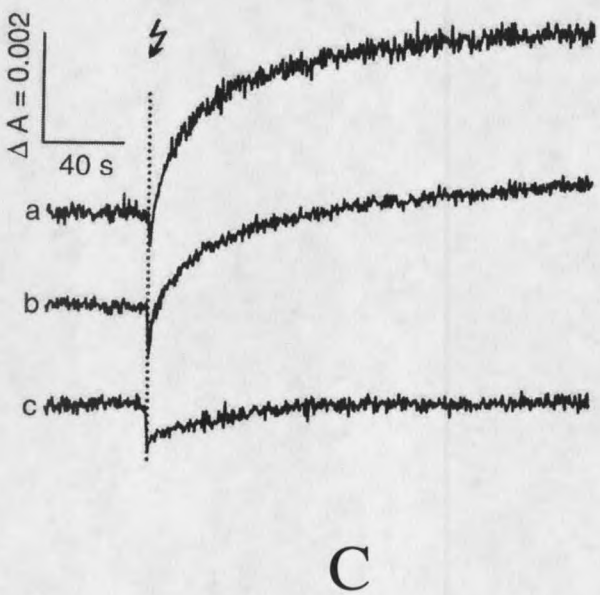


Solutions with and without various concentrations of competing peptides are all incubated with GTP-gamma-S35. After the incubation, solutions are suction filtered onto nitrocellulose filters, and washed with cold buffer to remove GTP-gamma-S35 not bound to transducin.Transducin with GTP-gamma-S35 bound sticks to the filter. Filters are dissolved in scintillation fluid and counted for radioactivity. As seen above, a plot of radioactivity vs peptide concentration yields an IC50 for the rhodopsin transducin interaction.

Filter Binding







C

Figure 15. Extra Meta II assay. A shift in the equilibrium between Meta I (478nm) and Meta II (380nm) absorbance is observed upon addition of transducin or transducin alpha C-terminal peptides. The extra absorbance at 380nm is directly proportional to the amount of transducin or peptide added. A) Static difference spectrum of Meta I and dark rhodopsin (top); Meta II and Meta I (bottom). B) Pictorial representation of Meta I to Meta II equilibrium. C) The "Extra Meta II Assay" is typically a time resolved difference spectrum. The signals are measured after a ~10% bleach flash, and represent the absorbance change at 380 nm minus the absorbance change at 417 nm, as a function of increasing transducin or peptide. The abrupt decrease after the flash is due to the rapid formation of Meta II precursors.

to Meta II causes a shift of the Meta I / Meta II equilibrium detected by an increased absorbance of the Meta II state. Later reports also indicated that the Metarhodopsin II is the conformation that binds tranducin and catalyzes nucleotide exchange (69). This binding event was also characterized by increases in light scattering of ROS membranes upon transducin binding (70; 71). Rhodopsin catalysis of nucleotide exchange, can also be characterized by increases in transducin tryptophan 207 fluorescence upon GTP binding (72; 73). Numerous studies have characterized the temperature, pH, ionic strength, and nucleotide dependence of these interactions (69; 73-79). Transducin and all G proteins have alpha, beta, and gamma subunits, of which the alpha is the most diverse. The alpha subunit releases GDP upon binding an activated GPCR, and then binds the GTP which is much more abundant in the cytosol.

Constitutive Activity of Rhodopsin and Transducin

A spontaneous exchange of GDP for GTP on the G alpha subunit takes place at very low levels the activated GPCR is not present, and the rapid exchange also requires G beta-gamma subuits. There are several classes of GPCRs based on sequence homology, with rhodopsin belonging to Class A which is the largest GPCR class. Rhodopsin and transducin are unique among the Class A GPCRs, in that both have a very low spontaneous or constitutive activity. In addition, opsin (rhodopsin without the chromophore retinal), can only activate transducin at very low levels. The low basal activity of wild type rhodopsin is an evolutionary adaptation of GPCRs unique to visual

receptors. Other GPCR's are 20-30% constitutively active (80) (the GPCR will catalyze nucleotide exchange without ligand binding).

Likewise G proteins other than transducin have a lower affinity for guanine nucleotides, and thus have a higher *basal* nucleotide exchange activity in the cytoplasm where GDP concentrations are much lower than GTP concentrations. The release of GDP is usually the rate limiting step in nucleotide exhange (76; 77). Light adapted rhodopsin catalyzes a 780 fold increase over *basal* transducin GTP binding. If ROS are urea stripped of their transducin and reconstituted with recombinant Gi, rhodopsin catalyzes only a 2-5 fold increase over *basal* Gi GTP-gamma35S binding. The initial rates of catalysis are 1304 umole/mole/s, (K_{app} 0.095/min) for rhodopsin/Gi1, and 3798 umole/mole/s for rhodopsin/transducin (K_{app} = 0.3/min) (62).

Role of Retinal in maintaining low basal rhodopsin activity

Reconstitution of opsin and 11-cis retinal in the dark leads to regeneration of the dark state of rhodopsin with equally low basal activity compared to the starting material, and has an absorbance max at 496nm. Maintenance of very low basal activity in dark rhodopsin is thought to be due to binding of 11-cis retinal (81) and also in part from a salt bridge between the Schiff's base K296 of helix seven (H-VII) and it's counterion E113 of helix three (H-III) (82; 83). As seen in Figure 16, photon absorption the 11-cis retinal isomerizes to trans retinal, and rhodopsis progresses in short intermediate steps from lumirhodopsin to the first long lived state, Metarhodopsin I (Meta I, absorbance max 478nm). E113 is then thought to accept a proton from the Schiffs' base linked K296

breaking the salt bridge, and shifting the retinal absorbance maximum from 478nm to 380nm . Deprotonation of the Schiffs' base and protonation of it's counterion E113, and the resulting blue shift occur during the transition from the Meta I to Meta II conformation. Mutating K296 or its counter ion E113 to a neutral residue leads to constitutive transducin activition (E113Q opsin has 23% of light activated wild type rhodopsin activity) (84)) (83; 85; 86; 86; 87).

Role of rhodopsin residues in maintaining low basal rhodopsin and transducin activity

Figure 10A summarizes the more important mutants described in this chapter. Examining mutants that cause opsin or dark adapted rhodopsin to activate transducin can lead to insight into identifying the dark state amino acid residues that maintain rhodopsin's very low basal activity, which are not directly involved in activation. All of rhodopsin's three cytoplasmic loops (C-I through C-III), and parts of their corresponding helixes have been implicated as interacting with transducin. Parts of loops C-I, C-II, C-III, and all of what was thought to be C-IV were found to be helical in the new dark structure of rhodopsin (52) and for practical considerations, this discussion will refer to mutation site positions relative to the new dark structure, even though these sites may be altered in the light conformation.

Han et al (84) reported mutations of E113Q, E134Q, M257X (X = any amino acid except L or R), F261V cause constitutive activities in opsin of 23, 3, 32 (M257Y),

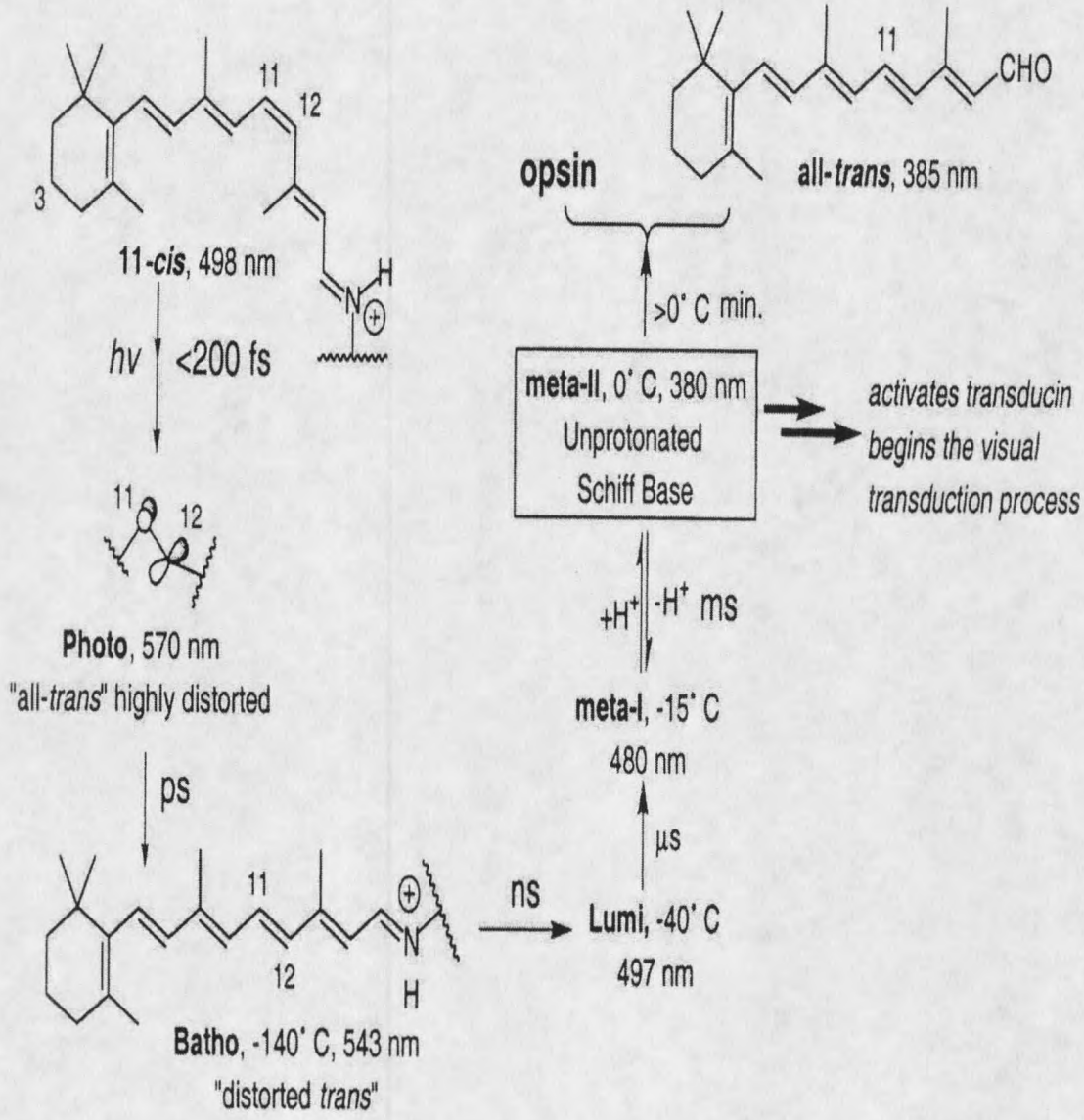


Figure 16. Spectroscopically detected intermediates in the photoisomerization of Rh. Initially, the 11-cis double bond is isomerized to a highly distorted trans intermediate (photo-Rh, cannot be isolated). Batho-Rh, a distorted 11-trans conformer, can be trapped at –140C, which upon warming to –40C yields lumi-Rh. A blue shifted intermediate (BSI) is in thermal equilibrium with the lumi-Rh intermediate but is not observed under cryogenic conditions; however, it can be observed with flash photolysis at ambient temperature. Meta-I-Rh, sequested at –15C, is in equilibrium with Meta-II-Rh at OC. Therefore, it is possible to trap each intermediate at specific temperatures and study the oreintation and movement of the chromophore with respect to the protein (199).

and 7.6 % of light activated wild type rhodopsin. Double mutant opsins, E113Q/M257A, E113Q/M257N, and E113Q/M257Y had 68, 74, and 81 % activity compared to wild type light activated rhodopsin.

Upon reconstitution with 11-cis retinal, all of the mutants' activity decreased to much lower levels, therefore, binding of 11-cis retinal can be an inverse agonist. Upon light activation of the mutants reconstituted with 11-cis retinal, the mutants M257A, M257C, M257F, M257I, M257K, M257L, M257Q, M257T, M257Y , E113Q, and E134Q had full activity compared to wild type.

All of the mutants (except M257L) had an increased ability to bind all trans retinal (ATR), reflecting the mutant opsins' conformational bias toward the active state. M257A, M257N, M257S, M257Y, and E113Q mutants in particular, had ~100% activity when reconstituted with ATR. When wild type opsin was reconstituted with ATR it had 14% of the activity of wild type opsin reconstituted with 11-cis retinal. This may reflect the reduced ability of wild type opsin to bind ATR.

The Meta I to Meta II transition is also accompanied by the uptake of a proton from solution by (74; 88; 89), although the function of proton uptake is not entirely clear. Many of the E134 rhodopsin mutants (in a conserved DRY of all GPCR's) of H-III are active in the dark state (84; 90; 91). Acharya et al reported the E134Q mutant to have a much higher opsin activity (46%), compared to Han et al's mutant E134Q opsin (3%). Han et al did report that the E134Q mutant had an increased ability to bind all trans retinal, with the ATR mutant having 51% of wild type activation. The E134Q mutant did not, however, have a decreased ability to bind 11-cis retinal as evidenced by its full light

activation compared to wild type. The E134D mutant has an ~50% decrease in transducin activation, and this decrease was independent of pH (92; 93). Acharya et al reported that while E134 to Q, I, and S increased the activity of opsin to about 50% of light activate wild type, they had little effect on the absolute rhodopsin light-activated rate, ***and moreover,*** E134 to L or F had no effect on opsin, dark or light activated rates of nucleotide catalysis.

Role of transducin residues in maintaining its low basal activity

Figures 12 and 13A & 13B summarize the more important transducin mutations discussed in this chapter. As mentioned before, transducin has a higher affinity for nucleotides than the 68% homologous Gi. Some mutatations have been shown to increase basal transducin activity. Muradov & Artemyev (94) reported that coupling between the transducin alpha subunit's N- and C-terminal domains is thought to be partly responsible for transducins low intrinsic GDP/GTP exchange in unstimulated transducin. They demonstrated that mutational interruption of the interaction between V30 and I339 could cause increased basal nucleotide exchange.

Posner et al (95) reported the A326S mutant of Gi1 alpha (analogous to A322 in the CAT of Gt alpha) to have an ~250 fold increased dissociation rate of GDP, while having little effect on the affinity for GTP-gamma-S, or the intrinsic GTPase activity. The protein crystal structure was nearly identical to the wild type, with the mutant having a slightly less occupied GDP binding site. The authors argue that this mutant is an approximation of the receptor activated state of Gi alpha. Mutations of C325S of Go

alpha, and A366S of Gs alpha have similar effects (96; 97). The location of the analogous Gt alpha residue is marked in Figure 13B. Peptides from this region can bind and stabilize the Meta II state of rhodopsin (98), and the peptide N-acetyl-311-329-amide is able to block rhodopsin catalyzed nucleotide exchange with an IC50 of 400 nM (to be discussed in Chapter 3).

Very recently, Marin et al (99) did an mutagenesis study of the residues at the interdomain cleft of Gt alpha. It was originally hypothesized that a large rearrangement of the interdomain cleft would have to occur to induce GDP release/nucleotide exchange (100). Most mutants had minimal to no effect on basal Gt alpha nucleotide exchange. The charge reversal of K276E increased basal nucleotide exchange the most (10X). None of the mutants had an effect on the rhodopsin catalyzed maximal nucleotide exchange rate. The authors argue based on these results, and data not shown (of Gt alpha 5 mutants that caused >150 increase in basal nucleotide exchange), that rearrangement of the interdomain cleft is not the mechanism of receptor catalyzed increases in nucleotide exchange. They note that other monomeric G proteins that do not have a helical domain at all (that makes it look like a sandwich) release GDP more slowly than some heterotrimeric G proteins (101).

The A326S mutant of Gi does have a 250X fold increase in the GDP release rate, and it's structure is nearly identical to the transducin GTP-gamma-S bound state, but it must be remembered that the crystal structure is probably the lowest energy state (it was crystallized with GTP-gamma-S bound), and presumably there is a higher energy intermediate nucleotide free state. As seen in Figure 17 from Posner et al, the A326S

mutant structure does show a loss interactions of C325 sulfur with the carbonyl of the guanine ring, of G45 amide with the alpha phosphate. Five other interactions are gained, and the sum of these interactions may favor the formation of the nucleotide free state.

Activation of Rhodopsin and Transducin

Retinal Activation of Rhodopsin

As seen in Figure 10B, retinal attached to K296, is sandwiched between H-III and H-VI. The 9-methyl group of the retinal is thought to interact directly with G121 of opsin in the middle of H-III, and is known to be one of the crucial steric determinants of of photoactivation (102). Removal of this group from retinal reduces the spectral shift from Meta I to Meta II and impairs rhodopsin catalytic efficiency to 8% of wild type (103). GPCR's other than rhodopsin, depend on a specific agonist ligand binding to stimulate formation of a active conformation that binds the G protein, releases its GDP, and catalyzes nucleotide exchange on the G protein. Retinal analogs have been synthesized with photo-activatable groups on the beta-ione, and these have been cross-linked in reconstituted wild type dark and light adapted rhodopsin (104; 105). Reconstitution of the retinal analog was about 50%, and about 20% of this cross-linked to dark adapted rhodopsin. In the dark and batho rhodopsin states, non-isomerizable retinal analogs the cross-linked mostly to W265 in H-VI, and to a lesser extent L266, as determined by Edmund sequencing.

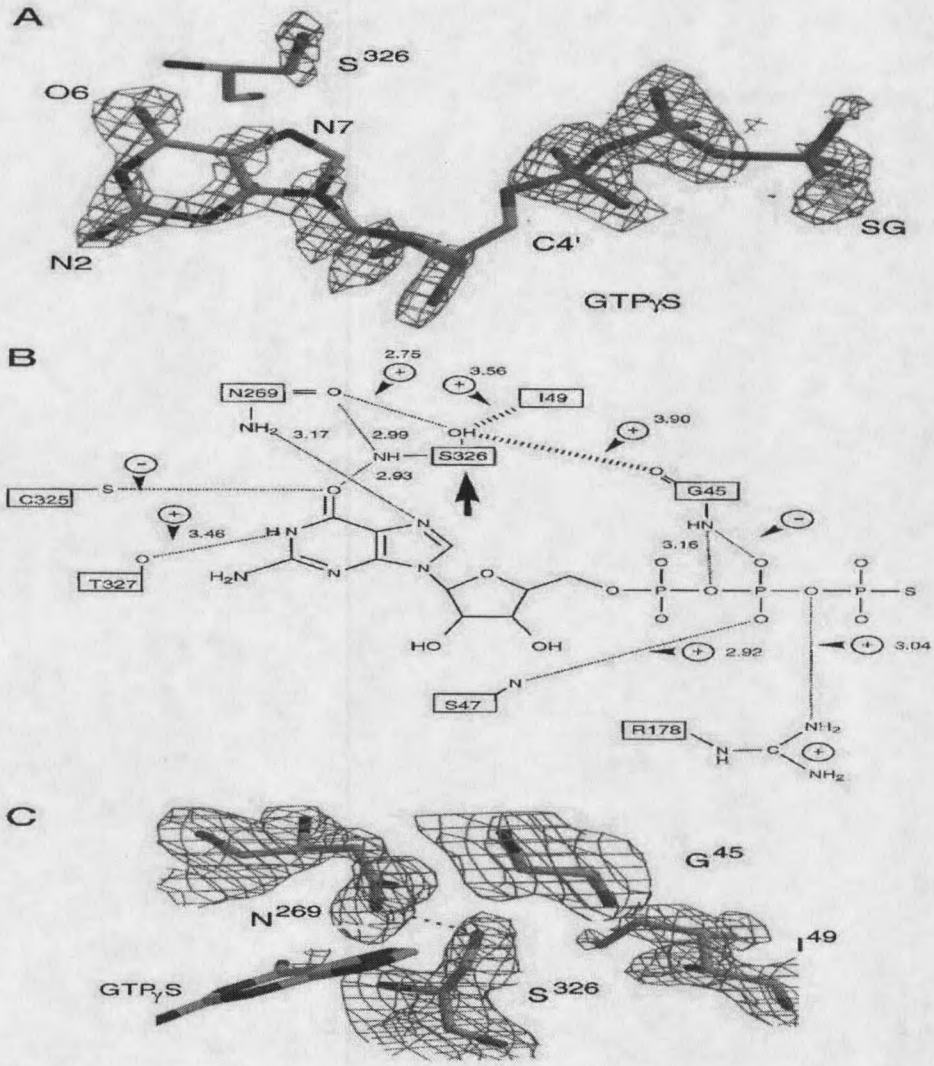


Figure 17. Stuctural Analysis of A326S Gi alpha-1 (95).

A, F_o - F_c map calculated from the model for A326S $G_i\alpha_1$-GTPγS-Mg^{2+} after molecular replacement and rigid-body refinement of the search model. The map has been contoured at 3.0 σ above the mean peak height. The electron density, colored in *orange*, indicates the location of the nucleotide and the mutant serine residue. The stick models indicate the position of the nucleotide and mutant serine in the refined model. *B*, noncovalent bonding interactions that have been perturbed in the active site of A326S $G_i\alpha_1$. Shown are hydrogen bonds (*dashed lines*) formed between protein residues and the nucleotide and van der Waals contacts (*thick hash marks*) between Ser326 and the protein that have changed in A326S $G_i\alpha_1$-GTPγS-Mg^{2+} relative to the wild-type complex. Interactions that have been gained (+) and that have been lost (—) in the mutant are indicated with the observed distances shown in *A*. Hydrogen bonds are defined as those interactions in which the donated hydrogen and acceptor atoms are separated by no more than 2.5 Å and the angle subtended by donor, hydrogen, and acceptor atoms is greater than 90°. *C*, examples of the electron density in a $2F_o$ - F_c map calculated from the refined model for A326S $G_i\alpha_1$-GTPγS-Mg^{2+}. $2F_o$ - F_c electron density map around Ser-326 contoured at 1.5 σ above the mean peak height using phases derived from the final model. Electron density for GDP; only the purine ring is included in the schematic for clarity.

1994]. With light adapted rhodopsin cross-linking was observed at multiple sites in H-III(104), and at A169 in H-IV (105). Only 1.5% of the radioactivity was recovered in Borhan et al's (105)identification of A169 as the cross-linkinking site. Isolating sites of cross-linking, and chemical modification in rhodopsin is a difficult process because it requires digestion of rhodopsin and isolation of very sticky fragments. Co-elution of rhodopsin fragments is common in HPLC separation of rhodopsin digest peptide fragments (106; 107). The HPLC co-elution of rhodopsin fragments, the low recovery of radioactive cross-linked fragment yield, and the multiple sites identified call into question the correct identification of the cross-linking sites observed for the light adapted rhodopsin. Multiple cross-linking sites certainly are possible in the light adapted state. It will be of interest to see if future cross-linking attempts with transducin bound cause a preference of cross-linking to a single (or fewer) site.

Role of rhodopsin residues in activation

Some rhodopsin and transducin residues have been directly correlated with activation (See Figures 10A, 13B). Mutation of these residues can lead to a decrease in transducin G-alpha-GTP formation. In rhodopsin (90; 108-110), the alpha1B-adrenergic receptor (111), chemokine receptor CX3CR1 (112), and muscarinic receptors (113; 114) R135 mutants of H-III virtually abolished G protein activation. The functional importance of this position is not universal to all GPCR's since other GPCR's are not as sensitive to substitutions at this position (115-117). Rhodopsin cysteine mutants of Y136, and V137-9 led to partial loss of transducin activation (118). Acharya et al (90) proposed

the YVVV of H-III and EKEVT of at the top of H-VI to form a pocket for the transducin C-terminal 340-350 peptide. Yamashita et al (93) were able to switch specificity of rhodopsin from Gt to Go by swapping the C-III loop with the C-III loop of the mAChR2, ETA, or ETB receptors. They also proposed that residues V138, E134, and C140 (which are opposite to R135, V139, and Y136 in helix C) were the most critical in maintaining full transducin activation.

Resek et al (119) made four single cysteine mutants H65C, C140, S240C, and C316. All other cysteines, except C110, 187 & 185 necessary for disulfide formation, were replaced with serines. These cysteines were derivatized by disulfide cross-linking to a tritiated photo-activatable probe. Only the derivatized mutant S240C from loop C-III was able to cross-link to Gt alpha upon exposure to UV light. The extent of cross-linking was very low (0.5% of the total radioactive label), and the site of cross-linking to Gt alpha was never located.

H-VII contains the site of retinal attachment to lysine 296. One might predict isomerization of 11-cis retinal to cause movement of H-VII relative to H-VI, and expose residues in H-VI critical to transducin activation. Disulfide cross-linking of 246C H-VI to 312C of H-VI, abolished transducin activation. A spin label at C316 of H-VIII, was reported to move apart from a label at position 65, at the amino terminus of transmembrane H-I, upon Meta II formation (120) . Yet disulfide formation between C65 and C316, had no effect on transducin activation (121). A highly constrained rhodopsin, with the cytoplasmic ends of H-I & -VII, H-III & -V, and the extracellular ends of H-III

& -IV, and H-V & -VI disulfided, still retains 60% of the ability to activate transducin compared to wild type (122).

Farrens et al (123), using cysteine mutants and spin labeling deduced that Meta II formation involves an outward movement of H-VI away from H-III. Cross-linking of H-VI to H-III by cysteine mutant disulfides or metal chelating agents (121; 124) (123) (125) also abolishes transducin activation. An M257 substitution of H-VI with any amino acid exept lucine and arginine causes constitutive activity (84). Dunham & Farrens (126) investigated residues nearby in H-VI to find residues involved in activation. They compared the ability of eight diffent cysteine mutants (near the residues at the top of H-VI in the Acharya study) to be chemically modified by the bulky PyMPO-maleimide probe and the enviromentally sensitive fluorophore mBBr (monobromobimane). They found that dark adapted mutants K248C, E249C, T251C, R252C and I255C could react with PyMPO, but V250C, M253C, V254C, and I256C could not. The V250C showed a dramatic increase in reactivity with PyMPO in the light. K248C, E249C, V250C, T251C, and R252C were reactive with mBBr in the dark, but M253C, V254C, I255C, and I256C showed little or no reactivity. The mBBr modified mutant V250C was the only mutant that showed a large blue shift upon conversion from dark to Meta II state, corresponding to a dielectric constant change of ~44 to ~17 (more hydrophobic). It's fluorescence quenching by KI reversed from being unquenchable in the dark state to quenchable in the Meta II state.

Studies of the H-VIII have been contradictory. Osawa et al's (127) N310A, K311A, and Q312A point mutants had no effect. Cai et al's (128) Q312C mutant reduced

Gt activation to 88% of wild type. Marin et al's (129) N310S K311P Q312D, K311P, and K311W reduced Gt fluorescence activation to 39, 87, and 74 % of wild type. This region, from N310 to T320, has been determined to be the 8th helix in the dark structure, and spin labels attached to positions 316, and 313 in the middle of C-IV undergo increased mobility after photolysis (120). The rhodopsin derived peptide 310-321 from this region can cause red shifting and a 10% increase in transducin tryptophan fluorescence (130).

Role of transducin residues involved in activation/coupling to rhodopsin

Some of the C-terminal transducin residues previously discussed to affect the basal nucleotide exchange rate, are also implicated in coupling to rhodopsin. These will be discussed more in the next section focusing on peptides. The C-terminus of G alpha can be a key modulator of of GPCR specificity. Substitutions in G alpha expressed in human embyonic kidney cells demonstrated that mutants of glycine in the -3 position (relative to the C-terminus) suffice to switch the GPCR specificity of the G alpha q/alpha i2 chimeras Certain mutations were able to switch the specificity of Gq to Gi2, Gq to Gs, and vice versa. The change in specificity, however, was only observed with particular GPCRs(131). Owasa et al (132)expressed transducin alpha subunit mutants invitro. Alanine mutants L344A, K345A, D346A, C347A, G348A, L349A, and F350A displayed 4%, 120%, 130%, 68%, 64%, 7%, and 70% of wild type binding. Mutations can lead to overall structural changes, and the binding of guanine nucleotide (a good test of structural integrity) can be measured by examining the resistance of the alpha subunit

to digestion by trypsin in the presence of GTP-gamma-S. G proteins have marked increases in resistance to trypsin digestion upon GTP-gamma-S binding (57; 58; 133; 134). These same mutants had 1%, 95%, 125%, 56%, 90%, 5% and 41% of wild type resistance to trypsin digestion. The highly conserved leucines were also more conservatively substituted with isoleucine, and these mutants L344I and L249I, demonstrated rhodopsin binding of 43 and 27% of wild type levels, and trypsin resistance of 69 and 50% of wild type levels.

Peptides as Probes of GPCR and G Protein function

There is an advantage to the use of peptides as probes of the wild type receptor/ligand interaction. This method does not suffer from the "making the news or reporting the news" problem associated with mutagenesis. Peptides (if derived from the proteins of interest) can give information about the specific residues responsible for receptor/ligand interaction. Peptides have been used to influence all stages of the signal transduction pathway. Measurement of the peptide influence at the first stage of signal transduction before the GPCR/ G protein interaction requires monitoring the ligand/GPCR interaction with radio or fluorescently labeled ligands (135-137). In the case of the visual pigment rhodopsin, peptide interference with rhodopsin coupling to transducin in the second stage can be measured using the UV/VIS "extra meta II assay" (68; 98; 138), the transducin fluorescence assay (129; 139; 140), or by monitoring GTP gamma S^{35} binding, GDP^{32} release, and/or P^{32} release from GTPase activity (67; 90; 141; 142). Measurement of peptide interference of signal transduction after the GPCR/G

protein interface requires downstream montitoring of the G alpha/effector interaction or G beta-gamma/effector interactions (135-137).

A number of studies have implicated the C-terminus of the alpha subunit of the G protein as mediating signal transduction. Hamm et al (98) found bovine C-terminal G alpha protein derived peptides that could inhibit rhodopsin/transducin interaction and/or stabilize the active conformation of rhodopsin (mimic the effect of transducin holoprotein) as measured by the "extra Meta II assay". Various Gt alpha peptides spanning residues 8-23, 311-329, and 340-350 could inhibit rhodopsin/Gt interaction, but only peptides derived from 311-329 and 340-350 could independently bind and stabilize the MetaII state. The peptides N-acetyl-311-329-amide (Ac311-329NH2) and 340-350 had the most activity with IC50's of 0.02 and 0.04 millimolar respectively for the rhodopsin/transducin interaction. The Ac311-329NH2 peptide contains the CAT guanine ring binding region of transducin, and it is the only peptide known to both bind rhodopsin and interact with the nucleotide. Ruiz-Avila et al (143)found the bovine Gt alpha Ac311-329NH2 peptide to be an inhibitor of taste cell membrane activation of rat transducin. Truncation of this peptide on either end lowered its activity, as did cyclizing it, or lengthening it. Different Transfer-NOESY NMR structures of the 340-350 peptide in complex with light activated rhodopsin have been reported (144-146). The alpha-5 helix of Gt alpha starts at threonine 325 and extends to various lengths in the reported crystal structures with the extreme C-termini disordered. One Gi alpha structure in complex with RGS4 (147) extends the C-terminal helix upto glycine 352 (analogous to G348 in transducin). The B-factors for the alpha carbons of I344, K345, N346, N347, L348,

K349, D350, C351, G352, L353, and F354 are 28, 26, 28, 31, 19, 19, 31, 37, 41, 30, 49 respectively.

Resenick et al (137) found two rat Gs derived carboxyl terminal peptides 354-372 and 384-394 could block beta-adrenergic stimulation of adenylyl cyclase in saponin-permeable C6 glioma cells, as measured by cAMP production, with IC50's of 20 and 50 micromolar respectively. Both peptides could also mimic the effect of Gs to increase the agonist isoproterenol's affinity (decrease the Ki) for the beta-andrenergic receptor, as measured by it's ability to inhibit receptor binding of the radioligand antagonist ^{125}I-pindolol (IPIN).

Martin et al (148) used combinatorial approach to find optimum bovine C-terminal Gt alpha peptides that mimic the extra Meta II effect of transducin binding to rhodopsin at low and submicromolar concentrations. Fourth round clones 8, 9, 10, 18, 23, and 24, as seen in Figure 18B and C had the most potency. Aris et al (149) explored these peptides further, and found that the K341L in 340-350 peptide analogs substitution had the greatest effect in producing a high affinity peptide analog to this region of Gt. Figure 19 combines Tables I – IV of Aris et al, summarizing the detailed peptide mutational analysis. Whereas some receptors activate multiple G proteins, A1 adensosine receptors are preferentially coupled to Gi/o proteins. Gilchrist et al (135) found C-terminal Gi1/2 alpha and Gt alpha peptides to modulate agonist binding or antagonist-agonist competition using cells overexpressing A_1 adenosine receptors. Gi1/2 and Go alpha peptides 344-354 both inhibited binding of agonist [^{3}H]N^6- (cyclohexyl)adenosine (CHA) to A1 adenosine receptor in rat cortical membraneswith IC50's of approximately 30

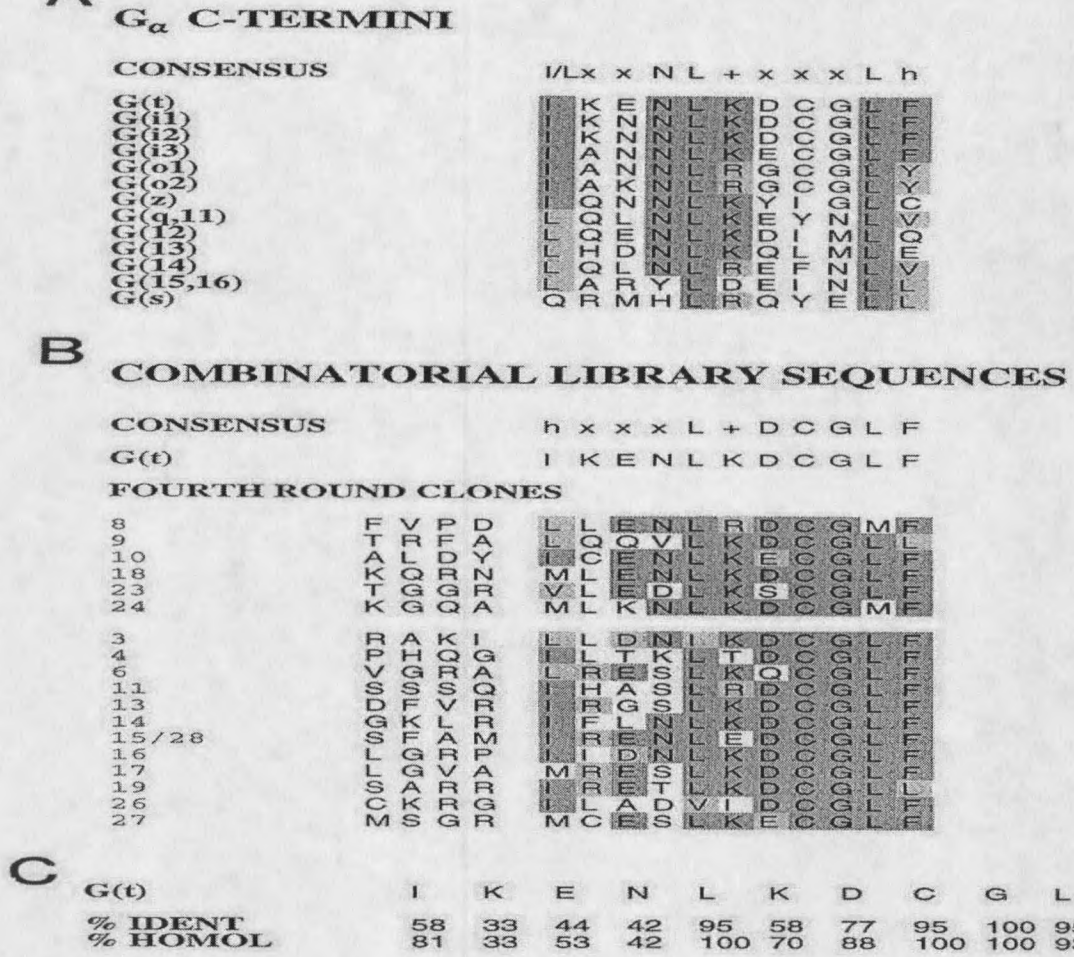


TABLE I

Binding to rhodopsin and Meta II stabilization by MBP fusion proteins and synthetic peptides

The dose response for the ability of each of the six high affinity MBP fusion proteins to compete with the LacI-Gtα-K341R-340–350 fusion protein for binding to light-activated rhodopsin was measured in an ELISA format. Microtiter wells were coated with 0.5 μg of ROS/well and blocked with BSA in the dark. Serial dilutions of purified MBP fusion proteins were added after light activation of the rhodopsin, incubated for 45 min at 4 °C. The LacI-Gtα-K341R-340–350 fusion protein was added, after 30 min the amount of bound LacI was detected by an anti-LacI primary antibody and AP-conjugated goat anti-rabbit secondary antibody, and the assay was developed with *p*-nitrophenyl phosphate. Meta II stabilization was measured as described under "Materials and Methods."

	MBP fusion protein			Synthetic peptides	
	Meta II binding IC_{50}	Meta II stabilization EC_{50}		Meta II binding IC_{50}	Meta II stabilization EC_{50}
	μM			μM	
MBP8	0.0078 ± 0.0003	0.94 (0.57–1.56)	8S	16 ± 5	8.3 (5.4–13)
MBP9	0.010 ± 0.003	1.05 (0.44–2.5)	9S	15 ± 4	12.0 (7.8–18.3)
MBP10	0.042 ± 0.02	5.4 (2.3–12.8)	10S	34 ± 20	24.0 (10.6–54)
MBP18	0.0038 ± 0.002	1.24 (0.74–2.0)	18S	10 ± 1	15.7 (8.3–29)
MBP23	0.020 ± 0.004	3.5 (1.66–7.3)	23S	0.64 ± 0.08	0.92 (0.74–1.15)
MBP24	0.0066 ± 0.002	0.49 (0.36–0.66)	24S	110 ± 40	152 (61–376)
MBP-K341R-340–350	6.0[a,b]	>100	K341R-340–350	200 ± 50	223 (155–321)
			18L	0.14 ± 0.05	1.60 (0.85–3.0)
			23L	0.21 ± 0.06	0.37 (0.37–0.54)
			G_t	0.084[b]	0.32 (0.26–0.39)

[a] Error not accurately determined since curve does not saturate.
[b] Experiment only conducted once.

Figure 18. A summary of 340-350 peptide analogs tested for their abilities to stabilize Metarhodopsin II (EC50), and for their abilities to inhibit a 340-350 K341R peptide fusion protein (IC50), as measured by ELISA (148).

Table I
Role of the charge at the *N* and *C* termini in Meta II stabilization by $G_t\alpha$-(340-350) analogs

The dose response for the ability of each of the listed $G_t\alpha$ analogs to stabilize Meta II was measured as described under "Materials and Methods." Bold letters indicate amino acid residues that differ relative to the native $G_t\alpha$-(340-350) sequence. Dose-response curves were analyzed by non-linear regression using a sigmoidal dose-response variable slope equation (GraphPad Prism) to obtain the EC_{50} values, S.E., and slope. The number of independent experiments, done in duplicate, is listed as *n*. The EC_{50} obtained for heterotrimeric G protein was 0.28 ± 1.12 μM, with a slope of 1.19 ($n = 8$).

Peptide	Sequence	EC_{50} ± S.E.	Slope	*n*
		μM		
Role of N terminus				
$G_t\alpha$-(340-350)	IKENLKDCGLF	1209.0 ± 2.7	0.82	4
$G_t\alpha$-(340-350)-K341R	IRENLKDCGLF	180.4 ± 1.2	1.40	3
Ac-$G_t\alpha$-(340-350)	*Ac*-IKENLKDCGLF	162.9 ± 2.0	0.78	3
Ac-$G_t\alpha$-(340-350)-K341R	*Ac*-IRENLKDCGLF	162.7 ± 1.3	0.89	7
Ac-$G_t\alpha$-(340-350)-K341R-K345R	*Ac*-IRENLRDCGLF	34.8 ± 1.2	1.18	3
Peptide 23	VLEDLKDCGLF	0.7 ± 1.1	1.06	2
Ac-peptide 23	*Ac*-VLEDLKDCGLF	0.5 ± 1.7	1.27	2
Ac-peptide 23-K345R	*Ac*-VLEDLRDCGLF	1.1 ± 3.6	0.78	3
Peptide 24	MLKNLKDCGMF	152.1 ± 1.8	0.89	3
Ac-peptide 24	*Ac*-MLKNLKDCGMF	9.7 ± 1.2	0.83	4
Ac-peptide 24-K342R-K345R	*Ac*-MLRNLRDCGMF	9.9 ± 1.2	0.81	3
Role of C terminus				
Ac-$G_t\alpha$-(340-350)-K341R-Amide	*Ac*-IRENLKDCGLF-Amide	395.7 ± 1.2	1.02	6

Table II
Role of Cys-347 and Gly-348 in Meta II stabilization by $G_t\alpha$-(340-350) analogs

The dose response for the ability of each of the listed $G_t\alpha$ analogs to stabilize Meta II was measured as described under "Materials and Methods." Bold letters indicate amino acid residues that differ relative to the native $G_t\alpha$-(340-350) sequence. The **Δ** symbol represents 2-aminobutyric acid (Abu). Dose-response curves were analyzed by non-linear regression using a sigmoidal dose-response variable slope equation (GraphPad Prism) to obtain the EC_{50} values, S.E., and slope. The number of independent experiments, done in duplicate, is listed as *n*.

Peptide	Sequence	EC_{50} ± S.E.	Slope	*n*
		μM		
Role of Cys-347				
Ac-$G_t\alpha$-(340-350)-K341R	*Ac*-IRENLKDCGLF	162.7 ± 1.3	0.89	7
Ac-$G_t\alpha$-(340-350)-K341R-C347Abu	*Ac*-IRENLKD**Δ**GLF	126.6 ± 1.2	1.42	6
Ac-$G_t\alpha$-(340-350)-K341R-C347A	*Ac*-IRENLKD**A**GLF	579.1 ± 1.2	3.10	5
Ac-$G_t\alpha$-(340-350)-K341R-C347D	*Ac*-IRENLKD**D**GLF	>1000	0.79	4
Ac-$G_t\alpha$-(340-350)-K341R-C347S	*Ac*-IRENLKD**S**GLF	>1000	1.11	4
Ac-peptide 23-K345R	*Ac*-VLEDLRDCGLF	1.1 ± 3.6	0.78	3
Ac-peptide 23-K345R-C347Abu	*Ac*-VLEDLRD**Δ**GLF	10.6 ± 1.2	1.09	4
Ac-peptide 23-K345R-C347M	*Ac*-VLEDLRD**M**GLF	11.0 ± 1.4	1.12	3
Ac-peptide 23-K345R-C347V	*Ac*-VLEDLRD**V**GLF	2.0 ± 1.3	0.71	3
Role of Gly-348				
Ac-$G_t\alpha$-(340-350)-K341R-G348A	*Ac*-IRENLKDC**A**LF	783.9 ± 1.6	1.33	3

Table III
Role of Lys-341 in Meta II stabilization by $G_t\alpha$-(340-350) analogs

The dose response for the ability of each of the listed peptide analogs to stabilize Meta II was measured as described under "Materials and Methods." Bold letters indicate amino acid residues that differ relative to the native $G_t\alpha$-(340-350) sequence. The **Δ** symbol represents 2-aminobutyric acid (Abu). Dose-response curves were analyzed by non-linear regression using a sigmoidal dose-response variable slope equation (GraphPad Prism) to obtain the EC_{50} values, S.E., and slope. The number of independent experiments, done in duplicate, is listed as *n*.

Peptide	Sequence	EC_{50} ± S.E.	Slope	*n*
		μM		
Role of Lys-341				
Ac-$G_t\alpha$-(340-350)-K341L-C347Abu	*Ac*-IL**E**NLKD**Δ**GLF	43.7 ± 1.3	0.67	4
Ac-$G_t\alpha$-(340-350)-K341L-C347M	*Ac*-IL**E**NLKD**M**GLF	19.6 ± 1.2	0.64	4
Ac-$G_t\alpha$-(340-350)-K341L-C347V	*Ac*-IL**E**NLKD**V**GLF	43.6 ± 2.7	0.54	2

Table IV
Role of the random linker sequences in Meta II stabilization by $G_t\alpha$-(340-350) analogs

The dose response for the ability of each of the listed peptide analogs to stabilize Meta II was measured as described under "Materials and Methods." Bold letters indicate amino acid residues that differ relative to the native $G_t\alpha$-(340-350) sequence. Dose-response curves were analyzed by non-linear regression using a sigmoidal dose-response variable slope equation (GraphPad Prism) to obtain the EC_{50} values, S.E., and slope. The number of independent experiments, done in duplicate, is listed as *n*.

Peptide	Sequence	EC_{50} ± S.E.	Slope	*n*
		μM		
Role of random sequences				
Peptide 23	VLEDLKDCGLF	0.7 ± 1.1	1.07	2
Peptide 23 long	TGGRVLEDLKDCGLF	0.4 ± 1.1	1.39	3
Peptide 24	MLKNLKDCGMF	152.1 ± 1.8	0.89	3
Peptide 24 long	KGQAMLKNLKDCGMF	10.1 ± 1.1	0.93	4

Figure 19. A summary of 340-350 peptide analogs tested for their abilities to stabilize Metarhodopsin II (EC50), (149).

micromolar. In contrast, neither Gs alpha 384-394 nor Gt alpha 340-350 inhibited agonist binding at concentrations of 200 micromolar, but some Gt alpha 340-350 analogs derived from Martin et al's combinatorial library could inhibit agonist binding to A1 adensosine receptors in CHO-K1 cells (peptides 19 & 24 had IC50's >100 micromolar). Peptides 8, 9, 15, 19, 23, 24, and Gi1/2 alpha 344-354 were tested for their ability to inhibit radiolabeled antagonist binding [3H]DPCPX by the full agonist R-PIA. Only peptides 8, 15, and 19 were able to ***increase*** the Ki values of full agonist R-PIA. Gilchrist et al also used whole cell electrophysiological recordings to measure peptide ability to inhibit activation of G protein coupled K+ channels through A1 adenosine or gamma-aminobutyric acid type B receptors in hippocampal CA1 pyramidal neurons. Peptides Gi alpha 1/2 344-354, 19, and 24 had the most significant effects on inhibition of adenosine stimulated holding current. Peptide 23 (rhodopsin high affinity peptide) had no effect. This negative result illustrates a concept important for drug design. It implies that small changes in peptide sequence can result in large changes in receptor specificity.

This review of peptides as probes of GPCR and G protein function, reveals that while peptides have the advantage of only "reporting the news", the "news reported" is highly dependent on the peptide sequence. Peptide binding to receptors is hindered by a large conformational entropy penalty. Small sequence changes can cause large changes in affinity. If neglible affinities are observed in a particular peptide, this may not necessarily imply that this sequence within the conformationally constrained protein (from which the peptide is derived) is not relevant. This concept will be further illuminated in Chapter 3.

CHAPTER 3

PROBING NON-COVALENT INTERACTIONS BETWEEN RHODOPSIN AND TRANSDUCIN BY PEPTIDE INHIBITON OF RHODOPSIN-CATALYZED NUCLEOTIDE EXCHANGE, AND CROSS-LINKING PHOTO ACTIVATABLE PEPTIDE ANALOGS TO RHODOPSIN

Abstract

Light-excited rhodopsin releases GDP from transducin, leaving a nucleotide-free intermediate which binds to GTP and goes on to stimulate the visual excitation cascade. Light excited rhodopsin rapidly forms an equilibrium mixture of metarhodopsin I and metarhodopsin II that absorb at 478 nm and 380 nm, respectively. Certain peptides derived from the transducin sequence stabilize metarhodopsin II (metaII). The peptide residues between 311-329 in the alpha subunit of transducin may be the most critical in mediating the catalysis of GDP / GTP exchange as evidenced by the inhibition of the binding of GTP-gamma-^{35}S to transducin. We found that the peptide Ac311-329NH2 inhibited 99% of GTP-gamma-^{35}S exchange in the rhodopsin/transducin system (IC50 </= 400nM), and also inhibited the homologous formyl peptide receptor/Gi system (IC50 =3uM). The 340-350 Gt alpha analog peptide AcVLEDLRSCGLF inhibited 99% of GTP-gamma-^{35}S exchange in the rhodopsin/transducin system (IC50 4-6uM), but had no effect in the FPR/Gi system. Rhodopsin activity was usually studied in the native retinal rod membranes which contain some residual transducin. Both C-terminal peptides

inhibited urea washed (transducin depleted) bovine retinal rod membrane catalyzed nucleotide exchange by exogenous bovine Gi/Go, but only with 70% maximal inhibition. The highest affinity Gt alpha C-terminal 340-350 peptide analogs have much higher MetaII affinity than the 311-329 analogs, but the 311-329 peptides are much more effective in inhibiting GDP/GTP exchange in the GTP-gamma-^{35}S assay. The amino acid substitution K341L in transducin-α-derived C-terminal peptides (340-350 or 336-350), which enhance meta II affinity by 150x (148) also increased the alpha helical propensity of the peptides 2-3 fold as measured by circular dichrosim in 50% TFE. The K341L substitution may favor formation of a conformation more similar to the active meta II binding conformation of the c-terminal portein of by decreasing the entropy of binding and thus increasing meta II affinity. A photo activatable 340-350 peptide analogue containing this high affinity substitution cross-links to rhodopsin with high specificity, and inhibits nucleotide exchange (IC50 4-6uM). These results provide further evidence for two recognition sequences for rhodopsin-catalyzed GDP/GTP exchange on transducin.

Introduction

Knowledge of the nature of the interface between transducin and rhodopsin is likely to be related to the coupling of other GPCR's to their G proteins (135; 136; 150-153). Evidence on the structural basis of this coupling has heretofor been limited to analysis of effects of site-specific mutants on G protein activation and on analysis of peptide interactions with rhodopsin and/or transducin. Crystal structures are available for

transducin complexed with GDP, with GDP and AlF_6^- (which mimics GTP action), and with GTP-gamma-S, as well as for dark adapted rhodopsin. The light-activated rhodopsin structure, and the light-activated rhodopsin in complex with transducin is still awaited.

Because of the large development horizon of methods for identification of non-covalent complexes by CRYO-IR laser desorption TOF (see Chapter 1 of this thesis), more conventional methods were initiated for the defining the photo-cross-linked molecular contacts involved in rhodopsin/transducin coupling. The method introduced here was modeled after the approach of Mills et al, and others (154; 155). As mentioned previously, conventional mass spectrometric instruments are capable of unit mass resolution up to about 6000 Da. Mass spec methods are also capable of "mass fingerprinting" the sequence of peptides below 2500 Da by analyzing the fragments of these peptides with post source decay experiments in TOF instruments, and with MS/MS experiments in ion trap and ion cyclotron instruments (107; 156). Thus while mass spectrometry will never yield the three dimensional structure of protein complexes, it can give resolution of interaction sites at the amino acid residue level using covalent stabilization of cross-linked complexes, if the complexes are reduced in size by enzymatic or chemical cleavage. Peptides with low to submicromolar affinity were found to mimic transducins binding to rhodopsin (98; 148). We synthesized flourescent photo-activatable analogs of these peptides as explained in this chapter. We verified the activity of these fluorescent photo-activatable peptides by radionucleotide measurement of GTP-gamma-^{35}S binding and by cross-linking competition experiments. In addition, other peptide candidates for cross-linking were identified. One peptide was 20X more

potent than the peptides previously identified for inhibition of GDP/GTP exchange, and was cross-reactive in the homologous formyl peptide receptor/ inhibitory G protein system (FPR/Gi). Mass spectometric methods to identify the sites of peptide cross-linking to rhodopsin will be discussed in the following chapter.

Materials and Methods

Peptides were synthesized using standard Fmoc chemistry and purified to >90% purity by reverse phase HPLC. Peptides were characterized by MALDI-MS using such and such as a matrix. Some peptides were synthesized on a Milligen 9050 using Fmoc amino acids purchased from Advanced Chem Tech, while other peptides were purchased from Macromolecular Resources (Fort Collins, Colorado). 6-(fluorescein-5-carboxamido)hexanoic acid succinamidyl ester (5-SFX) was purchased from Molecular Probes (product # F-6106) and coupled to the epsilon amino group of the N-acetylated, N-terminal lysine of selected peptides. Urea washed rod outer segment membranes and transducin were prepared as described (157; 158) as provided by Professor Heidi Hamm. The formyl peptide receptor was overexpressed in stabley transfected Chinese hamster ovary cells as described (171) and provided by Dr. John Mills. Gi/o was purified from bovine brain as described (159). GTP-gamma-S, and GDP were purchased from Sigma, while GTP-gamma-^{35}S (1000 Ci/mmole)was purchased from Amersham Pharmacia. Whatman 0.45 micron nitrocellulose filters were purchased from VRW, and scintillation

counting was performed in ScintiSafe (Fischer) scintillation fluid on a Beckman LCS 100 scintillation counter.

Transducin GTP-gamma-S35 binding assays were performed in 720uL of solution containing approximately 75 nM rhodopsin, 24nM transducin, 10uM GDP (or in 200uL of a solution containing 6 nM FPR, 93nM transducin, 1uM GDP), in 100mM NaCl, 1mM Mg+2, 5mM Hepes, pH 7.5. Assays were performed in sets of ten samples from the same stock solutions of rhodopsin and transducin. To improve assay reproducibility, it was imperative to sonicate ROS membranes in buffer and to disaggregate them, breaking them into smaller pieces. The sonicated membranes were then centrifuged (14K 2 minutes) and the supernatant containing the finest membrane particles in suspension were used for the assays. Assays were begun by equilibration of the assay mixture on ice and then the addition of GTP-gamma-^{35}S (0.05-0.1 micro curie per assay, equivalent to 100-200K counts), typically run for 10 minutes. Assays were terminated by rapid filtration through nitrocellulose membranes, and immediate washing with 2mL cold buffer. All assays were performed in duplicate, and the radioactivity was counted for 2-5 minutes. It was important to ad GDP to reduce the rate of GTP–gamma-^{35}S binding, as explained under results.

Cross-linking experiments were performed with ~5 micromolar rhodopsin, and 5 micromolar photo-activatable peptide in 100mM NaCl, 5mM Hepes, 1mM Mg+2 , pH 7.5. Samples were flushed with argon, bleached with white light, and stirred at zero degrees celcius in a UV-transparent cryo dewar, followed by exposure to a 200W Ultra High pressure Hg lamp filtered through a 313nm interference filter (OptoSigma) for 15

minutes. The interference filter was cooled by a fan to keep it from overheating. Labeled membranes were collected and separated from free uncross-linked peptide by centrifugation at 35K 40 minutes. Pellets were sonicated in 1 milliliter of dH2O and centrifuged again. This washing step was repeated 3 times, after which pellets were dissolved in SDS or LDAO detergent. Total cross-linking yields were assessed by quantitating total fluoroscein fluorescence (495 excitation 530nm emission), compared to a known fluorescent standard. The standard was quantitated using a fluorescein extinction coefficient of 70,000 $M^{-1}cm^{-1}$. The extent of cross-linking was assessed from the ratio of the fluorescence from the peptide cross-linked to rhodopsin relative to UV aromatic amino acid absorbance from the bleached rhodopsin recovered during HPLC gel filtration in 0.5% SDS, 10mM phosphate, 0.05% NaN3 pH 7.5, at 0.3mL/min flow rate on a TOSOHASS super SW2000 column. 280 Absorbance was monitored on a TSP UV2000 detector and fluoroscein fluorescence (530nm emission, 495 excitation) was monitored on a Perkin-Elmer 650S HPLC fluorescence detector. Aliquots of cross-linked membranes were washed and dissolved in 0.5% SDS and injected on the column and the ratio of the 530nm fluorescence emission to 280nm absorbance were calculated from peak heights at the appropriate retention time. Tris-tricine acrylamide SDS gels were run as described (160) and imaged on a BioRad Fluor-S Imager. It should be noted that running dye should not be used in gels if intrinsic fluorescence is to be assessed, because the dye sticks to rhodopsin and produces fluorescence not due to peptide cross-links. Instead 500-1000 picomoles of fluorescent standard was run in an end lane of the gel and the migration rate of the gel front was assessed visually.

Results

Peptides that mimic portions of the alpha subunit of transducin were found to be stabilze Meta II in a similar manner to the intact heterotrimeric G protein, transducin (98). Martin et al (148) found several high affinity analogs corresponding to residues 340-350 of transducin's alpha subunit (Gt alpha) by screening peptide libraries. In our photo cross-linking studies we utilized synthetic photo-activatable analogs of the 18L peptide reported in Martin et al. The sequence of the 18L peptide is shown in Table 2. The 18L peptide was reported to have ~1 micromolar Meta II stabilization. Lysines in the 340-350 Gt peptide destabilize Meta II by attacking the retinal binding site, but this effect is obviated by replacement of the lysines with arginines (144). Replacement of K341R and/or K346R enhance the affinity of the 340-350 peptide for Meta II (149). In order to synthesize a fluorescently labeled photo activatable analog for cross-linking we substituted arginine for lysine, aminobutyric acid (Abu) for cysteine, valine for methionine (to facilitate cyanogen bromide cleavage without losing the fluorophore), benzoyl phenylalanine for phenylalanine, and also N-acetylated the N-terminal lysine before deprotection of the peptide.These substitutions yielded peptide-1 in Table 2. The Cys to Abu substitution was shown to have minimal effect on activity (149), and avoids undesirable cysteine reactions. In the last step of the synthesis we attached a fluorescein hexanoyl to the epsilon amino group of the N-terminal lysine, to yield peptide-2. Another fluorescently labeled peptide analog with the benzoyl

Table 2. Characteristics of Transducin alpha subunit C-terminal peptide analogs

No.	Sequence[a]	MetaII Stabilization EC50 (uM)	GTP-y-S binding IC50(uM)[e]	Molar Ell. per residue[f]
18L	KQRNMLENLKDCGLF	1.6 (0.85-3.0)[b]	ND[c]	ND[c]
1	Acetyl-KQRNVLENLRD-Abu-GL-Bpa	1.6 (0.85-3.0)[b]	6	8182
2	Acetyl-K(epsilon-fl)QRNVLENLRD-Abu-GL-Bpa	NM[c]	6	ND[c]
3	Acetyl-KQR-Bpa-LLENLRD-Abu-GLF	NM[c]	6	ND[c]
4	Acetyl-K(epsilon-fl)QR-Bpa-LLENLRD-Abu-GLF	NM[c]	15	ND[c]
5	Acetyl-VLEDLRSCGLF	0.5+/-1.2[d]	6	7609
6	Acetyl-IRENLRDCGLF	34.8+/-1.2[d]	150	2857
7	AcDVKEIYSHMTCATDTQNVK-amide (transducin Ac311-329NH2)	20	0.4	ND[c]
8	DVKEIYSHMTCAT (transducin 311-323)	150	150	NDc
	Transducin Holo-protein	0.3uM[bd]	NA	NA
	Melittin	NA		16498

a)Abu = aminobutyric acid, Bpa = Benzoylphenylalanine, fl = hexanoylfluorescein

b) as reported Martin et al 1996

c) NM = not measurable because of fluorescein absorbance, ND = not determined

d) as reported Aris et al 2000

e) IC50 = 50% inhibition of 75nM rhodopsin catalyzed GTP-gamma-^{35}S binding by 25nM tranducin in 10uM GDP, 25 picoM GTP-gamma-^{35}S, 100mM NaCl, 1mM Mg+2, 10mM Hepes pH 7.5, 0 degrees celcius.

f) Molar Ellipticity per residue measured at 222nm

phenylalanine in the 4 position was similarly synthesized, yielding peptides 3 & 4 respectively.

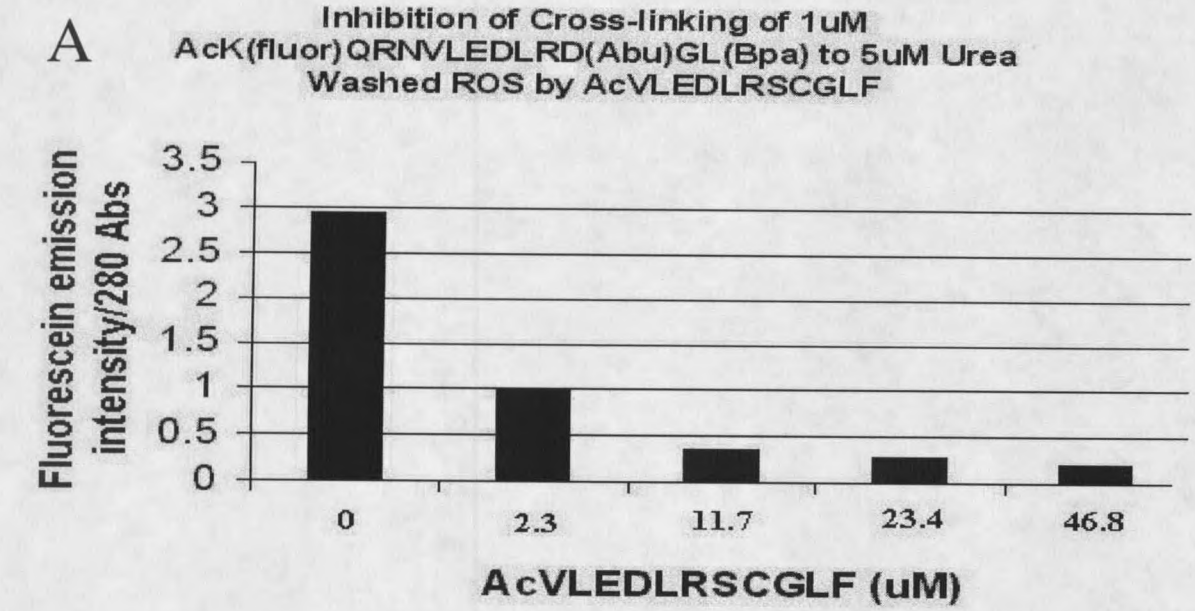
All of the peptides used in Table 2 were tested for inhibition of excited rhodopsin catalyzed GTP-gamma-^{35}S binding by Gt alpha. Peptides 1-6 correspond to peptide analogs of the C-terminal portion of Gt alpha 340-350. Peptides 7 & 8 correspond to peptide analogs of the C-terminal portionGt alpha 311-329. Photo-activatable analogs of these two peptides have not yet been made, and their activities are discussed later in this paper. The IC50 values for the peptides 1-6 reported here are similar to the Meta II stabilization values reported by Hamm et al (98)), Martin (148)), and Acharya et al. (90). None of the substitutions made in 18L were found to severely affect their activity. The substitution of Bpa in the 4 position and L in the 5 position to produce peptide 3 did not affect the IC50 , however, the addition of the hexanoyl fluorescein to make peptide 4, lowered the IC50 2 fold.

Various concentrations of the photo activatable fluorescent peptides added to suspensions of bleached ROS membranes were exposed to 313nm filtered light from a focused high pressure 200W Hg lamp for various times in the presence and absence of non-fluorescent non-cross-linking competitive inhibiting peptides. After UV exposure, ROS were spun down, and washed with water to remove noncovalently bound peptide. Membrane pellets were dissolved in SDS or LDAO detergent and total fluorescein fluorescence was measured to quantitate total cross-linking yield by comparison to fluorescent standards as described in the Materials and Methods. Aliquots of these same samples were analyzed by HPLC gel filtration in detergent buffered to pH 7.5 to maintain

fluorescein fluorescence. The ratio of fluorescence emission to 280 absorbance was calculated from peak height at the appropriate retention time to quantitate peptide cross-linking normalized for rhodopsin recovered. Labeled samples were also run on 16.5% acrylamide tris-tricine SDS gels and analyzed by exposure to broad band 302nm UV radiation on a BioRad Fluor-S Imager to analyze cross-linking. Figures 20a-c demonstrate that the cross-linking of peptide 2 to rhodopsin is specific (competable by an unlableled peptide), and reproducible, where as Figure 20c shows that the cross-linking of the lower affinity peptide 4 is poorly competable.

Modifications of the N-terminal portion of the C-terminal Gt alpha peptide strongly affect affinity (149). The C-terminus of Gt alpha in the various crystal structures is alpha helical through asparagine 344 (100), while residues 345-350 are disordered. We analyzed the helical propensities of C-terminal peptides in solution by circular dichroism. A solvent containing 50% water, and 50% trifluoroethanol was used to favor latent helical structure. Figure 21 shows that the alpha helical content of the peptides containing the K341L substitution are enhanced 2-3 fold compared to the K341R peptide.

Total fluorescence meausurements of peptide 2 covalently cross-linked to rhodopsin (after washes to remove non-covalently bound peptide) indicate that 3-5% of the light exposed rhodopsin could be cross-linked with photo activatable peptide. Increases in peptide concentration beyond 10uM or exposures beyond 15 minutes did not increase cross-linking yields, however, total yield did correlate linearly with peptide concentration and exposure time variation below these values (data not shown). Light scattering from ROS membranes limited penetration of 313nm photo cross-linking light.



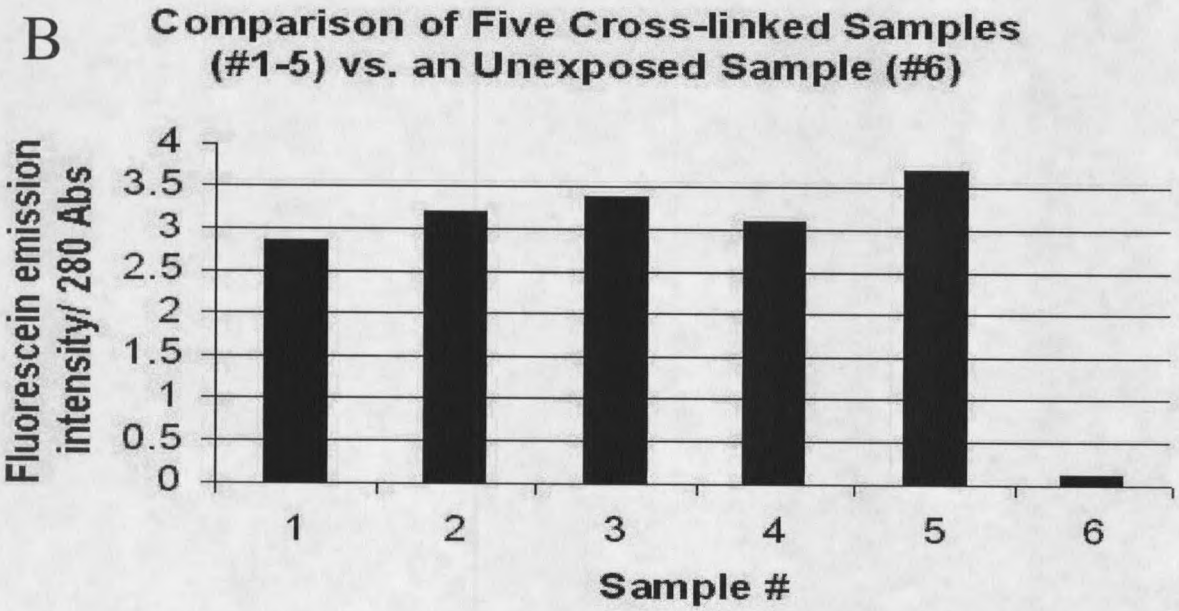


Figure 20. Fluorescent peptide-2 crosslinking experiments.
A) HPLC gel filtration assessment of peptide inhibition of cross-linking.B) HPLC gel filtration assessment of identical cross-linking experiments vs. an uncross-linked sample.

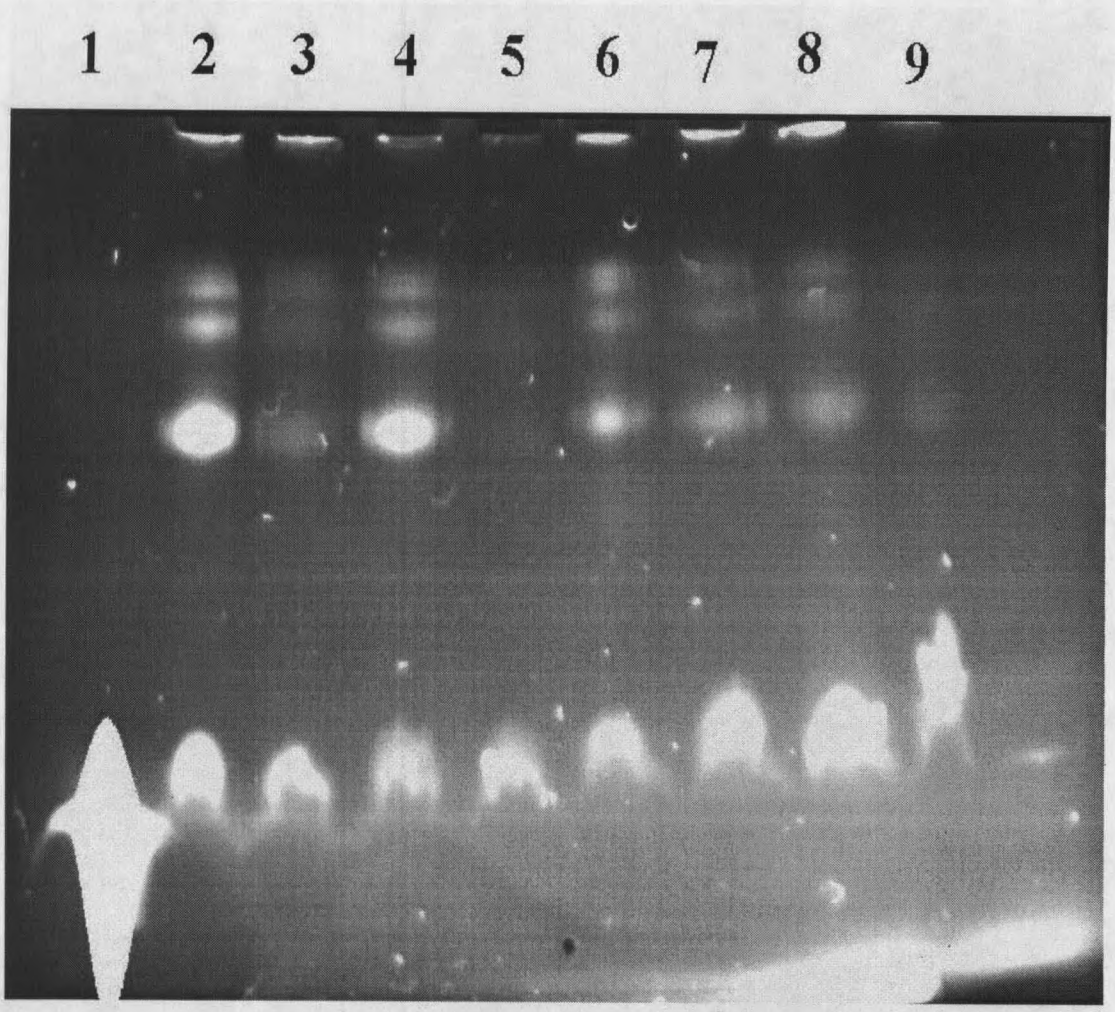


Figure 20C. SDS-PAGE confirmation of cross-linking specificity.

Photo of 302 broad band excitation of a 16.5% tris/tricine gel loaded with various cross-linking experiments.Lanes 1, 5, &9 had no UV exposure. All other lanes had 15 minutes UV exposure.

Lane 1	Fluorescent Peptide Standard
Lane 2	5uM Peptide 2, 5uM Ac311-329-amide, 5uM ROS, 15 min UV exposure
Lane 3	5uM Peptide 2, 100uM AcVLEDLRSCGLF, 5uM ROS, 15 min UV exposure
Lane 4	5uM Peptide 2, 5uM ROS, 15 min UV exposure
Lane 5	5uM Peptide 2, 5uM ROS, **NO UV exposure**
Lane 6	5uM Peptide 4, 5uM Ac311-329-amide, 5uM ROS, 15 min UV exposure
Lane 7	5uM Peptide 4, 100uM AcKQR(Bpa)LLENLRS(Abu)GLF, 5uM ROS, 15 min UV exposure
Lane 8	5uM Peptide 4, 5uM ROS, 15 min UV exposure
Lane 9	5uM Peptide 4, 5uM ROS, **NO UV exposure**

Stirring of the membrane suspension helped maximize total cross-linking yields. 365nm UV light exposure accelerated the decline in rhodopsin activity significantly, however, 313nm radiation did less so. As seen in lanes 2 &6 of Figure 20c, addition of Ac-311-329-amide peptide to the cross-linking reaction enhanced the yields of cross-linked peptide 2. The enhancement due to the Ac311-329NH2 was approximately 20%, as measured by HPLC gel filtration comparison (data not shown) of multiples samples (n=6) under the same conditions in Figure 20c. Isolation and identification of cross-linking sites of peptide-2 to rhodopsin is discussed in Chapter 5.

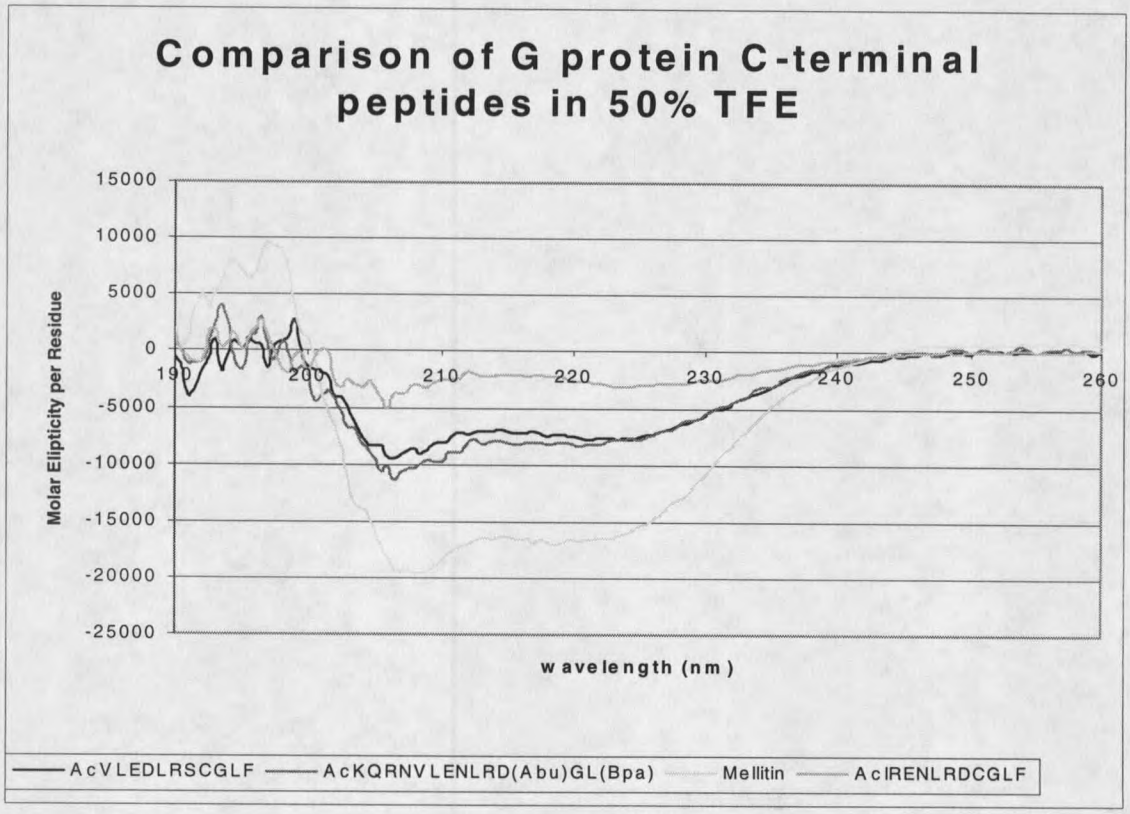


Figure 21. Circular Dichroism analysis of Transducin 340-350 peptide analogs in 50% trifluoroethanol.

In a search to identify other sequences within transducin suitable for cross-linking, we tested peptides 7 & 8 for their ability to block nucleotide exchange. Peptides 7 & 8 were previously characterized by the extra meta II assay (98). Table 2 shows peptide 7 & 8's sequences, their corresponding IC50's for GTP-gamma-^{35}S, and their reported EC50 meta II stabilization. Most of the peptides IC50's for GTP-gamma-^{35}S binding correspond quite well with reported EC50's for meta II stabilization, with the exception of the peptide comprising the residues 311 to 329. The Ac311-329NH2 peptide has 50X more activity inhibition of GTP-gamma-^{35}S binding than it's reported meta II stabilization (400X more than the acetylated native 340-350 peptide's EC50 for meta II stabilization). The unacetylated 311-323 peptide has a GTP-gamma-^{35}S binding IC50 that is 375X weaker, which corresponds well with its reported EC50 meta II stabilization.

The Ac311-329-amide peptide is about 13X more potent than the high affinity AcVLEDLRSCGLF peptide for inhibiting GTP-gamma-^{35}S binding and the two peptides were anaylyzed in the same assay to verify that the apparent differences in potency were not due to assay to assay variation. Figure 22 compares GTP-gamma-^{35}S exchange observed with equivalent concentrations of competing peptides vs. no inhibiting peptide. The Ac311-329NH2 peptide is clearly much more potent than AcVLEDLRSCGLF, with 4.4uM Ac311-329NH2 peptide inhibiting nucleotide exchange almost as much as the non-radioactive GTP-gamma-S control. The assays described in Figure 22 were performed on ice in the presence of 10 micromolar GDP. The GDP was included to slow the GTP-gamma-^{35}S exchange to a more easily measurable and linear rate. The effect of

GDP concentration on the affinity of Gt for rhodopsin, and its subsequent effect on the ability of peptides to compete with Gt for rhodopin, has been described (161). The assay design for rhodopsin GTP-gamma-^{35}S binding by tranducin is not similar to previously described peptide inhibition of GTP-gamma-^{35}S binding assays (90). Typically an excess of GTP-gamma-^{35}S is included in the reaction with little or no added GDP. Large GDP concentrations, and low GTP-gamma-^{35}S concentrations relative to transducin make the reaction rate first order, and effectively lowers the rate GTP-gamma-^{35}S binding by lowering the transducin concentration. Linearity of GTP-gamma-^{35}S binding was maintained by incubating 5 fold less time for 1uM GDP than for 10uM GDP, while maintaining the same rhodopsin concentration. With rhodopsin and transducin concentrations constant, lower GDP concentrations significantly increased the IC50's of both peptides (data not shown). Figure 23A shows the alpha carbon trace of the three dimensional structure of the transducin chimera with GDP bound as reported by Lambright et al (162). The beta-gamma subunits are rotated to the back and are colored green and dark blue respectively. The alpha subuint is in light blue. An expanded view of the the C-terminal Gt alpha residues is 311-344 and GDP is shown in Figure 23B. Hydrophobic, polar, positive and negative residues are green, yellow, blue, and red respectively. The Ac311-329NH2 peptide is reported to bind and stabilize the Meta II conformation of rhodopsin (98).

The crystal structures of bovine Gt alpha with GDP, and GTP-gamma-S, Gi1 alpha with GDP, and bovine Gs with GTPyS have been reported (100; 133; 163; 164). The 311-329 sequence is quite conserved among G proteins. In Gt, the residues D324,

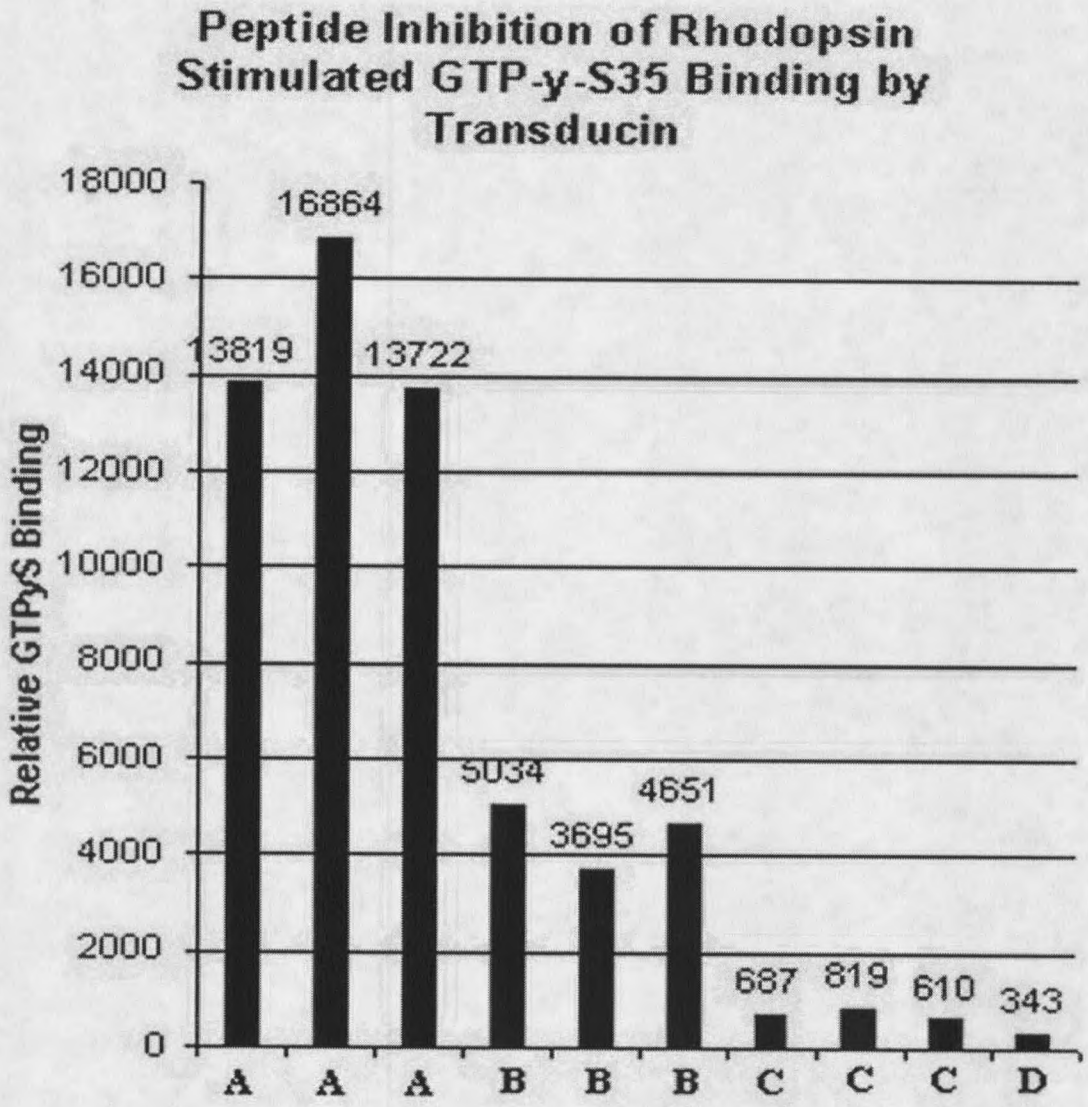
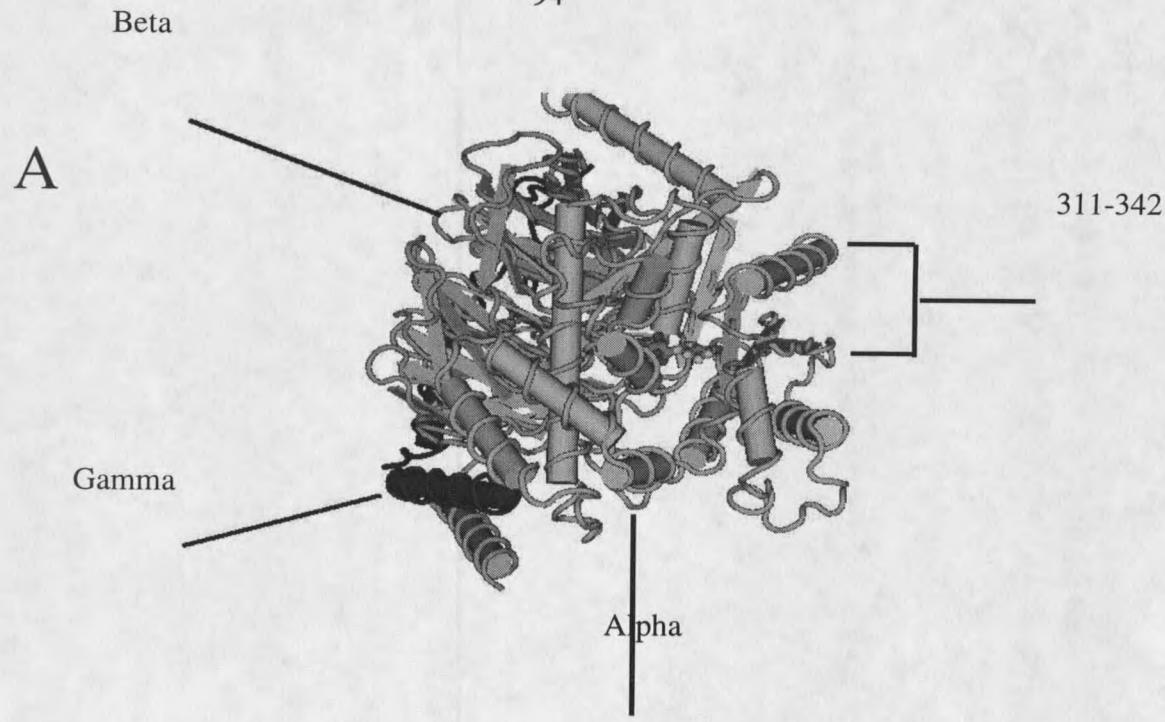
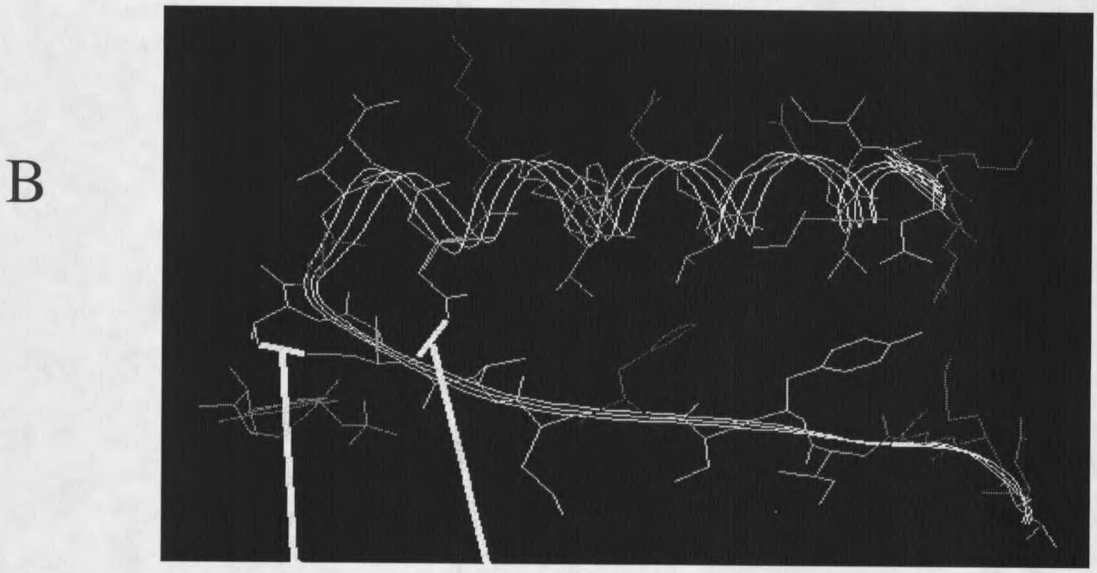


Figure 22. Comparison of Uninhibited, N-acetyl-VLEDLRSCGLF, and N-acetyl-311-329-amide inhibited GTP-gamma-^{35}S binding in urea washed ROS with exogenous transducin added. All assays were performed on ice simultaneously from the same stock solutions. All assays contained 50nM urea washed ROS, 25nM exogenous Gt, 10uM GDP, 250picoM GTP-gamma-^{35}S, 1mM Mg, 10mM Hepes pH 7.5, Zero Celcius. Lanes A have no inhibiting peptide. Lanes B contain 4.2uM AcVLEDLRSCGLF. Lanes C contain 4.4uM Ac-311-329-NH2. Lane D is a control and contains excess non-radioactive GTP-gamma-S.





311DVKEIYSHMT**CAT**DTQ**N**V(K329)FVDAVTDIIIKE 342

Figure 23. A) Ribbon and tube model of Heterotrimeric G protein, transducin. B) Expanded view of C-terminal residues 311-342.

T325, Q326, N327, and V328 (*i* through *i*+4, respectively) make up a Type I beta turn that is stabilized by helix strand interactions. The amide of A322 hydrogen bonds with the guanine ring of GDP, and C321 and T323 make Van der Waals contacts. Figure 24 shows the C-terminal sequence homology between Gi, Gt, and Gs subunits. Differences between the sequences are highlighted. The strand, turn, helix motif is conserved in Gi, Gt, and Gs with the residues comprising the turn having the highest homology. The proline in Gs does not affect the structure of this motif.

```
Gi1   311 KRKD--TKEIYTHFTCATDTKNVQFVFDAVTDVIIKNNLKDCGLF 353
Gt    308 MRRD--VKEIYSHMTCATDTQNVKFVFDAVTDIIIKENLKDCGLF 350
Gs    350 TASGDGRHYCYPHFTCAVDTENIRRVFNDCRDIIQRMHLRQYELL 394
                .   :  *.*:***.**:*:: **:   *:* : :*::  *:
```

Figure 24. Sequence Alignment of the C-terminus's of Gi1, Gt, and Gs.

Because of this high sequence and structural homology, it was of considerable interest to test the activity of bovine transducin Ac-311-329-amide and the bovine transducin high affinity analog of Ac-340-350 in another GPCR/G protein coupled system. Rhodopsin has been reported to couple to Gi, Go, and Gs to varying degrees (62; 134; 165). Gt is most similar to Gi, having ~70% sequence homology. The formyl peptide receptor (FPR) is a GPCR coupled to Gi2 (80; 166; 167), and has been studied extensively (85; 166; 168-171) . Similar to a report by Sheikh et al (124), we have found that a brief 4M urea wash, as described in the Materials and Methods was critical to

observe the coupling of exogenous transducin to FPR. Urea washing removed 30-40% of the protein content of the membranes, and improves the enhancement of fMLF stimulation from 2-3 fold to 4-6fold. Figure 25, shows that human FPR is capable of stimulating bovine Gt in an fMLF-dependent matter. Figure 26 shows a titration of Ac311-329-amide inhibition of FPR catalyzed GTP-gamma-^{35}S binding to Gi endogenous to chinese hamster ovary cells (IC50 ~3uM).The C-terminus of Gi , as seen in Figure 24, does have some significant sequence differences than bovine transducin. In the bovine transducin 311-329 sequence, mutations of V312T, S317T, Q326K, and K329Q, are required to yield the analogous Gi2 sequence. In the bovine transducin 340-350 sequence, a single mutation of E342N, would yield the analogous Gi2 sequence. Niether the high affinity AcVLEDLRSCGLF 340-350 peptide analog, nor the Gi2 peptide analogous to the Gt Ac311-329NH2 inhibit FPR catalyzed GTP-gamma-^{35}S binding to Gi endogenous to chinese hamster ovary cells.

Because the peptides Ac311-329-NH2 and the high affinity K341L 340-350 peptides may not have a strong affinity for FPR, a better system to test of their potency would be in a sytem containing urea washed, Gt depleted, bovine rod rhodopsin with exogenous bovine brain Gi/o added. Figure 27 displays a peptide inhibition study in this system. In our preparations, rhodopsin catalyzed GTP-gamma-^{35}S binding by transducin with about a ten fold greater rate than by bovine brain Gi/o. This difference was compensated in the assay design by reducing the incubation time with GTP-gamma-^{35}S by 10 fold while maintaining the same rhodopsin and GDP concentrations. Both the high affinity 340-350 and the Ac311-329-NH2 Gt alpha peptides were able to inhibit bovine

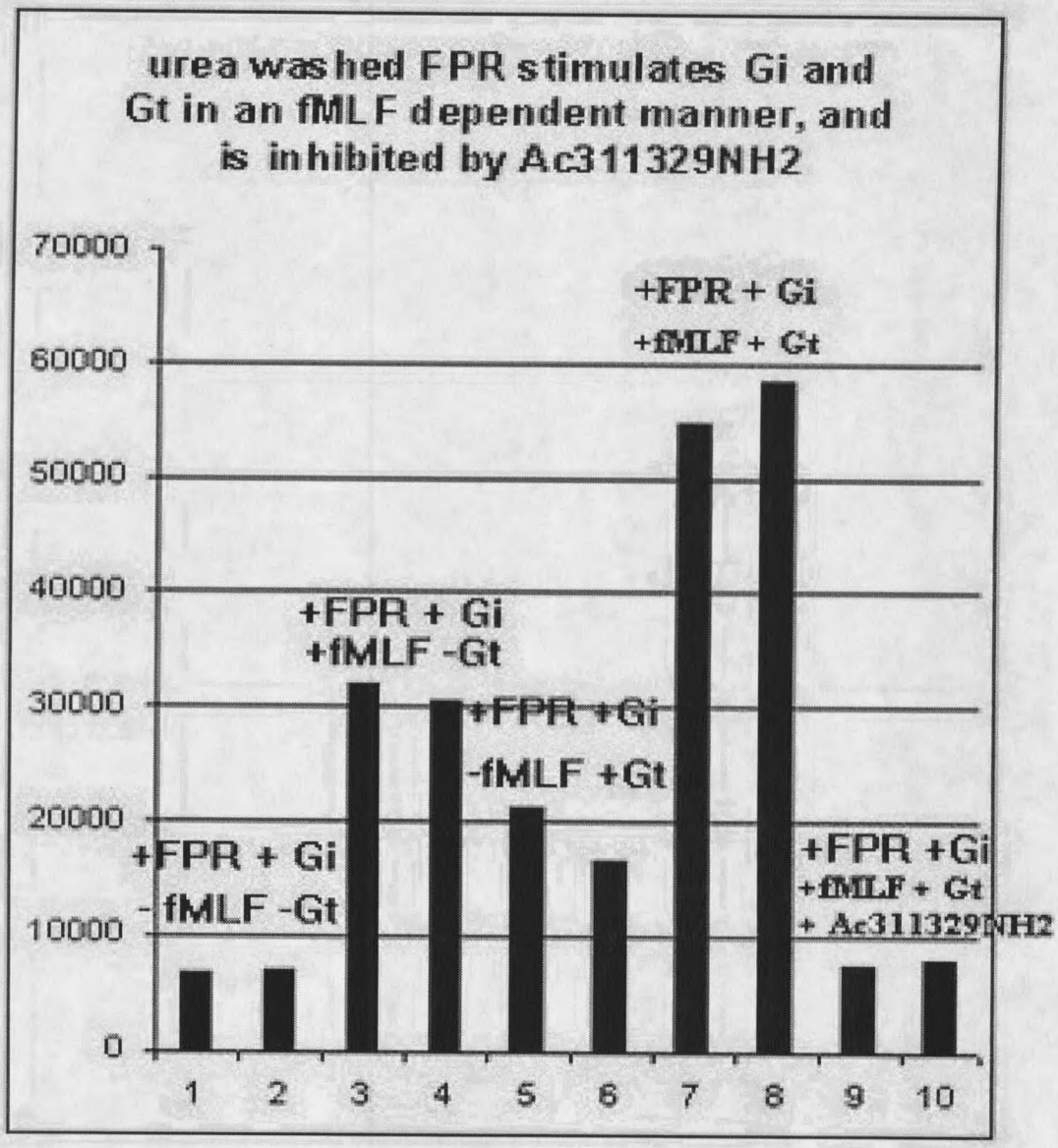


Figure 25. Agonist formyl-MLF stimulated Human Formyl Peptide Receptor catalyzed GTP-gamma-^{35}S binding by Transducin. FPR overexpressed in CHO cells were briefly urea washed, centrifuges and then resuspended in buffer. Columns 1,2 have FPR, endogenous Gi, and no fMLF. Columns 3,4 have FPR, endogenous Gi, plus fMLF. Columns 5,6 has FPR, endogenous Gi, exogenous Gt (93nM), and no fMLF. Columns 7,8 have FPR, endogenous Gi, exogenous Gt (93nM), plus fMLF. Columns 9,10 have FPR, endogenous Gi, exogenous Gt (93nM), fMLF, and 50uM Ac311-329NH2.

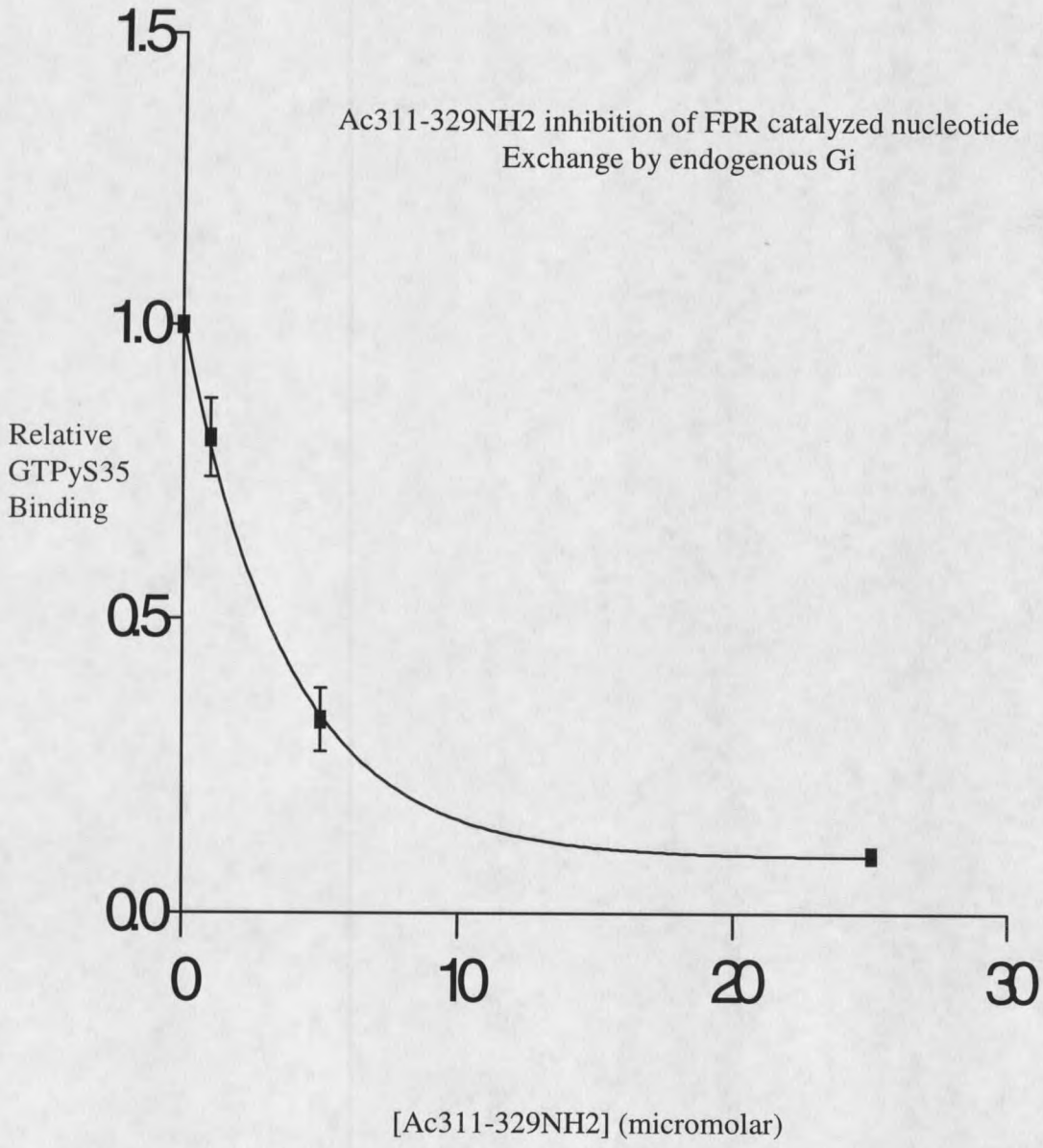


Figure 26. Ac311-329NH2 titration of agonist formyl-MLF stimulated Human FPR catalyzed GTP-gamma-^{35}S binding by Gi2. Assays contained urea washed membranes overexpressing FPR. Urea washing removed background GTPase activity, and preserved endogenous Gi activity.

rhodopsin catalyzed GTP-gamma-^{35}S binding by bovine brain Gi/o alpha with IC50's of 40 and 20 micromolar respectively. At low peptide concentrations, the high affinity 340-350 and Ac311-329NH peptides were able to inhibit rhodopsin catalyzed GTP-gamma-^{35}S binding by bovine Gi/o, with similar potency, to GTP-gamma-^{35}S binding by transducin. Neither peptide was able inhibit GTP-gamma-^{35}S binding by Gi/o to the same extent as they could inhibit GTP-gamma-^{35}S binding by Gt. Maximum peptide inhibition of GTP-gamma-^{35}S binding was 70% for rhodopsin/Gi and 99% for rhodopsin/Gt. Peptide solubility limited the maximum allowable peptide concentration useable for the Ac311-329NH2 to 50-100 micromolar.

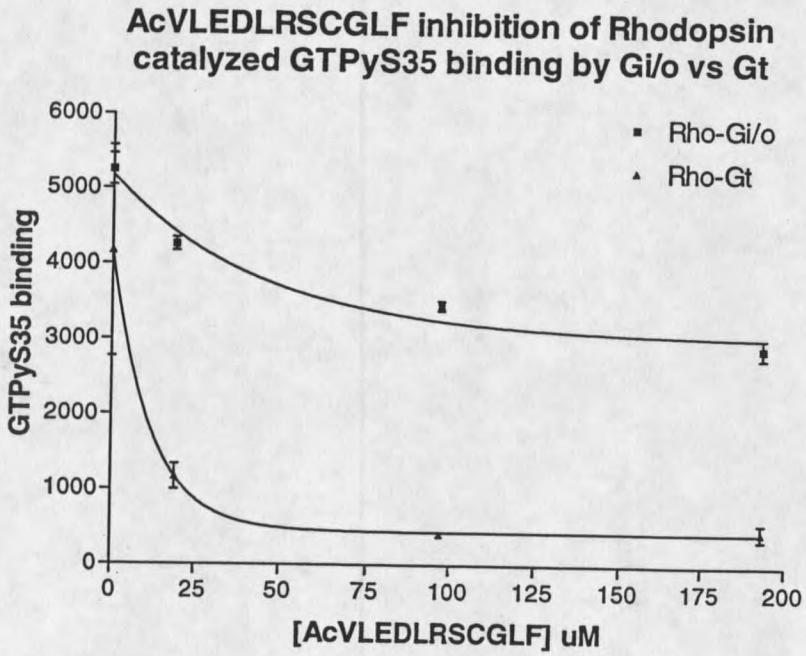


Figure 27. Peptide Inhibition of urea washed (Gt depleted) bovine rhodopsin catalyzed GTP-gamma-^{35}S binding by exogenous bovine Gi/o.

Discussion

The search to define the points of contact between the c-terminal sequence of the G protein and GPCR's is ongoing in order to better understand the mechanism of this ubiquitous signaling system. Some structural information can be implied from site-specific mutagenesis analysis of the G-holo-protein, GPCR, and interfacial peptides (81; 84; 90; 98; 103; 148; 149; 172) however, without a crystal structure of the complex between a G protein and a GPCR, the site specific mutagenesis data is difficult to interpret. Photo-cross linking of ligands to receptors followed by mass spectrometry for analysis is capable of defining molecular contacts with amino acid residue resolution (168; 173), and thus can lead directly to knowledge of the functional interactions of pharmacological interest. We report the first successful effort to cross-link peptides, corresponding to the c-terminus of tranducin, to rhodopsin. These peptides were found to have activity in both receptor stabilization, and in inhibiting nucleotide exchange when added in low micromolar amounts. In Figures 20a-c, we have shown the interaction of the c-terminal 340-350 sequence (and it's analogues) with bovine rhodopsin to be specific through competition measurements by fluorescence quantitation of cross-linked products, and by inhibition of nucleotide exchange. Benzoyl phenylalanine has been reported to require long exposure times for complete photolysis (174-176), however, the yields reported here are 3-10X higher than that of previous photo cross-linking experiments (105; 177). Hamm et al 1988 (98), reported the 340-350 peptide and the 311-329 peptide to work in synergy, lowering the EC50 of Meta II stabilization. As seen in

Figure 20c, addition of the Ac-311-329 peptide increased cross-linking yields significantly. Higher yields are typically associated with higher affinity photo-probes in cross-linking experiments (174; 175; 178). The 20% enhancement in yield as assessed by gel filtration HPLC may be a conservative observation. The experiment was performed with 5uM of each peptide and rhodopsin, and it is expected that most of the photo cross-linking peptide would be already bound under these conditions and so little stimulation of cross-linking may be possible. More importantly, the Ac311-329NH2 enhancement of cross-linking yields by peptide 2 indicates that it does not compete with the cross-linking of peptide 2, and that the sites of interaction are separate. Identification of the sites cross-linked by digestion and mass spectrometry is the next step in identifying the specific residue interactions, and is a topic that will be discussed in a future publication.

The origin of the increase in affinity due to the K341L mutation is of special interest, since the affinity increases far above the native sequence and the random peptide library experiments show that this is the only substitution that does so. Martin et al and we found that 340-350 analogues with the K341 L mutation inhibit nucleotide exchange at similar concentrations, studied by the Meta II peptide stabilization assay. Acetylation of the N-terminus of the peptide, or a K341R substitution also increases the Meta II affinity, although not nearly as much as the K to L (149). The increase in affinity of this peptide by the K341L substitution could be caused by a decrease in electrostatic repulsion, an increase in hydrophobicity, or by biasing the solution conformation toward the active bound conformation. The alpha subunit of transducin is alpha helical between residues 325 and 343 but residues 344 to 350 are disordered in the crystal structures

reported by Noel et al (100) and the other structures as well. One structure reported extended the helix up to glycine 348 (179). However, crystal packing forces may affect the conformation of surface regions of the protein. Circular dichroism of peptides in alcohols or in water/alcohol mixtures is reported to be a useful method to measure the propensity to form alpha helices (180). Our circular dichroism measurements as shown in Figure 21, indicate a 2-3X increase in alpha helical content in the Gt alpha 340-350 peptide analog by the K341L substitution. An increase in helical propensity may decrease the conformational entropy of the peptide allowing it to bind more strongly because it may more closely mimic the native bound/active conformation in solution.

In our studies of GTP-gamma-^{35}S binding assays to verify the biological activity of the photo-activatable peptide analogs, it quickly became apparent that including GDP was useful to compete with GTP to make rate changes in GTP binding more observable, and to also reduce the required quantity of radioactive GTP-gamma-35S, rhodopsin, and transducin. GDP concentration can also affect the ability of a peptide to compete with transducin. Similarly, Kahlert et al (161) described the diphosphate beta position of GDP as being critical to its ability to displace transducin from rhodopsin. Using the rhodopsin peptide 310-321, they demonstrated that the IC50 for the peptide inhibiting the meta II/rhodopsin complex dropped from 126uM to 5uM if the GDP-beta-S concentration was increased from zero to 100 micromolar (GDP is about 3 times more effective than GDP-beta-S). Large GDP concentrations, and low GTP-gamma-^{35}S concentrations, relative to transducin, make the reaction rate first order, and effectively lower the rate of GTP-gamma-^{35}S binding by lowering the transducin concentration. The Kd of rhodopsin and

transducin with GDP bound is ~200nM, and with nucleotide free transducin it is ~5nM. The GTP-gamma-S assays were performed at ~75nM rhodopsin, 25nM transducin; therefore at this rhodopsin/transducin concentration increasing the amount of GDP bound transducin reduces the amount of transducin bound to rhodopsin. The Kd of GDP binding to transducin (when rhodopsin and transducin are bound) is 20uM (181), thus in the assays performed with 1uM GDP, most of the rhodopsin and transducin are bound, but at 10uM GDP the bound transducin concentration significantly decreases, resulting in significantly lower peptide IC50s of GTP-gamma-^{35}S binding.

Other regions of G proteins, besides the extreme C-terminus of the alpha subunit, are reported to make functional contacts with their corresponding GPCR. The C-terminus of the G gamma subunit, the N-terminus of the alpha subunit, and a sequence (311-329) just upstream from the extreme C terminal residues have been the subject of much research. These interactions have been studied by making peptides to these regions, and are reported have activities in the 100-200 microlar range for stabilization of Meta II (98; 153; 182). As seen in Figure 22, we found that the Acetyl-311-329-amide peptide, derived from transducin's alpha subunit, to inhibit rhodopsin catalyzed GTP-gamma-^{35}S binding by transducin at submicromolar concentrations. As seen in Figures 25 & 26, the same transducin Ac-311-329 amide peptide also inhibited GTP-gamma-^{35}S binding in the homologous FPR/Gi system. This is the only sequence in the transducin structures that contacts both the guanine ring of GDP and rhodopsin (100; 163). A Type I beta turn exists in the protein in the sequence of this peptide, and a truncation of this peptide (311-323) causes a 375X decrease in IC50. Thus, rhodopsin may recognize this beta turn in Gt

alpha, and the Ac311-329-amide peptide is able to bind to the rhodopsin residues critical to catalyzing GDP release. The turn encompassed by this peptide's sequence is conserved in all G alpha crystal structures reported. Gq's may also have this turn conserved as evidenced by the sequence homology and the ability of the thrombin receptor to activate transducin (139). An A326S mutation (analogous to A322 of Gt) of (as discussed in Chapter 2) of the turn in Gi causes a 250X decrease in transducin GDP affinity, without altering it's affinity for GTP-gamma-S, or its GTPase ability (95).

The very high potency (approaching that of the G holo protein) of the Ac-311-329-amide peptide in inhibiting nucleotide exchange adds to the extensive evidence for the critical involvement of the Gt alpha C-terminus in the mechanism of GPCR catalysis of nucleotide exchange. The Ac311-329-NH2 sequence and most of the rest of the C-terminus (that is resolved in the x-ray structure) is clearly exposed in the homologous G protein crystal structures reported thus far. This evidence makes it unlikely that the beta/gamma dimer exposes the C-terminus of Gt alpha for recognition (as proposed by Kisselev's conformational switch model, (183)).The beta/gamma subunits are required for nucleotide exchange (57-59; 61; 184), however, the c-terminal gamma peptide mimetic used thus far exhibits a low affinity interaction as measured by meta II stabilization (183) . The role of the beta/gamma dimer's effects on nucleotide exchange, may be more linked to the beta regions in direct contact with the alpha subunit (162; 185). The farnesyl group is essential for the activity of the c-terminal gamma subunit peptide. The minimal segment of the c-terminal gamma peptide that shows activity is farnesyl cysteine itself, which was reported to inhibit nucleotide exchange in both the

FPR/Gi and rhodopsin/Gt system with an appoximate 100uM IC50m (153). Furthermore, the gamma subunit C-terminus is at least 40 angstroms from the alpha C terminus in the Gt GDP bound crystal structure (and is even further from the GDP binding pocket), which would imply that farnesyl cysteine may effect the conformation of the important rhodopsin sites that interact with G alpha rather than being indicative of a Gt region of involved in rhodopsin nucleotide catalysis. The potency and specificity of the Ac311-329-NH2 and K341L 340-350 peptides in influencing the rhodopsin/transducin system suggests that GDP release and receptor specificity functions may be largely confined to the rhodopsin region contacting the Gt alpha C-terminus. As seen in Figure 22 and Table 2, the acetylated 23S peptide (and our photoactivatable analogs) inhibit rhodopsin catalyzed GTP-gamma-^{35}S binding by transducin with much less potency than the Ac311-329NH2 peptide. The acetylated 23S is unable to detectably inhibit FPR catalyzed Gi GTP-gamma-^{35}S binding (data not shown), but it is able to inhibit rhodopsin catalyzed Gi GTP-gamma-^{35}S binding (Figure 27). The Ac311-329NH2 peptide is capable of inhibiting GTP-gamma-^{35}S binding in the "native" rhodopsin/Gt (Figure 22) and FPR/Gi systems (Figures 26), and in the "non-native" rhodopsin/Gi couple(data not shown), and FPR/Gi/Gt systems (Figure 25). Gilchrest et al (135)similarly investigated the activity of the homologous Gi1/2 alpha 344-354 peptide (numbering in Gi1/2 shifted relative to Gt), and several Gt alpha 340-350 peptide analogs derived from the Martin et al (148)combinatorial library in the Al adenosine receptor system. The A1 adenosine receptor sytem is reported to exclusively couple to Gi, and our investigation parallels theirs in many ways. Namely, given the 70%+ sequence homology between Gt and Gi,

and the 22% sequence homology (40% positive) between rhodopsin and FPR (17% identity, 39% positive, between rhodopsin and A1 ADR), to what extent do these signaling systems overlap, and what is are the sources of similarities and differences?

FPR is reported to couple to Gi2. As seen in Figure 24, comparison of human Gi2 and bovine transducin sequence reveals near identity in the entire C-terminal region. Both the high affinity 340-350, and the Ac311-329NH2 peptides were selected for their ability to stabilize the meta II conformation of rhodopsin (98). Rhodopsin and transducin have co-evolved, and rhodopsin catalyzes a 780X increase in nucleotide exchange on Gt, but only a 3-5X increase on Gi (62). While the 340-350 peptide analogs bind to rhodopsin, they may not bind to FPR because of amino acid residue differences. Less likely, but not excluded, is the interpretation that FPR may catalyze nucleotide exchange in an entirely different manner, and these Gt peptide analog sequences may not be as important in catalysis of nucleotide exchange. The Ac311-329NH2 peptide and its analogous sequence in Gs have been previously reported to inhibit other G protein/GPCR interactions (137; 186).

Conklin et al's (131) site-specific mutagenesis experiments have implicated the C-terminus of G alpha as a modulator of the specificity of GPCR coupling.Understanding of the mechanism of this specificity could favor development of new drug leads. Substitutions of glycine in the -3 position (relative to the C-terminus) suffice to switch the GPCR specificity of the G alpha q/alpha i2 chimaeras. Certain mutations were able to switch the specificity of Gq to Gi2, Gq to Gs, and vice versa. These reports note that

these changes in specificity are particularly dependent on the GPCR the G protein is coupled to.

This emphasizes the importance of measuring the effects of inhibitors on GPCR's that couple to similar G proteins. Gilchrist et al (135), noted the 23S peptide from Martin et al (148) that is very potent in stabilizing Metarhodopsin II, is incapable of inhibiting the A1 Adenosine receptor's catalysis of nucleotide exchange on Gi2. Our variable peptide inhibition results with the 340-350 peptides correlate with Conklin's and Gilchrist's results (ie the extent of interaction of the extreme C-terminus of the G-alpha is specific to the the GPCR). But, while we demonstrated that transducin can interact with FPR, our negative results with the acetyl 23S peptide inhibition of FPR/Gi interaction do not necessarily prove that FPR does not catalyze GTP-gamma-^{35}S binding by transducin (or Gi2) via the same mechanism as rhodopsin does transducin. Our inhibition results of both rhodopsin and FPR nucleotide catalysis with the Ac311-329NH2 peptide indicate that this region of G-alpha may be more conserved with respect to the mechanism of the catalysis of nucleotide exchange. The results also suggest the mechanism of catalysis of nucleotide exchange could be separate of that of the mechanisms controlling specificity between G protein and GPCR.

The increased rate of GTP-gamma-^{35}S binding in the rhodopsin/Gt system as compared to the rhodopsin/Gi system reported by us and Skiba et al (62), may have evolved from an increased role the interaction of rhodopsin with the 340-350 sequence of Gt alpha. Evidence for this is seen in Figure 27, where the AcVLEDLRSCGLF peptide has a higher IC50 (40uM vs 4-6 uM) and lower maximal inhibition (70% vs

99%) in the Rho/Gi vs the Rho/Gt system. These results could be interpreted in at least two ways. The peptide could be recognizing the rhodopsin/G protein complex, and not just rhodopsin. The Hill Coeficient of nucleotide exchange is approximately 2, and this cooperativity has been attributed to the alpha subunit (75). Alternatively, Gi could bind rhodopsin tighter than Gt . The gamma subunit of Gi is geranylated and the gamma subunit of Gt is farnesylated. Gt is virtually completely removed from ROS with a 4M urea wash. Gi is not removed from membranes with a 4 M urea wash (which we used to our advantage), but rather requires detergent extraction to separate it from the membrane. Mutational analysis of the C-terminus of transducin by Osawa & Wiess (132) led them to conclude the C-terminus of transducin more important for its nucleotide and rhodopsin binding than it is for other G proteins. Gi and Gs are much less sensitive to mutations in the C-terminus.

Future projects include MS identification of the site that peptide-2 cross-links to on rhodopsin, and synthesis of photactivatable analogues of the Ac-311-329-amide sequence. Peptides analogous to Ac311-329NH2 have activity in the beta andrenergic/Gs and A1 adenosin/Gs systems, and these peptides may be suitable for cross-linking studies in these systems. The molecular interactions responsible for GPCR/G protein interactions may be defined by cross-linking and mass spectrometry, and may facilitate the design of small molecule mimetics that are specific to a particular GPCR. The Ac-311-329-amide peptide and the high affinity 340-350 peptide may also serve as tools for probing other aspects of G-protein signal transduction.

CHAPTER 4

MASS SPECTROMETRIC ANALYSIS OF CYANOGEN BROMIDE FRAGMENTS OF INTEGRAL MEMBRANE PROTEINS AT THE PICOMOLE LEVEL: APPLICATION TO RHODOPSIN

Abstract

Advances in time of flight mass spectrometry allow unit mass resolution of proteins and peptides up to about 6,000 Dalton molecular weight. Identification of larger proteins and study of their post-translational or experimental modifications by mass analysis is greatly enhanced by cleavage into smaller fragments. Most membrane proteins are difficult to mass analyze because of their high hydrophobicity, typical expression in low quantities, and because the detergents commonly used for solubilization may be deleterious to mass analysis. Cleavage with cyanogen bromide is beneficial for analysis of membrane proteins since the methionine cleavage sites are typically located in hydrophobic domains and cleavage at these points reduces the size of the hydrophobic fragments. Cyanogen bromide also gives high cleavage yields and introduces only volatile contaminants. Even after cleavage membrane proteins often contain fragments that are difficult to chromatograph. Matrix assisted laser desorption ionization mass spectrometry (MALDI MS) is capable of analyzing complex mixtures without chromatography. We present a MALDI MS method that quickly and reliably identifies the cyanogen bromide fragments and post-translational modifications of reduced and alkylated bovine rhodopsin from as little as 30 picomoles of rhodopsin in detergent solubilized retinal rod disk membranes, using 1-5 picomoles of digest per sample. The amino acid sequences of some of the peptides in the digest were confirmed by post source decomposition MS analysis of the

same samples. The method appears to be general and applicable to the analysis of membrane proteins and the protein composition of membrane preparations.

Introduction

Optimization of mass spectrometric methods with uncross-linked rhodopsin digests was necessary before isolation of the cross-linking sites between photo-activatable peptide and rhodopsin, as described in Chapter 3. The development of matrix-assisted laser desorption ionization (187) and electrospray ionization (188) for biological mass spectrometry has revolutionized many aspects of analytical biochemistry. Although, this revolution has yet to decisively spread to integral membrane proteins. Integral membrane proteins present many difficulties for mass spectrometry because their high hydrophobicity causes solubility problems, and reagents that are used for solubilization and purification often interfere with mass spectrometry.

Bacteriorhodopsin, and rhodopsin are the principal integral membrane proteins that have been characterized extensively via mass spectrometry, due to the relative ease of purification of these proteins. Rhodopsin makes up over 90% of the protein content in washed retinal rod outer segment (ROS) membranes (189; 190). ROS membranes contain about 40% rhodopsin and 60% lipids by weight (191; 192), which is a rather typical lipid-to-protein ratio for biological membranes. In contrast, most integral membrane proteins are expressed in complex mixtures in cells at much lower quantities, and thus require extensive purification for study. Bacteriorhodopsin is even easier to isolate for study than rhodopsin, but bacteriorhodopsin occurs in a crystalline membrane, which contains an unusually low fraction of lipid and is not a typical case. A number of mass spectrometry methods have been developed to study bacteriorhodopsin (107; 193-

195). We have chosen to focus our present efforts on optimizing protein biochemical methods for mass spectrometric analyses of vertebrate rhodopsin that are also compatible with gel filtration, and gel electrophoresis. Rhodopsin is a member of the large G protein-coupled receptor (GPCR) superfamily. The GPCR superfamily is particularly important because these proteins are the targets of a large fraction of pharmaceuticals and genomic analysis indicates that perhaps 5% of the proteins coded by the human genome are GPCRs (196).

Functional interactions of membrane proteins in signaling or adhesion pathways are often studied via photo cross-linking of peptides or radioligands to the proteins (197-199). Detailed structural information can be provided by MS analysis of the cross-linking sites (198; 200). In order to localize cross-links and other modifications with currently available mass analysis technology, it is essential to cut the protein into smaller peptides, using chemical and/or enzymatic cleavage. Purification and analysis of membrane proteins must usually occur in detergents to facilitate solubilization, penetration of enzymes and other reagents, chromatography, aliquoting, and accurate concentration determinations; however, most commonly used detergents tend to interfere with mass spectral analysis (201). Membrane proteins and their hydrophobic fragments tend to adhere to glass, plastic, or the surfaces of chromatographic supports, which can result in very significant sample losses upon manipulation. Fortunately, the detergent lauryldimethylamine oxide (LDAO) has been found to be a favorable detergent for effective solubilization and gel filtration analysis of rhodopsin and other hydrophobic proteins. LDAO can be largely removed, if needed, and most importantly LDAO does not interfere with MALDI MS (201).

For the reasons described above, mass spectrometric analysis of membrane protein digests requires enhanced methods that are highly sensitive, and that can tolerate

contamination. There have been few studies that have been able to mass identify fragments of membrane proteins, most have not been able to identify all fragments, had low sensitivity and/or incomplete sequence coverage. Orlando et al (202) reported a FAB/MS/MS method capable of identifying nine of the ten expected cyanogen bromide fragments of bacteriorhodopsin, and provided sequence information on six of the peptides. After trypsin digestion and HPLC in the detergent octyl glucoside and MALDI analysis, Barnidge, et al.(106) was able to recover all but one large hydrophobic fragment of rhodopsin. Trypsin cleaves largely near the membrane surfaces and yields highly hydrophobic peptides that are difficult to recover from chromatography. LeCoutre et al. (203) reported a method capable of identifying all the cyanogen bromide fragments of OmpA, the most abundant outer membrane protein in a crude extract of *Escherichia coli* membranes. Recently, it was reported (107) that all of the cyanogen bromide peptides of rhodopsin could be detected and sequenced by LC/MS, but this method required rather large amounts (4-6 nanomole) of starting material. Methods that require affinity purification and/or two dimensional gel electrophoresis before mass spectrometry have been reported (204; 205) that accurately identify membrane proteins of low copy number in cells. We report a simple method employing TCA concentration, ethanol extraction of contaminants, and CNBr digestion. When starting with as little as 30 picomole of rhodopsin in detergent-solubilized membranes it is sufficient to spot 1-5 pmole of digest on a MALDI sample well to obtain 99% sequence coverage.

Materials and Methods

Bovine retinal rod outer segment (ROS) membranes were prepared under dim red light (63; 190) and washed with water containing EDTA or 4M urea to strip off surface-bound proteins. Rhodopsin concentrations were determined by UV/VIS spectroscopy,

using an extinction coefficient of 42,700 M-1cm-1 at 500nm or 72,590 M-1cm-1 at 280nm (206). Typically 125 micrograms of rhodopsin in washed ROS were dissolved in 1mL 1% LDAO under dim red light, after which a difference optical absorption spectrum was measured before and after bleaching with white light to determine rhodopsin concentrations (207). Most aliquots were reduced with dithiothreitol (~15mM DTT) for one hour and alkylated with iodoacetamide (~100mM) for 2-3 hours. Some samples were reduced with 5mM DTT and alkylated with 15mM 5-iodoacetamido fluorescein (Molecular Probes) for later SDS PAGE analysis of the efficiency of CNBr cleavage. Samples were gassed with nitrogen or argon, tightly capped and tumbled during these incubations.

TCA precipitation is a useful method for recovering and concentrating proteins after chromatography in detergent (208) and for removing reagents used for protein chemistry. Rhodopsin irreversibly aggregates after TCA precipitation, and becomes insoluble in anything but neat TFA or formic acid. Formic acid was not used to avoid partial formylation of serines and threonines. Fortunately, the CNBr reaction proceeds efficiently in 80% TFA/ 20% water. 10-100 microliter aliquots of 3-5 micromolar rhodopsin dissolved in LDAO were precipitated with 10% TCA and spun on a tabletop centrifuge at 14K rpms for 2 minutes. The pellet was washed by bath sonication in 95% ethanol and the washed precipitate was collected by centrifugation to remove lipids, TCA and other reagents. The ethanol wash was repeated three times, after which the pellet was dissolved in 100% TFA, containing 500 molar excess CNBr per methionine in the sample. Distilled water was then added to make the final TFA concentration 80%. Samples to be digested were flushed with argon, and sonicated in a programmable bath sonicator intermittently (0.2 Hz, 1 sec pulses) in the dark for 24hrs during digestion. Digests were then diluted three fold with distilled water, and freeze dried. Small portions

were dissolved in SDS (at room temperature) for PAGE analysis. Tricine gels were purchased from BioRad, and gel electrophoresis was performed as previously described (209). Digests were dissolved in a minimum amount (20-50 microliters) of 50/50 water/acetonitrile, and freeze dried again to remove traces of TFA and CNBr. This latter step was repeated two to three times, and it was very helpful to obtain suitable matrix crystals for MALDI MS. A dilution series of the digest to be analyzed was made in 20/80 water/acetonitrile before mixing 1:1 to 3:1 with saturated MALDI matrix in 20/80 water/acetonitrile (alpha-cyano-4-hydroxycinnamic acid, or 2,5-dihydroxybenzoic acid). Typically, 0.1 to 0.3 microliters of matrix/sample mixture was spotted per well. Using the above procedure, we found that 10 microliters of 3 micromolar rhodopsin starting material (30 picomoles) was the minimum amount of rhodopsin required to obtain 99% sequence coverage. Fresh and high purity (99%) DHB and ACHA are recommended. Chemicals were purchased from Sigma/Aldich Chemical Co. except for LDAO (Calbiochem). High purity (>99%) cyanogen bromide should be used fresh to reduce tryptophan oxidation (210). MALDI TOF spectra were performed on Bruker BiFlex III or Perceptive Biosystems Voyager RP. Typical accelerating voltages were 20kV, and delayed extraction times on the BiFlexIII ranged from 100 to 400 nanoseconds. Spectra were averaged over 100 to 300 laser shots.

Results

Rhodopsin is perhaps the best-studied member of the vast GPCR superfamily. The x-ray structure of rhodopsin was recently reported (52), which reveals new features of its structure and confirms many aspects long anticipated (191). GPCRs span the membrane bilayer seven times and Figure 28 shows a diagram of the transmembrane

topology of bovine rhodopsin together with the amino acid sequence. The sixteen methionines, which are the sites of CNBr cleavage, are highlighted, as are the ten cysteines, which are important in the mass spectral analysis. Cysteines 321 and 322 are palmitoylated in the native protein. We find, consistent with a recent report (107), that it appears to be essential to alkylate cysteines to optimize recovery of peptides in mass spectral analysis. Asparagines two and fifteen bear N-linked glycosylation, which generate mass heterogeneity, due to differing numbers of sugars at these positions. Chemical cleavage of methionines with CNBr (211) is typically quite efficient, although reduced cleavage efficiency is reported for methionines followed by serine or threonine (212) and there is one Met-Ser and one Met-Thr in the bovine rhodopsin sequence.

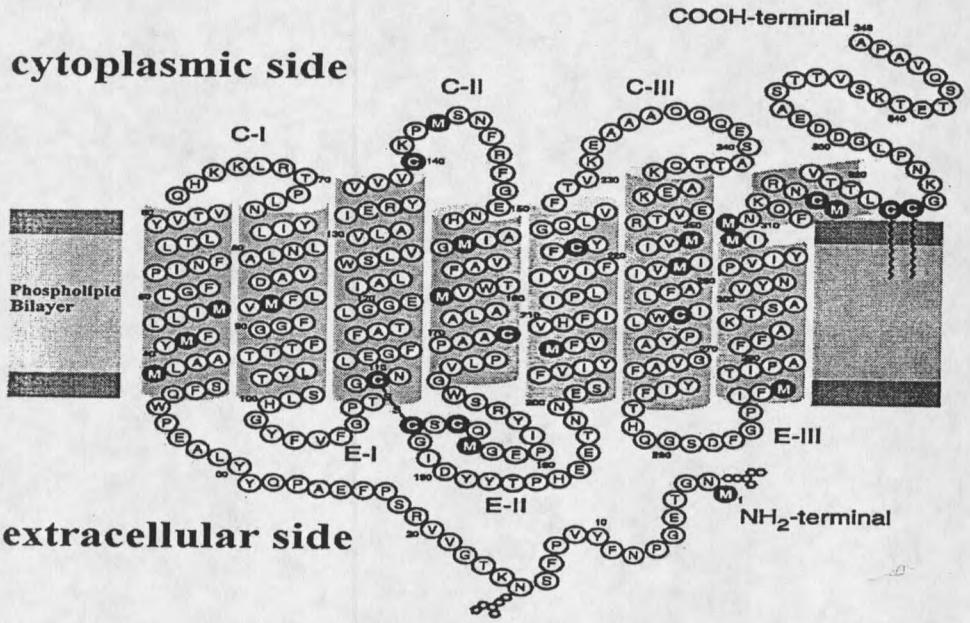


Figure 28. Transmembrane topological model of rhodopsin with highlighted methionines, which are cleaved by CNBr, and highlighted cysteines, which are best alkylated for these studies. This figure (52)is schematically reflective of the organization of the recently reported rhodopsin crystal structure (28).

The several post-translational modifications, as well as solubility problems with many of the peptides, complicate complete analysis of rhodopsin digestion products. To minimize the number of fragments and increase the ease of accurately mass analyzing digests, it is important to optimize the cleavage conditions to minimize missed cleavages. SDS-PAGE in tricine gels was found to be a useful method for routinely assessing the fraction of rhodopsin that is cleaved; however, protein staining on PAGE gels strongly favors detection of high molecular weight species. To more accurately measure CNBr digestion, we labeled rhodopsin sulfhydryl groups with iodofluorescein after DTT reduction and observed the digests by fluorescence on the gels. Figure 29 shows fluorescein-labeled, CNBr digested rhodopsin and undigested fluorescein-labeled rhodopsin on 16.5% tricine SDS-PAGE gels, which are able to resolve small peptides. Seven of the CNBr fragments of rhodopsin contain cysteine residues and can be labeled by alkylation with iodo-fluorescein. Gels were imaged with a BioRad Fluor-S MultiImager. Figure 29 shows a fluorescence emission image of a tricine gel, using broad band UV excitation centered at 302nm. Lane 3 contains about 50 picomoles of fluorescently labeled, undigested rhodopsin. The monomer (MW ~40kDa) is predominately detected in lane 3, with faint noncovalent multimers of rhodopsin present at higher molecular weights. Lane 1 contains 280 picomole of a synthetic fluorescein-labeled peptide standard of approximately 2400 Da. Lane 2 contains about 300 picomole of fluorescently-labeled, CNBr digested rhodopsin and shows that no undigested rhodopsin can be detected. The estimated detection limit at this exposure level is about 10 picomoles.Some of the smaller fragments (<4000 Da) in Lane 2 run so closely on the gels that they could not be clearly resolved. The highest molecular weight clearly detected in Lane 2 migrates below 10,000 Da. This band is most likely fragment 87-143 (MW~ 6800) with one or two cysteines tagged with iodofluorescein. Essentially complete

delipidation and removal of detergent through TCA precipitation and washing by sonication in ethanol was necessary to achieve good resolution on the tricine gels. LDAO completely solubilizes but does not denature dark-adapted rhodopsin (207) and LDAO was also found to be compatible with the mass spectral methods used in the present work. LDAO solubilized rhodopsin (10-100 microliters, 3-5 micromolar) was reduced with DTT and the sulphydryls alkylated for most experiments. Iodoacetic acid was previously reported to give poor detection of cysteine-containing fragments in LC/ESI/MS (107), therefore reduction of disulfides with tributyl phosphine and sulphydryl alkylation with vinyl pyridine in 50% n-propanol was recommended. We found that this latter method irreversibly aggregated the rhodopsin and thus interfered with gel filtration analysis of undigested rhodopsin. Reduction and alkylation were found to go to completion with DTT and the non-ionic sulfhydryl alkylation reagent iodoacetamide, if ROS were solubilized in LDAO or SDS detergent. We found that gel filtration analysis was important for monitoring protein labeling in other experiments and for monitoring digestion with CNBr, and thus we used the DTT/iodoacetamide method for reduction, alkylation, and analysis of the proteins before digestion.

Prior to CNBr digestion, aliquots were usually subjected to 10% trichloroacetic acid (TCA) precipitation, and several steps of washing with ethanol, during bath sonication, to remove TCA, detergent, lipids, and reducing and alkylating reagents. TCA precipitation was not required to obtain MALDI spectra; however, it served to concentrate dilute rhodopsin in pellets in microfuge tubes after centrifugation and thus facilitated the recovery of small amounts of protein material. Contaminants, such as detergents, lipids, and reducing and alkylating reagents, could be tolerated if the starting concentration of rhodopsin was high, but once the protein concentrations reach the low micromolar range it was essential to concentrate by TCA precipitation and remove non-

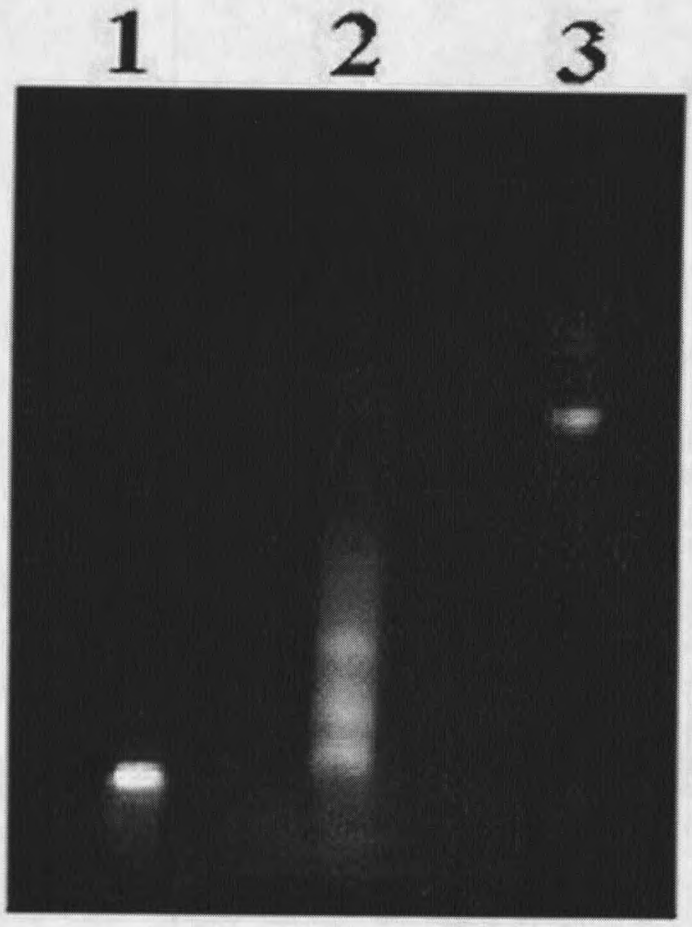


Figure 29. SDS-PAGE analysis of fluorescein labeled proteins and peptides. Fluorescence image of a 16.5% tricine gel, as explained in Materials and Methods. Lane 1, 280 picomole of fluorescein labeled peptide standard, MW ~2400; Lane 2, CNBr digest of fluorescein labeled rhodopsin; Lane 3, fluorescein labeled undigested rhodopsin.

protein contaminants by ethanol washing to obtain MALDI spectra. Proteins solubilized in other detergents (such as octyl glucoside) will TCA precipitate, and contaminants can then be removed by ethanol washing. Proteins solubilized in SDS will not TCA precipitate without an RNA carrier (23), and therefore SDS was not used. While contaminants were not always detrimental to MALDI spectra, we found that they severely interfered with LC-ESI-MS of the digests, if not removed (data not shown). Washed TCA pellets were dissolved in 100% trifluoroacetic acid containing 500 M excess of CNBr relative to protein methionines. After dissolution, distilled water was added to 20%, tubes were flushed with nitrogen and capped. The added water was found to be essential for efficient CNBr digestion. The digestion tubes were sonicated intermittently in a water bath overnight (~24hrs) in the dark. MALDI analyses indicated that sonication helped foster cleavage to completion (data not shown), presumably by enhancing the access of the reagents to the bonds to be cleaved. Samples were diluted 2-3X with water after digestion and freeze dried. Several subsequent cycles of dissolution of the digests in a minimum amount (10-20 microliters) of 50/50 water/acetonitrile, and freeze drying, more completely removed volatile contaminants, improved MS resolution, and concentrated small sample amounts. MALDI sample preparation is discussed further in the Materials and Methods section. We found that starting with 10uL of a 3 micromolar rhodopsin solution solubilized in 1% LDAO, containing ~ 30 picomole rhodopsin, was sufficient material for sample work-up to obtain mass spectra covering 99% of rhodopsin's sequence, missing only two single methionines. A total of 1-5 picomole of the 30 picomole sample was needed for MALDI, leaving the remainder for other analyses.

A portion of a MALDI MS spectrum (acquired on the Bruker Biflex III) of a CNBr digest of rhodopsin is shown in Figures 30. This spectrum was acquired near the

laser intensity threshold for obtaining signals to maximize resolution and mass accuracy. This spectrum contains 91% sequence coverage. The matrix, alpha-cyano-4-hydroxycinnamic acid (ACHA), consistently yielded higher resolution than 2,5-dihydroxybenzoic acid (DHB). Ion intensities were quite variable from spot to spot on the sample plate, as is often seen in MALDI. To greatly reduce chemical noise produced by matrix ions, and to obtain the best resolution and intensity for all fragments,

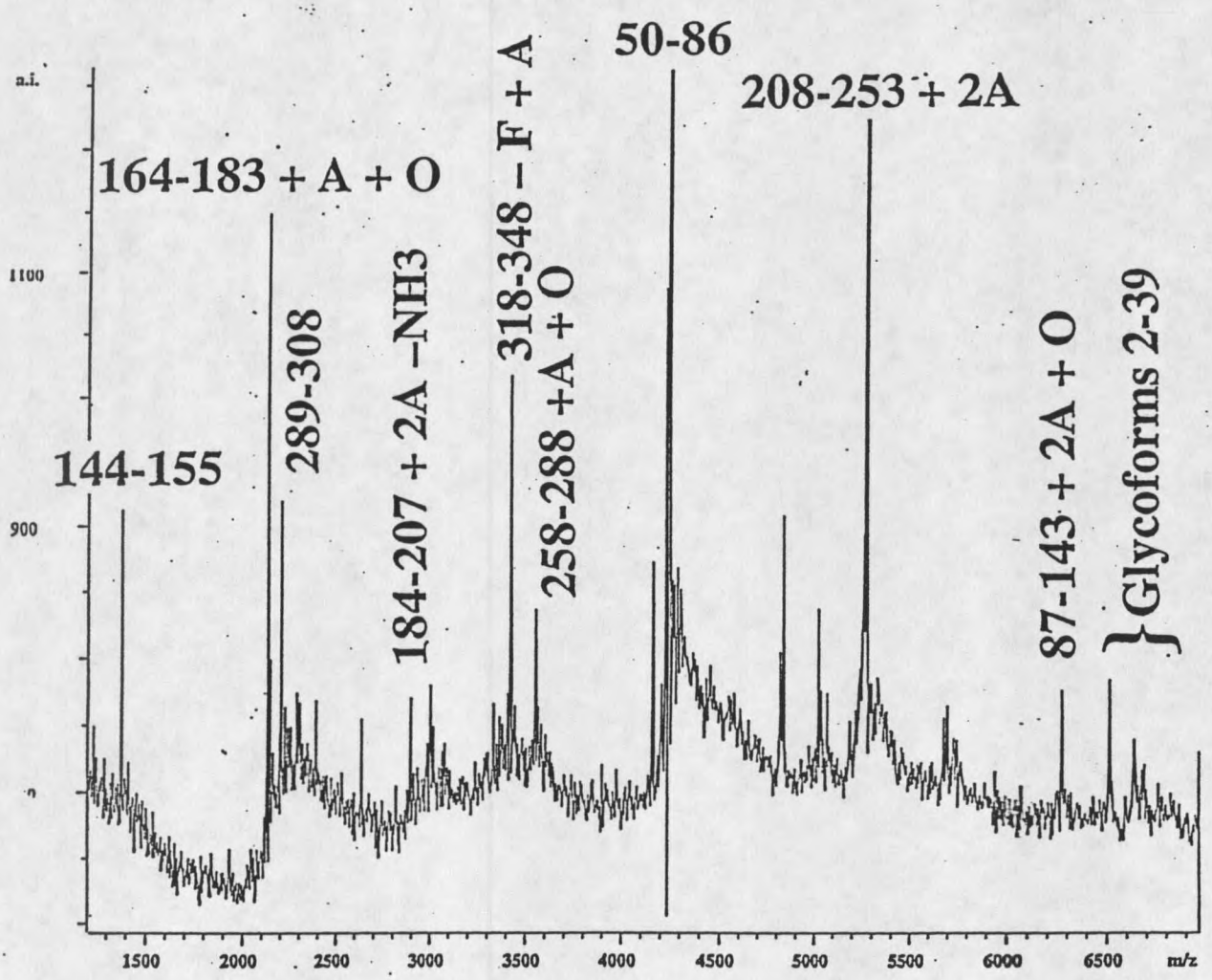


Figure 30. Delayed extraction and reflected MALDI spectrum of 2 picomole of reduced and thiol alkylated rhodopsin cyanogen bromide digest in alpha-cyano-4-hydroxycinnamic acid.

the deflector was set to 400 and acquisition conditions were optimized for a broad range. Markedly improved resolution and mass accuracy could be obtained on any single ion of interest by optimizing the laser power, extraction delay, and second stage extraction voltage for its particular mass range and searching for sweet spots on the sample. We could obtain monoisotopic mass resolution on rhodopsin peptides up to about 5300 Da using ACHA as a matrix, as shown in Figure 31. Rhodopsin CNBr fragments larger than 5300 were usually observed as their average mass.

The masses that were attributed to rhodopsin, together with their corresponding theoretical rhodopsin CNBr fragment masses, are shown in Table 3. Internal calibration with monoisotopic masses of selected rhodopsin CNBr fragments resulted in the observed masses shown in Table 3. The entire sequence was identified except for fragments 1 and 309, which are the remains of single methionines. These methionine fragments must be present in the digests, because their neighboring fragments are detected, but they are obscured by matrix ions even without the use of a low mass gate. Many peaks that were detected with significant signal to noise ratio do not match rhodopsin CNBr fragments. These unassigned peptide peaks are not labeled in the spectra and are not listed in Table 3. The masses of the unknown peaks do not match *expected* incomplete cleavage products of rhodopsin to within 0.05% error. Some of the unidentified peaks might be explained by modified incompletely cleaved fragments of rhodopsin, if CNBr intermediates (213), oxidation, fragmentation, and/or neutral losses are posited. Further analysis is ongoing to identify unknown peaks.

We found that fragments containing cysteines tend to yield substantially better sensitivity after reduction and alkylation of the sulfhydryl groups, consistent with the

LC/MS results of Ball et al (107). The sample shown in Figure 3 is from 2.0 picomole of a CNBr digest from reduced and alkylated rhodopsin spotted in the sample well. Differences between the the unreduced and unalkylated vs. reduced and alkylated spectra included mass shifts of +57 due to the addition of one acetamide for fragments 164-183, 208-253, and 258-288 which contain one cysteine, and mass shifts of +114 due to the

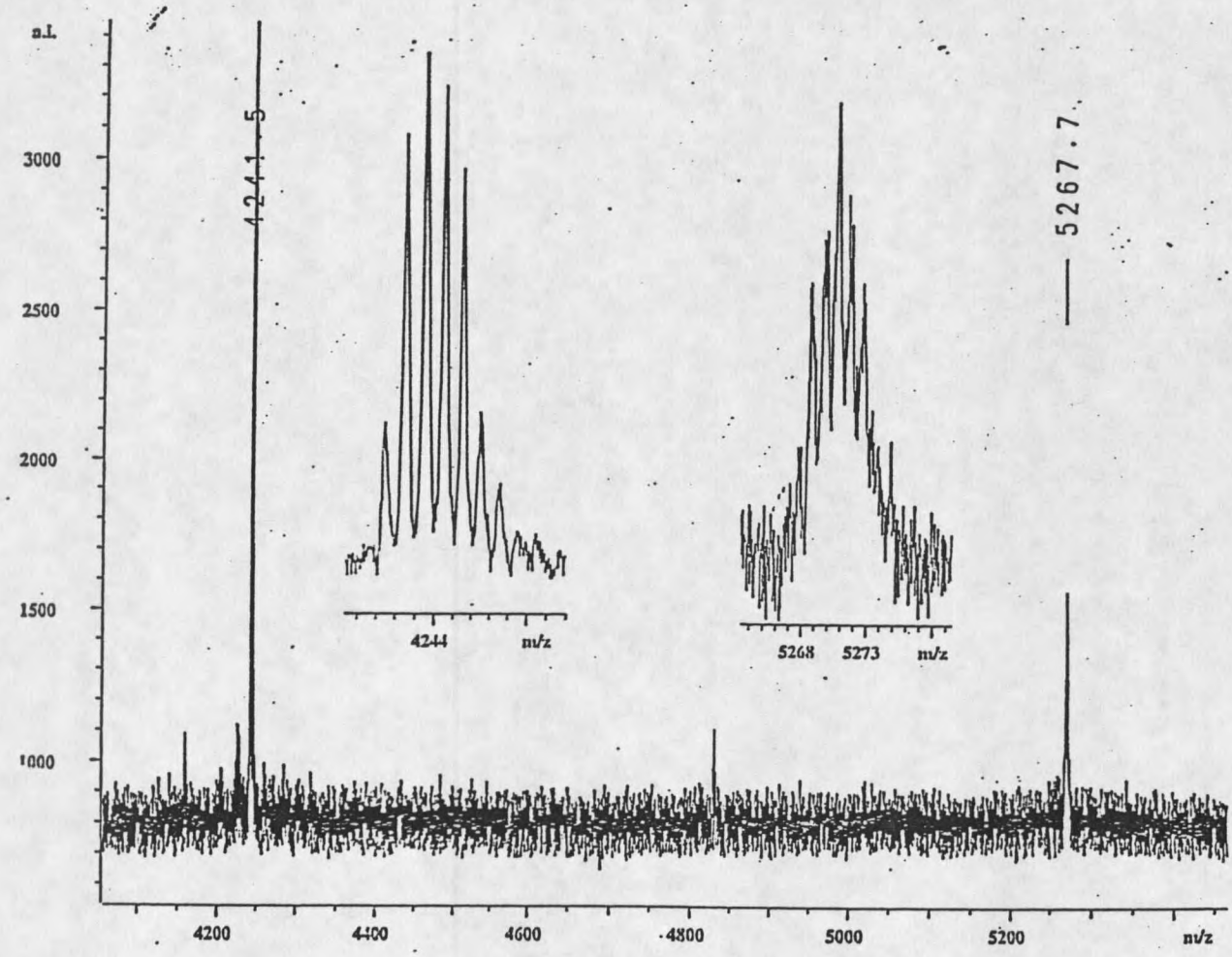


Figure 31. Unsmoothed (to clearly display monoisotopic resolution of the insets) reflected and delayed extraction MALDI spectrum of 4 picomole of reduced and thiol alkylated rhodopsin cyanogen bromide digest in alpha-cyano-4-hydroxycinnamic acid.

addition of two acetamides for fragments 87-143 and 184-207, which contain two cysteines. Palmitoyl groups are bound to cysteines by thioester linkages in fragment 318-348, and are labile to removal by transesterfication with DTT. Removal of fatty acids was not driven to completion under the analysis conditions for the sample shown in Figure 30. If a high enough fresh DTT concentration (40 millimolar) is used, both cysteines can be deacylated and then completely alkylated. Fragment 318-348 contains one deacylated and acetamide alkylated cysteine and one remaining palmitoyl group. All in four possible forms of the 318-348 fragment have been observed in different experiments (as listed in TABLE 3). Fragment 184-207 is primarily detected as a pyroglutamate. Many glycoforms of fragment 2-39 are detected. The most intense glycoform is approximately 6501.8 molecular weight, as previously reported (107). This glycosylation adds 2194.7 Da to the unmodified 4307.1 Da molecular weight of fragment 2-39. Often, an almost equally intense ion is found at 6298.6 molecular weight (spectrum not shown), which corresponds to one N-acetylglucosamine less than the major glycoform. This rhodopsin CNBr fragment contains one of the core oligosaccharides with three mannose and two N-acetylglucosamines, that is the basis for addition of sugars to form heterogeneous glycoproteins (214).

Tryptophan-containing fragments (2-39, 87-143, 164-183, 258-288), show a mixture of oxidized (+16) and unoxidized products. As previously reported (210) the use of fresh CNBr reduced tryptophan oxidation (results not shown). It is important to note that fragments containing cysteines and no tryptophan did not show detectable oxidized products

TABLE 3

Rhodopsin Cyanogen Bromide Fragments

OBSERVED MASS	THEORETICAL MASS Monoisotopic	Average	SEQUENCE IDENTIFICATION	ION TYPE
427.1*	427.3	427.6	254-257	MH+
449.3*	449.3	449.6	254-257	Na+
520.3*	520.3	520.6	40-44	MH+
588.4*	588.4	588.8	45-49	MH+
610.5	610.4	610.8	45-49	Na+
626.5	626.4	626.8	45-49	K+
862.4*	862.4	863.0	156-163	MH+
878.4*	878.4	879.0	156-163 + O	MH+
1049.5*	1049.5	1050.2	310-319 + A	MH+
1107.4	1107.6	1108.5	40-49 (-30)	MH+
1374.6*	1374.7	1375.5	144-155	MH+
2054.0	2054.1	2055.4	164-183	MH+
2110.9*	2111.1	2112.5	164-183 +A	MH+
2127.1*	2127.1	2128.5	164-183 +O,A	MH+
2198.3*	2198.2	2199.6	289-308	MH+
2220.9*	2221.2	2221.6	289-308	Na+
2398.6	2299.2	2300.8	289-309 (-30)	MH+
2778.6	2778.2	2780.0	184-207 -NH3	MH+
2892.2*	2892.2	2894.1	184-207 +2A-NH3	MH+
2909.1*	2909.2	2911.1	187-207 +2A	MH+
3124.3	3123.5	3125.4	318-348 -2F	MH+
3237.6*	3237.5	3239.6	318-348 -2F+2A	MH+
3418.8*	3418.7	3420.9	318-348 -F+A	MH+
3536.7	3532.8	3535.1	258-288 +A	MH+
3548.5*	3548.8	3551.1	258-288 +A+O	MH+
3604.1	3599.9	3602.3	318-348 (+2F)	MH+
4224.1*	4224.4	4227.1	50-86 -NH3	MH+
4241.5	4241.4	4244.1	50-86	MH+
5267.4*	5267.8	5271.1	208-253 + A	MH+
6274.8*	6273.2	6277.3	87-143 +2A+O	MH+
6300.2	6294.8	6298.6	2-39 +G	MH+
6314.3*	6310.8	6314.6	2-39 +G +O	MH+
6502.3	6497.8	6501.8	2-39 +G	MH+
6516.9*	6513.8	6517.8	2-39 +G+O	MH+

O = oxygen NH3= ammonia
W= water F= palmitoyl -30 = CNBr intermediate (33)
A = acetamide G= glycosylations

* Low masses calibrated internally with monoisotopic DHB matix dimer (309.061) and fragment 310-319 + A (1049.495) and/or fragment 144-155 (1374.655). High masses were calibrated internally with monoisotopic masses of fragment 310-319 +A, and fragment 50-86 (4241.425).

Table 3. Peptide masses matched to within 0.05% of the masses expected for the cyanogen bromide digest of rhodopsin. Cysteines were alkylated with iodoacetamide.

Sensitivity was better in linear mode than in reflector mode, which indicates there was significant metastable ion decay before reflection. Figure 32 was acquired in linear mode with the matrix DHB, and displays the fragments 254- 257(427.1 Daltons), 40-44(520.3 Daltons), 45-49(588.4 Daltons),156-163(878.4 Daltons), and 310-317(1049.6 Daltons). Typically, it was not possible to obtain the MH+ ion of the lowest mass fragments 254-257, and 40-44 in reflector mode, where as the larger fragments 45-49, 156-163, and 310-317 were easy to observe in reflector mode. The lowest mass fragments 254-257, and 40-44 were observable with the matrix DHB, but not ACHA. Figure 32 was acquired with the low mass gate set to 200 Da, and calibrated internally with the monoisotopic mass of a matrix dimer and the monoisotopic mass of fragment 310-317 at 1049.5 Daltons. Although not shown in this particular figure, the lower mass fragments often ionize as Na+ and K+ adducts, and these adducts were useful in assigning fragments 254-257, 40-44, and 45-49.

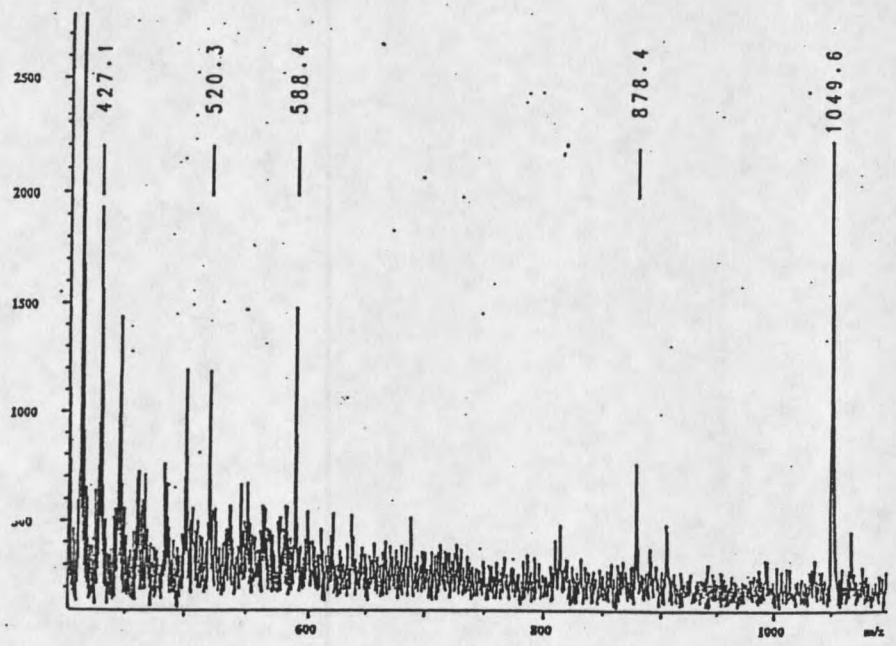


Figure 32. Linear mode, delayed extraction MALDI spectrum of 4 picomole of reduced and thiol alkylated rhodopsin cyanogen bromide digest in 2,5-dihydroxybenzoic acid.

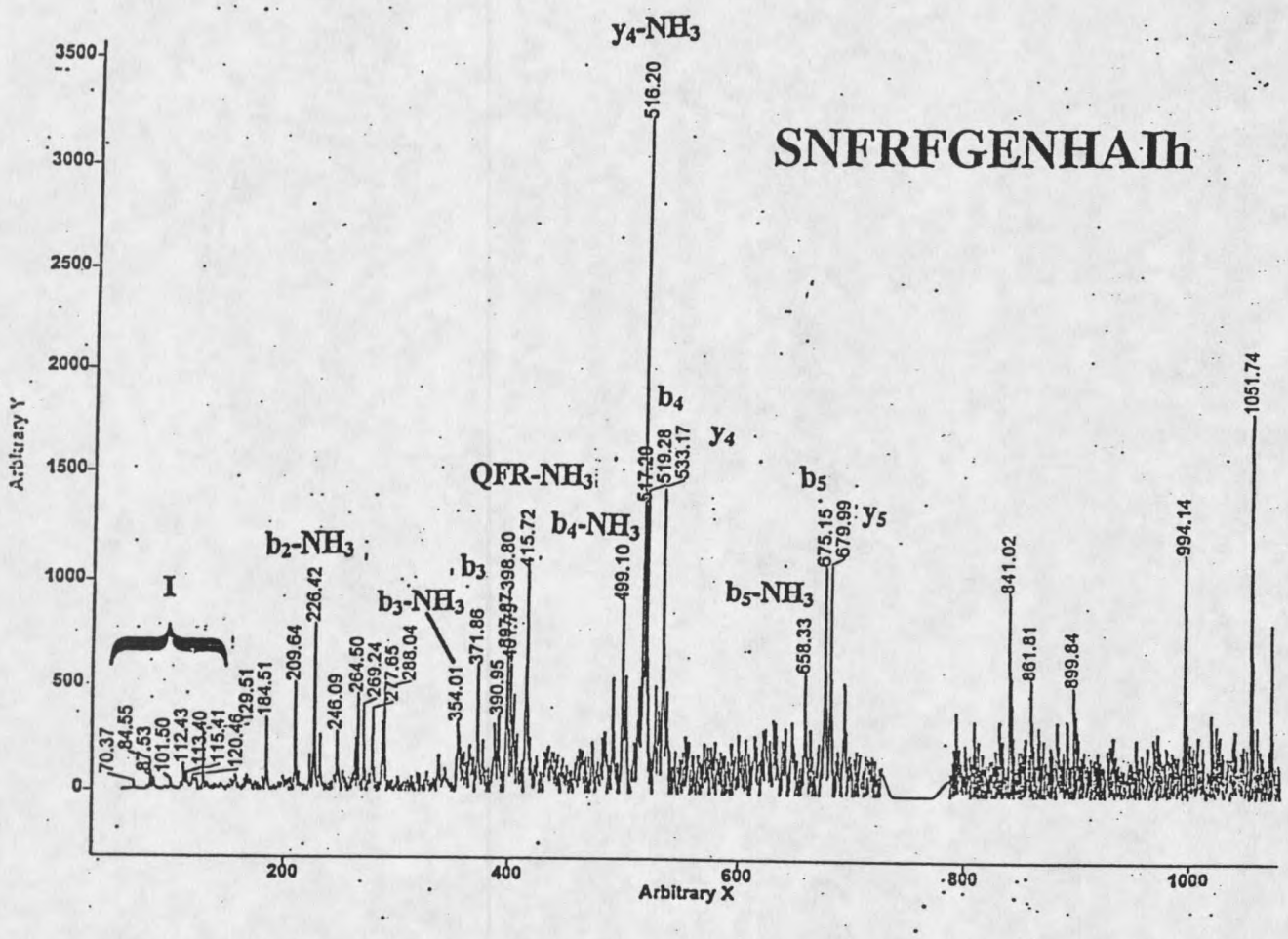


Figure 33. MALDI post source decay (PSD) spectrum of fragment 310-317. Standard one letter amino acid residue abbreviations are used for the peptide sequence (h = homoserine lactone) and fragment ions are labeled accordingly (36).

Post source decay (PSD) fragmentation carried out at higher laser power can identify sequences by their "mass finger print" (156). Figure 33 displays, for example, a PSD spectrum of fragment 310-317, derived from the parent ion of molecular weight 1051.74 Da (the calibration of this particular spectrum is slightly high for all masses). Primarily "b- and y- ions" (215) are detected, and are labeled accordingly. In addition, immonium ions for N, K, Q,

F and R are detected between 70 and 129 Da. supporting the composition of this peptide. While PSD was not the primary focus of the method development targets in this paper, it was also used to confirm the identities of the sodiated fragment 254-257 (449.3 Daltons), and fragment 144-155 (1374.6 Daltons).

Discussion

Investigation of the function of eukaryotic integral membrane proteins and their site-specific mutations necessitates the use of eukaryotic expression systems to obtain proper folding, and post-translational modifications. Eukaryotic membrane proteins are typically expressed in very low levels and thus the study of these proteins requires the use of radioactive or fluorescently labeled ligands for functional detection. Bovine rhodopsin and bacteriorhodopsin are the only integral membrane proteins that have been directly sequenced by mass spectrometry and their post-translational modifications fully analyzed. The sequences of other membrane proteins are most often deduced indirectly from their cDNA, and many of their post translational modifications are not measured directly. Methods that increase sensitivity are highly desirable to extend the capabilities of mass spectrometry to study membrane proteins. Mass spectrometric detection limits are often quoted as 50 femtomole or lower for highly purified proteins (187; 216). For most proteins, background from contamination raises detection limits in practice, and picomole amounts are often required for mass spectrometric detection (201; 217-219). One microliter of one micromolar protein solution yields a picomole of protein. In order to obtain even low micromolar concentrations, most membrane proteins have to be purified in detergent and concentrated. Optimization of reduction and alkylation yield and cleavage methods is also essential to achieve high sensitivity in mass spectrometric detection of membrane protein fragments. The fluorescein labeling and cyanogen

bromide digestion of rhodopsin depicted in the tricine gel in Figure 2, demonstrates that the digestion methods used in this study are effective. TCA precipitation and ethanol washing serves to rapidly concentrate dilute protein solutions, and to remove protein modification reagents, lipids, and detergents which may be detrimental to mass spectral analysis. Sample losses in chromatography tend to be large for hydrophobic fragments of membrane proteins. Chromatography was avoided in the present studies by the use of MALDI, and the removal of contaminants led to improvements in sensitivity, enabling detection of all cyanogen bromide digestion product peptides from 10 microliters of 3 micromolar rhodopsin. As little as 1 picomole of the digest could be spotted, using the MALDI MS method described in this paper, and still obtain 99% sequence coverage. Partial peptide sequences could be obtained on the same samples using PSD. In general, the fragments having the highest relative intensity have lower masses, lowest detection limits, and have higher numbers of charged residues in the sequence. Some of the fragments of rhodopsin show sub-picomole detection limits. Ion intensities similar to those seen in Figure 3 are typically found in many spectra; however, 5-10X variation in ion intensity was common for all ions. The older Perceptive Biosystems RP MALDI, without delayed ion extraction, was also capable of yielding 99% sequence coverage (albeit with much less resolution and mass accuracy and much greater uncertainty of ion assignment) with one picomole samples (data not shown).

Ion suppression and concomitant loss or reduction of ion signals is a common phenomenon in MS of protein/peptide mixtures, and thus separation of mixtures by liquid chromatography before MS is desirable. Reverse phase LC-MS is an excellent method for achieving this goal if the mixture contains well-behaved proteins/peptides in sufficient quantity. Ball et al. (107) report an LC/MS method for identifying most of the bovine rhodopsin CNBr fragments during a 90 minute chromatographic run. The Ball

method required 6 nanomole (~250 micrograms) of starting material, which is 200 fold more material than the 30 picomole required for the MALDI method described here. A later paper by Ablonczy et al (210) using the Ball et al method (107), reported similar results for rat rhodopsin with a similar quantity of starting material (approximately 4 nmoles/175 micrograms). MALDI analysis is very fast, and the data analysis is relatively straightforward, since MALDI produces primarily singly charged ions and thus no spectral deconvolution is required.

Since rhodopsin is 90% + pure in the rod outer segments, and the rhodopsin CNBr fragments have been previously characterized (107; 210), the primary focus of this work was to optimize biochemical methods to observe all rhodopsin CNBr fragments by mass spectrometry at the picomole level. It was difficult to obtain the 300 ppm instrument specified mass accuracy for external calibration over the broad range of 300-7000 Da. This difficulty with mass accuracy is most likely because the large number of fragments to assign, and the laser threshold for these hydrophobic peptides was significantly higher than the synthetic standards used for external calibration. In this regard, the calibration of the LC-MS method reported by Ball et al is significantly easier, since the external calibration of an ion trap (or quadrapole mass filter) of peptide ions produced by electrospray does not suffer from the inherent kinetic energy differences produced by laser desorption. Ball et al reported average masses for fragments greater than 2000 Da, while with the Bruker Biflex III were able to obtain monoisotopic mass resolution up to about 5300 Da. Multiple internal calibrations using monoisotopic masses of CNBr fragments attributed to rhodopsin were required to obtain the best mass accuracy. All of the internally calibrated masses in Table 1 have mass accuracies <100ppm, except for fragment 254-257. The mass error on the fragment attributed to the 254-257 peptide of almost 500 ppm, calls its identification into question. It's sodium adduct, on the other

hand, had no significant mass error, and was mass fingerprinted by PSD (data not shown). PSD analysis was not the focus of this work, but future PSD analysis of unknowns not mass matched to expected CNBr fragments of rhodopsin seems feasible, and may lead to their identification.

Conclusion

Sensitivity improvements and the essentially full sequence coverage of rhodopsin reported in this biochemical method for detergent-solubilized retinal rod membrane digests is a significant step towards practical MS analysis of membrane proteins. This method may also be useful for mass spectrometric studies of other membrane systems containing numerous different proteins without fractionation. Membrane proteins have been difficult to analyze and most membrane proteins occur in highly complex mixtures in low quantities in native membranes, requiring gel filtration, gel electrophoresis, antibody precipitation, chromatography or other purification in detergent prior to the application of the mass analysis protocol presented.

Acknowledgements

We thank Paul Kowalski, Nigel Ewing, and Maryann Shen at Bruker Daltonics Corporation; David Ledman and Cheny Krishnan at PE Biosystems; and Richard Barry and Blaine Roberts at Montana State University for assistance with measuring some of the mass spectra. We thank Heide Hamm for ROS membrane preparations, and Jan Sunner and Daniel Knapp for useful discussions. This work was partially supported by NIH EY06913 and NSF MCB 9904009 (to EAD).

CHAPTER 5

CONCLUSIONS AND FUTURE WORK

We have made significant progress on four fronts during the course of this thesis research: 1) desorption of proteins and peptides from aqueous solutions, and discovery of some the fundamental mechanisms involved in MALDI (220); 2) synthesis of biologically active photo-activatable peptides and cross-linking to rhodopsin; 3) identification of a new more potent peptide candidate for cross-linking to rhodopsin, the formyl peptide receptor, and possibly other GPCR's implicated in the mechanism of nucleotide exchange; 4) discovery of the conditions for observation of all of cyanogen bromide fragments of rhodopsin by MALDI-MS with picomole sensitivity(221). Despite this progress, we have not achieved an initial goal of observing specific non-covalent interactions by IR laser desorption mass spectrometry. Neither have we conclusively identified the amino acid residues in contact between transducin and rhodopsin by photo cross-linking.

Preservation of non-covalent complexes in laser desorption experiments.

In the current laser desoption method of mass spectrometry from aqueous solutions, "Cryo-IR SALDI", only non-specific clustering has been observed between proteins. The strong protein complexes (trypsin & trypsin inhibitor, myoglobin & heme) are mostly observed in their dissociated monomeric states (data not shown). Non-specific clustering between proteins is predominant in most spectra (see Chapter 1). This has also

been observed by Berkenkamp et al (222). What is novel about our method is the ability to observe very high charge states on proteins in thymine and ACHA solid suspensions. The highest charge states observed so far, +14 on cytochrome C (data not shown), have been with evaporated sucrose thymine or ACHA solid suspensions at room temperature. It is clear that these are preformed ions, as discussed in Chapter 1. A smooth single distribution of charge states is observed with all solid suspensions, whether they yield high or low mass/charge ratios. Thus it is thought that one ionization process is responsible for both. Some evidence suggests that increases in the rates of electron-protein recombination result a reduction in charge and in a shift from low to high mass to charge ratios. Protein and peptide ions are always observed as MH_n+, and rarely MH+X, where X = an atomic counter anion. The source of such a rate difference could be water shielding of electron-protein interactions in the plume. Experiments with diethylamine mixed in cryo-protein-solid suspensions indicated that proton exchange interaction from MH+ ions to the neutral diethylamine were markedly lower than those observed in FAB TOF MS (220). Electron capture in the plume or immobilization of electrons on the solid surface by the matrix could also contribute to differences in electron-protein recombination. Experiments in the negative ion mode may provide evidence for whether or not electron-protein recombination is the ionization mechanism resulting in different mass/charge ratios. In negative ion mode it should be proton-protein recombination that is responsible for mass/charge ratio difference, and since protons should have significantly lower mobility than electrons in the electric field, one might expect to observe even higher charge states (lower mass to charge ratios) in negative ion mode.

Adding metal powders/filings to the suspensions should provide a good source of electrons upon laser excitation of the suspension, and this could shift the mass/charge ratio higher. If water is the most important factor in producing high charge states, experiments that alter the dielectric constant of the plume reveal may reveal evidence for this mechanism. Experiments in which the electric field was lowered from 20 to 10 KV did not produce noticeable changes in protein mass to charge ratios, but the instrument that these experiments were preformed on used a single stage constant extraction. The new Bruker Biflex III installed at Montana State University has delayed ion extraction capabilities, and an extra port for the IR laser. The introduction of a field free time period after the laser desorption may produce a change in protein charge to mass ratios with the neutral thymine solid suspension.

The mechanism of the ionization process (or the mechanism of the ion-recombination process) is critical not only for preserving specific non-covalent protein complexes, but also for determining sensitivity and resolution of large analytes. Most laser desorption TOF experiments currently do not preserve specific non-covalent complexes. The mass limit of laser desorption TOF mass spectrometry is about 1 million Daltons (223). Unit resolution extends to about 6000 Da, but it drops rapidly to about 70 mass/delta mass for larger molecules. A critical observation is that the distribution of protein peaks with different mass to charge ratios is pH independent (pH 1 to 8). One ***distribution*** of protein peaks, whether they be high or low mass to charge ratio, are observed in with all SALDI solids. If ions are preformed, and high electron protein recombination rates are responsible for observation of high mass/charge ratios (low

charge states), one might conclude that all proteins and peptide start from a fully charged state (ie in positive ion mode all amines and carboxylic acids protonated). This state would likely not preserve specific non-covalent complexes.

A more likely place to find preservation of specific non-covalent complexes may be in the delayed ablation products. The ions observed in Cryo-IR SALDI and traditional UV-MADLI are "dry" monomolecular ions desorbed in few nanoseconds of the laser pulse. Ion peak widths are less than a microsecond long even for small proteins (so little water is bound to each protein). Cummings & Walsh (224) characterized the desorption process by measuring the length of time of IR that the product of IR laser ablation appear, using a helium-neon laser parallel to the sample surface. Ablation products peaked at 5 microseconds and continued for 50 microseconds. Similar observations were made with laser post ionization measurements of the plume on our own instrument (data not shown). Frozen analyte solutions yield no ions upon IR laser ablation, but post ionization with a 248nm excimer laser focused on the plume of frozen tryptophan solutions, allowed mapping of the plume. Tryptophan intensity was measured with increasing time delay between the IR laser and the excimer laser. Williams et al (225; 226) was able to desorb and collect very large intact DNA fragments from thin aqueous frozen films on an electrode opposite the desorption site, but typically no ions were observed. We and Berkenkamp et al (222) also observed no ions from bulk aqueous protein solutions, even though the IR laser ablation gives very high ablation yields (227). The problem may be that the desorbed material is mainly neutrals. It may also be that the analyte molecules in the delayed ablation products are large clusters that either never hit the detector or create

a signal that is so broad that it is never resolved. Clustering is observable from IR laser desorption of frozen water/glycerol/salt solutions in the absence of protein (data not shown). Others have also observed very large clusters in laser desorption TOF MS (222; 223). Experiments with a second IR laser focused on the plume may be able to reduce the size of these clusters and make observation of monomolecular species. A very low UV wavelength laser (193nm, 157nm, or 93nm) may prove better than IR for post-source ionization/dehydration. Excitation with this wavelength may not preserve non-covalent complexes, but it may desolvate analytes more efficiently since the extinction coefficient of water rises rapidly below 200nm (228; 229). A softer ionization method recently described (230) should also be considered. An electron gun instead of a very low UV laser aimed at the plume in the experimental setup described by Jongma et al (229) proved useful for ionizing large molecular weight laser ablation products. Post ionization of delayed ablation products may not suffer from extensive surface charging problems that are posited in the mechanism of traditional laser desorption/ionization experiments (220), and thus may offer a means of preserving specific non-covalent complexes.

Defining the amino acid molecular contacts between rhodopsin and transducin.

We have made many attempts to isolate the site of cross-linking between benzoyl phenylalanine containing Gt alpha peptides and rhodopsin, but so far we have not been able to confidently assign the cross-link site. Figure 34 summarizes the cross-linking and isolation strategy used with cyanogen bromide digestion (for further details see Methods

and Materials Chapters 3&4). Assessment of cross-linking yield is also provided at each step. After extensive washing to remove unbound peptide, we currently obtain 3-5% yield of fluorescent peptide-rhodopsin cross-link relative to the total rhodopsin. In a typical experiment, 1mL of 5uM fluorescent peptide and 5uM rhodopsin is exposed to 15 minutes of 313nm filtered UV light from a high pressure mercury lamp. Thus of 5000 picomole of total rhodopsin, about 150-250 picomoles have fluorescent peptide cross-linked to it, as determined by comparison to a fluorescent standard. Typically the cross-linked material from 6 to 8 experiments are pooled, reduced and alkylated, and digested with cyanogen bromide in 80:20 TFA:water for 24 hrs. Reductions in fluorescence after cyanogen bromide cleavage are 10-50%. Too much CNBr can quench all fluorescein fluorescence; too little results in inefficient cleavage. Anti-fluorescein antibodies attached to CNBr-Sepharose beads are able to bind about 50% of detergent (1% LDAO) solubilized fluorescent peptide-rhodopsin fragments. Elution from the beads then yields 310-800 picomole of fluorescent peptide cross-link from the original pooled samples. If this elution were 100% pure, MALDI-MS identification would be trivial. MALDI-MS has identified many peaks, many of which are known rhodopsin cyanogen bromide fragments (data not shown). The laser power required for ionization threshold for peaks identified has been very high suggesting that many impurities are eluted from the affinity beads along with the desorbed peptides. As a result of the high laser power the peaks have been of low resolution, and have not consistently implicated cross-linking to particular rhodopsin cyanogen bromide fragments. 16.5% acrylamide tris-

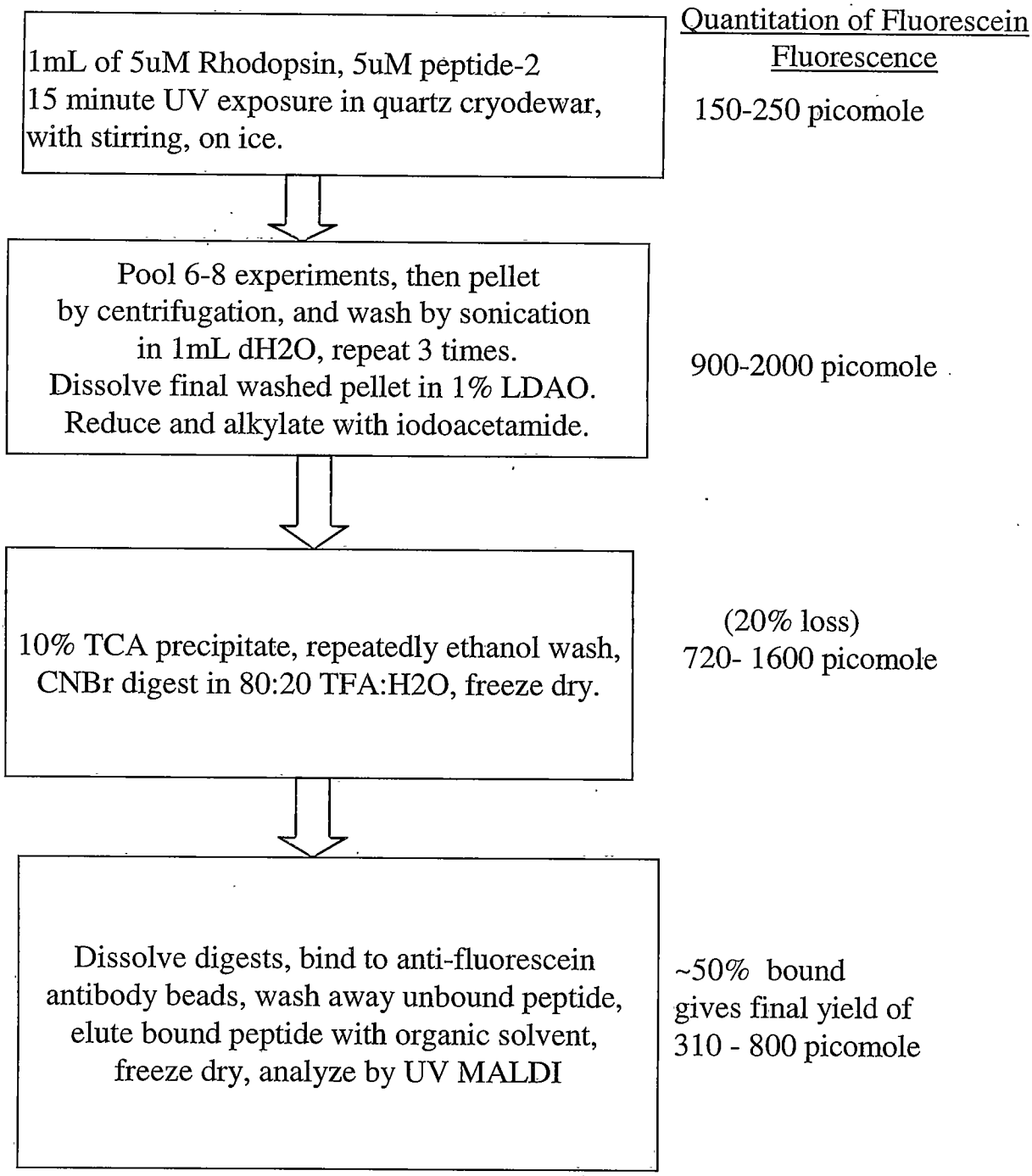


Figure 34. Flow chart of cross-link isolation.

tricine gels resolve peptides to some degree and can give low resolution peptide mass information about rhodopsin cyanogen bromide fragments (209; 221). Figures 35A shows a 16.5% acrylamide tris-tricine gel of CNBr digests of peptide 2 cross-linked to rhodopsin. Cyanogen bromide digestion appears be very efficient (221), and therefore is the method of choice because efficient digestion makes the MS identification much easier. Protein masses greater than 50Kda typically cannot penetrate the separating gel of 16.5% acrylamide tris-tricine gels (209). The fluorescent bands at the top of Lanes 2&3 are a small percent (as estimated from Coomassie staining of the same gels) of the total rhodopsin digest that cannot penetrate the stacking gel. No distinct band from monomeric undigested rhodopsin is detected in either Lane 2 or 3. Lane 1 was loaded with unexposed fluorescent peptide-2. Lane 3 is the cyanogen bromide digest of peptide-2 cross-linked to rhodopsin. It is unclear whether the lowest molecular weight band in Lane 3 is free peptide that was not washed away before digestion, or if it really is the peptide cross-linked to a rhodopsin fragment. As seen in Lane 2, spiking the digest with free peptide revealed that the presence of the digest caused the free peptide to travel slower than free peptide alone. Lane 4 is undigested rhodopsin and peptide-2 that were mixed, but not exposed to UV light. The rhodopsin peptide mixture was ultracentrifuged, washed and digested to the same extent as the other samples, and thus served to measure the efficiency of the washing. The band observed at the end of Lane 4 is mostly peptide that was not washed away, but some retinal contamination

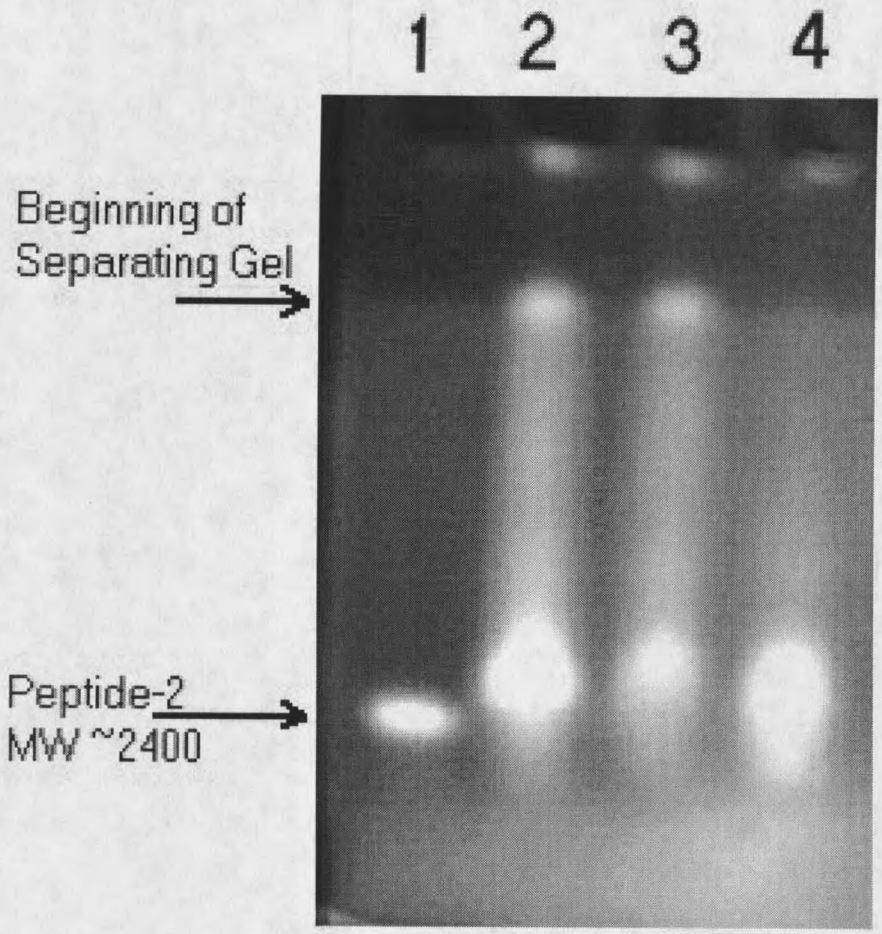


Figure 35A. Fluorescence image of 16.5% acrylamide tris-tricine gel of cyanogen bromide digest of peptide-2 cross-linked to rhodopsin. Lane 1 contains peptide-2. Lane 2 contains a CNBr digest of peptide-2 cross-linked to rhodopsin, plus a small amount of free peptide-2. Lane 3 contains a CNBr digest of peptide-2 cross-linked to rhodopsin. Lane 4 contains a CNBr digest of rhodopsin washed free of non-covalently bound peptide-2.

also contributes to the observed fluorescence. Comparison of Lanes 2&3 to Lane 4 indicates the presence of some undigested cross-linked rhodopsin that is unable to penetrate the separating gel in at the top of Lanes 2&3, and also the presence of unresolved cross-linked products throughout the mass range. The lack of a fluorescenct band at the top of Lane 4, and the lack of fluorescence thoughout the lane (except at the bottom) indicates that without UV exposure, cross-linking cannot occur. 50-80 micrograms of cyanogen bromide digested rhodopsin was loaded in this gel in order to observe the 3-5% of the fluorescent cross-linked material without a long UV exposure, and to make certain that lack of sensitivity in the fluorescence signal was not to blame for not being able to see a distinct fluorescent band. These results imply that either 1) the size of peptide-2 cross-link to rhodopsin CNBr fragment is too small to be resolved from free peptide, 2) the cross-link may be labile to the harsh conditions of the cyanogen bromide digestion, and as a result mostly free peptide is observed at the end of the gel 3) the low yield of cross-linked peptide-2 relative to the uncross-linked rhodopsin CNBr fragment prevents chromatographic resolution in the gel, or 4) the is the cross-linking of peptide-2 is non-specific. Explanations 1, 2, & 3 are certainly possible. Explanation 4 seems improbable because the cross-linking occurs at low peptide and rhodopsin concentrations, the cross-linking can be nearly completely inhibited by non-photo reactive peptide, and lastly, the peptide shows activity in GTP-gamma-^{35}S inhibition assays (Chapter 3, peptide IC50 4-6uM with [rhodopsin] = 75nM, and [Gt] = 25nM).

Enzymatic digestion proceeds at neutral pH and avoids the harsh conditions of CNBr digestion that the cross-link may be labile to. There are no lysines in the peptide

reactive to Lys-C digestion (fluorescein is attached to the epsilon of the N-terminal lysine), and Figure 35B shows a 16.5% acryalmied tris-tricine gel of a Lys-C digestion of peptide-2 cross-linked rhodopsin. On the left is a fluorescence image, and on the right is an image of the Coomassie stain of the same gel. Lanes 1&2 contain undigested peptide-2 cross-linked rhodopsin. 50% of the undigested rhodopsin does not significantly penetrate the separating gel, and 50% is detected as monomeric rhodopsin (~40K Da). Lanes 3&4 contain the same cross-linked rhodopsin as in Lane 1&2, except they were digested with Lys-C for 24hrs. Digestion was far from complete, with about 50% residual undigested monomeric rhodopsin detected. A second distinct band is detected after the 40K Da undigested monomer. This band has significant fluorescence and stained well with Coomassie Brilliant Blue. Many other weaker fluorescent bands are detected but are barely visible at this UV exposure. A slightly stronger more distinct band is discernable at the end of Lanes 3&4, and it migrates approximately the same as the free peptide-2 loaded in Lane 5. This band could be peptide-2 cross-linked to a small rhodopsin Lys-C fragment, or free peptide that was not washed away. The free peptide of Lane 5 fluorescence brilliantly in image A, but is is not seen in image B because peptides less than 10 K Da do not stain well with Coomassie Brilliant Blue. The Lys-C digestion does give some low resolution information about the cross-link location. Most of the fluorescence partitions into the first band in the digest which is about 30K Da. This is probably a large fragment of rhodopsin with the N and/or C-termini clipped off, therefore, one could conclude that peptide-2 is not cross-linking to either terminus. The

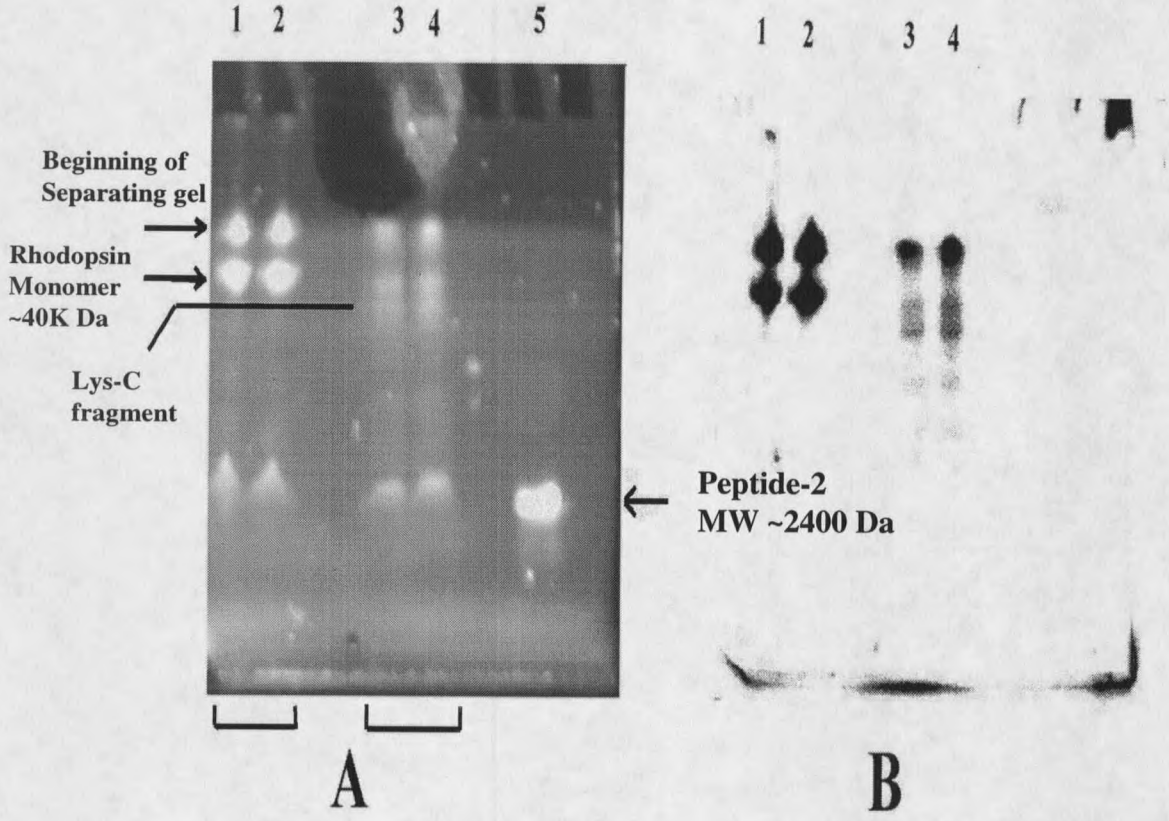


Figure 35B. Fluorescence image (A) and Coomassie stain image (B) of the same 16.5% acrylamide tris-tricine gel of a Lys-c digestion of peptide-2 cross-linked to rhodopsin. Lanes 1&2 are undigested ROS cross-linked with peptide-2. Lanes 3&4 are ROS cross-linked with peptide-2 and Lys-C digested 24hrs. Lane 5 is free peptide-2 MW 2407 Da.In lanes 1&2 unresolved rhodopsin multimers that have been cross-linked with peptide-2 are the lesser bands at the top of the gels, barely penetrating the separating gel. Below this is rhodopsin monomer cross-linked with peptide-2.At the bottom of Lanes 3&4 is retinal and/or free uncross-linked peptide that did not wash away. Lanes 3&4 contain additional flourescent peptide bands from Lys-C digestion.

inefficiency of the digestion, however, prevents any further identification. None of the fluorescent bands in Figures 35A or 35B were present in a high enough concentration to be make their extraction and UV-MALDI possible. Anti-fluorescein antibody bead purification has not yet been attempted in combination with Lys-C digestion, and MS method development on uncross-linked Lys-C digests of rhodopsin is still pending.

There are several experimental improvements that can be made to help in the identification of the cross-linking sites and thus the amino acid molecular contacts between rhodopsin and transducin. A low 3-5% cross-linking peptide to rhodopsin yield is the most significant problem preventing identification. Reasons for low cross-linking yields include: 1) bleaching and/or destruction of the fluorescein on the photo-activatable peptide; 2) during photolysis benzoylphenylalanine is not very reactive and use of long exposure times is required for good yields (174; 176) 3) Metarhodopsin II is partially destroyed upon UV exposure, and this may cause loss of peptide binding; 4) the peptide-rhodopsin cross-link may be labile to cyanogen bromide digestion; 5) the peptide-rhodopsin fragment may be too large, and/or too hydrophobic for efficient recovery and detection; 6) the benzoylphenylalanine may be in a position in the peptide that is not suitable for cross-linking to rhodopsin (ie the Bpa faces the solvent most of the time in the bound state), or the peptide may cross-link to itself; 7) contamination remaining in the antibody purification of peptide protein cross-links is interfering with mass spectrometric identification; 8) the peptide may not have high enough affinity for efficient cross-linking; 9) low resolution and mass accuracy with the Perceptive Biosystems Voyager RP UV MALDI-TOF used to date in this project.

Benzoylphenylalanine has been reported to give yields as high as 50-80% (174; 175) with long exposure times at 365nm. The Meta II conformation of rhodopsin that binds the photo-activatable peptide has an absorbance max at 380nm. The absorbance band is very broad and has a high extinction coefficient (38,000 M-1,cm-1). We found that we could obtain higher cross-linking yields and maintain nucleotide binding longer using a 313nm filter in front of our mercury lamp. 308, 302, and 254nm light will efficiently activate benzoylphenylalanine, and should be tried as a means of maintaining rhodopsin activity longer, and thus hopefully improve cross-linking yields.

Benzoylphenylalanine may not be reactive enough, or it's cross-link may not be sufficiently stable to CNBr digestion (174). Benzoylphenylalanine in the peptide could be substituted with a more reactive cross-linking reagent, that also yields a more stable cross-link. Many chemical and photo reactive groups are commercially available with succinymidyl ester (Pierce, Molecular Probes) leaving groups that could be added to the peptide if the peptides are made with amino-alanine (Adv. Chem Tech). The best alternative may be the synthesis of a 3-[p-(trifluoromethyl)-3H-diazirin-3-yl]-L-phenylalanine (200). This phenylalanine analog reacts in a few nanoseconds, and upon photo-excitation generates a carbene that is expected to yield a stable carbon-X covalent cross-link.

It is still possible the benoylphenylalanine is in the wrong position for the most efficient cross-linking to occur. For this reason we synthesized a similar photo-activatable peptide with the Bpa in the 4 position. This peptide had a 2 fold lower affinity and also had 2 fold lower cross-linking yields. Photo-activatable groups should be scanned in

every position of the peptide to verify another position would not yield more efficient cross-linking. Williams and Shoelson (231) did such an experiment with a phospho-peptide that binds the p85 SH2 Domain of a phospho-binding protein. They found that only three of twelve residues in the peptide led to cross-linking of >50%. One of these substitutions that efficiently cross-linked actually decreased the peptides affinity by 50-100 fold, therefore reductions in affinity do not always correlate with increased cross-linking yields.

Measured increases in fluorescenct peptide-rhodopsin cross-linking yields plateau after 15 minutes of UV exposure (Chapter 3 results not shown). Photo-bleaching of the fluorescein attached to the epsilon amino of the N-terminal lysine may give the false impression of low cross-linking yields. Mills et al (198) reported greater than 50% yields in similar cross-linking experiments with a fluorescein labeled penta-peptide. The efficient cross-linking observed with this peptide may be a result of its much stronger binding to it's receptor (EC50 of GTP-gamma-^{35}S binding = 3nM). Peptide-2's EC50 for rhodopsin Meta II stabilization is about 1uM. Synthesis of peptide-2 with the epsilon amino lysine labeled with ^{125}iodine (200; 232) would increase the sensitivy of detection of cross-links and eliminate concerns over chemical modification/quenching of fluorescein by cyanogen bromide or photo-bleaching. It would also reduce the size of the peptide by ~300 daltons. The peptide could be further reduced in size to ^{125}I-VLEDLRS(Abu)L(Bpa) (mw ~1400). This is a 1000 Da decrease in molecular weight over the current mass of peptide-2 (mw ~2400) which could significantly increase the mass spectrometric sensitivity and resolution if the cross-linked fragment could be

purified by gel electrophoresis or HPLC. Elimination of the fluorescein eliminates the possibility of anti-fluorescein antibody bead purification, but increases in sensitivity may make it a worthwhile approach.

Current attempts to purify peptide-2 cross-links with antifluorescein antibody beads are performed in 1% LDAO to minimize non-specific binding by uncross-linked rhodopsin cyanogens bromide fragments. In mass spectrometric experiments with uncross-linked rhodopsin it was found that mass accuracy and resolution were extremely dependent on the purity of the cyanogen bromide digest (221). High resolution and mass accuracy is dependent on obtaining suitable matrix-analyte crystals. Despite extensive washing with dH2O after antibody bead binding, significant contamination was present after the elution from the antibody beads, causing poor MALDI matrix crystallization, and necessitating the use of high laser power in UV MALDI-MS. Organic solvent washing of the sepharose beads before derivatization with antifluorescein antibody, and elimination of detergent during the purification of fluorescent peptide-2-rhodopsin fragments may decrease contamination. Use of acrylamide beads for antibody derivatizaiton my also decrease contamination.

Lastly, the Perceptive Biosystems Voyager RP has significantly lower mass resolution and mass accuracy than our recently acquired Bruker Biflex III UV MALDI-TOF with delayed extraction, and Esquire 3000 LC-MS (with photodiode array absorbance and fluorescence detectors) Ion Trap. Just these improvements in mass spectrometry at Montana State University may be sufficient to allow mass identification of peptide-2-rhodopsin fragments without any of the suggested improvement mentioned

above. These instruments are also much more powerful for providing peptide sequence information, and therefore are absolutely required for defining molecular contacts at amino acid resolution.

REFERENCES

1) Hillenkamp, F.; Karas, M.; Beavis, R. C.; Chait, B. T. *Anal. Chem.* **1991**, *63*, 1193A-1203A.

2) Stults, J. T. *Curr. Opin. Struct. Biol.* **1997**, *5*, 691-698.

3) Karas, M.; Bachmann, D.; Bahr, U.; Hillenkamp, F. *Int. J. Mass Spectrom. Ion. Proc.* **1987**, *78*, 53-68.

4) Fenn, J. B.; Mann, M.; Meng, C. K.; Wong, S. F.; Whitehouse, C. M. *Science* **1989**, *246*, 64-71.

5) *Low Temperature Biotechnology*; The American Society of Mechanical Engineers: New York, 1988.

6) Fahy, G. M.; Lilley, T. H.; Lindsell, H.; Douglas, M. S.; Meryman, H. T. *Cryobiology* **1990**, *3*, 1630.

7) Williams, P. *Int. J. Mass Spectrom. Ion. Proc.* **1994**, *131*, 335-344.

8) Berkenkamp, S.; Karas, M.; Hillenkamp, F. *Proc. Natl. Acad. Sci. USA* **1996**, *93*, 7003-7007.

9) Eisenberg, D.; Kauzmann, W.*The Structure and Properties of Water*; Oxford: New York, 1969; pp 228-253.

10) Overberg, A.; Karas, M.; Bahr, U.; Kaufmann, R.; Hillenkamp, F. *Rapid Commun. Mass Spectrom.* **1990**, *4*, 293-296.

11) Overberg, A.; Karas, M.; Hillenkamp, F. *Rapid Commun. Mass Spectrom.* **1991**, *5*, 128-131.

12) Berkenkamp, S.; Karas, M.; Hillenkamp, F.In *Proceedings of the 43rd ASMS Conference on Mass Spectrometry and Allied Topics, Atlanta, May 21-26*; **1995;** p. 1247.

13) Nordhoff, E.; Ingendoh, A.; Cramer, R.; Overberg, A.; Stahl, B.; Karas, M.; Hillenkamp, F.; Crain, P. F. *Rapid Commun. Mass Spectrom.* **1992**, *6*, 771-776.

14) Cramer, R.; Hillenkamp, F.; Haglund, R. F. *J. Amer. Soc. Mass. Spectrom.* **1996**, *7*, 1187-1193.

15) Berkenkamp, S.; Menzel, C.; Karas, M.; Hillenkamp, F. *Rapid Commun. Mass Spectrom.* **1997**, *11*, 1399-1406.

16) Niu, S.; Zhang, W.; Chait, B. T. *J. Am. Soc. Mass Spectrom.* **1998**, *9*, 1-7.

17) Tanaka, K.; Waki, H.; Idao, Y.; Akita, S.; Yoshida, Y.; Yoshida, T. *Rapid Commun. Mass Spectrom.* **1988**, *2*, 151-153.

18) Siegel, M. M.; Kunz, A.; Bell, D.; Berkenkamp, S.; Karas, M.; Ingendoh, A.; Hillenkamp, F.In *Proceedings of the 42nd ASMS Conference on Mass Spectrometry and Allied Topics, Chicago, Illinois, May 29 - June 3*, **1994**, p. 967.

19) Juhasz, P.; Costello, C. E. *Rapid Commun. Mass Spectrom.* **1993**, *7*, 343-351.

20) Juhasz, P.; Biemann, K. *Proc. Natl. Acad. Sci. USA* **1994**, *91*, 4333-4337.

21) Sadeghi, M.; Olumee, Z.; Tang, X.; Vertes, A.; Jiang, Z. X.; Henderson, A. J.; Lee, H. S.; Prasad, C. R. *Rapid Commun. Mass Spectrom.* **1997**, *11*, 393-397.

22) Cummings, J. P.; Walsh Jr., J. T. *Appl. Phys. Lett.* **1993**, *62*, 1988-1990.

23) Vodopyanov, K. L. *J. Chem. Phys.* **1991**, *94*, 5389

24) Cummings, J. P.; Walsh Jr., J. T. *SPIE* **1992**, *1646*, 242-253.

25) Nelson, R. W.; Rainbow, M. J.; Lohr, D. E.; Williams, P. *Science* **1989**, *246*, 1585-1587.

26) Nelson, R. W.; Thomas, R. M.; Williams, P. *Rapid Commun. Mass Spectrom.* **1990**, *4*, 348-351.

27) Schieltz, D. M.; Chou, C. W.; Luo, C. W.; Thomas, R. M.; Williams, P. *Rapid Commun. Mass Spectrom.* **1992**, *6*, 631-636.

28) Williams, P.; Nelson, R. W.In *Methods and Mechanisms for Producing Ions from Large Molecules*; Standing, K. G., Ens, W. Eds.; Plenum Press: New York, **1991**, pp 265-273.

29) Hunter, J. M.; Lin, H.; Becker, C. H. *Anal. Chem.* **1997**, *69*, 3608-3612.

30) Alimpiev, S. S.; Belov, M. E.; Mlinsky, V. V.; Nikiforov, S. S. *Analyst* **1994**, *119*, 579-582.

31) Alimpiev, S. S.; Mlynski, V. V.; Belov, M. E.; Nikiforov, S. M. *Anal. Chem.* **1995**, *67*, 181-186.

32) Belov, M. E.; Alimpiev, S. S.; Mlynsky, V. V.; Nikiforov, S. M.; Derrick, P. J. *Rapid Commun. Mass Spectrom.* **1995**, *9*, 1431-1436.

33) Sunner, J.; Dratz, E.; Chen, Y. C. *Anal. Chem.* **1995**, *67*, 4335-4342.

34) Alimpiev, S.; Chen, Y.-C.; Dratz, E.; Kraft, P.; Sunner, J.In *Proceedings of the 44th ASMS Conference on Mass Spectrometry and Allied Topics, Portland, Oregon, May 12-16*, **1996**, p. 641.

35) Touloukian, Y. S.; Powell, R. W.; Ho, C. Y.; Klemens, P. G. *Thermophysical Properties of Matter. Vol. 2*, Plenum: New york, **1970**.

36) Lane, L. B. *Ind. Eng. Chem.* **1925**, *17*, 924

37) Boutron, P. *Cryobiology* **1984**, *21*, 183-191.

38) Alimpiev, S.; Dratz, E.; Kraft, P.; Sunner, J.In *Proceedings of the 44th ASMS Conference on Mass Spectrometry and Allied Topics, Portland, Oregon, May 12-16*, **1996**, p. 644.

39) Sunner, J. *Org. Mass Spectrom.* **1993**, *28*, 805-823.

40) Dreisewerd, K.; Schurenberg, M.; Karas, M.; Hillenkamp, F. *Int. J. Mass Spectrom. Ion. Proc.* **1995**, *141*, 127-148.

41) Bohon, R. L.; Conway, W. T. *Thermochimica Acta* **1972**, *4*, 321-341.

42) Franks, F.In *Developments in Biological Standardization. International Symposium on Biological Freeze-Drying and Formulation, Bethesda, USA, 1990*; Karger: Basel, **1991;** pp 9-19.

43) Feng, R.; Konishi, Y. *J. Amer. Soc. Mass Spectrom.* **1993**, *4*, 638-645.

44) Buttrill Jr., S. E.; Fleming, R. H.; Rossi, M.; Gohl, W.; Goeller, L. N.In *Proceedings of the 29th Annual Conference on Mass Spectrometry and Allied Topics, Minneapolis,* **1981;** pp. 594-595.

45) Sunner, J.; Ikonomou, M. G.; Kebarle, P. *Int. J. Mass Spectrom. Ion. Proc.* **1988**, *82*, 221-237.

46) Vestal, M. L.; Juhasz, P.; Martin, S. A. *Rapid Commun. Mass Spectrom.* **1995**, *9*, 1044-1050.

47) Brown, R. S.; Lennon, J. J. *Anal. Chem.* **1995**, *67*, 1998-2003.

48) Fleissner, G.; Hallbrucker, A.; Mayer, E. *Chem. Phys. Lett.* **1994**, *218*, 93-99.

49). Heck,M. and Hofmann,K.P. (2000) *J.Biol.Chem.*

50) Horn,F., Weare,J., Beukers,M.W., Horsch,S., Bairoch,A., Chen,W., Edvardsen,O., Campagne,F., and Vriend,G. (1998) *Nucleic Acids Res.* **26**, 275-279.

51) Strathmann,M. and Simon,M.I. (1990) *Proc.Natl.Acad.Sci.U.S.A* **87**, 9113-9117.

52) Palczewski,K., Kumasaka,T., Hori,T., Behnke,C.A., Motoshima,H., Fox,B.A., Le,T.I., Teller,D.C., Okada,T., Stenkamp,R.E., Yamamoto,M., and Miyano,M. *Science 2000.Aug.4.;289.(5480.):739.-45.* **289**, 739-745.

53) Drenth, J. Principles of Protein X-Ray Crystallography. 1999. Springer-Verlag New York, Inc.

54) Oliveira, L, paiva, ac, Sander, C, and vriend, g. A common step for signal transduction in G protein-coupled receptor. Trends Pharmacol.Sci. **15**, 170-172. 1994.

55) Lichtarge,O., Bourne,H.R., and Cohen,F.E. (1996) *Proc.Natl.Acad.Sci.U.S.A* **93**, 7507-7511.

56) Horn,F., van der Wenden,E.M., Oliveira,L., Ijzerman,A.P., and Vriend,G. (2000) *Proteins* **41**, 448-459.

57) Fung,B.K. and Nash,C.R. (1983) *J Biol.Chem.* **258**, 10503-10510.

58) Fung,B.K. (1983) *J Biol.Chem.* **258**, 10495-10502.

59) Kelleher,D.J. and Johnson,G.L. (1988) *Mol Pharmacol.* **34**, 452-460.

60) Phillips,W.J., Wong,S.C., and Cerione,R.A. (1992) *J.Biol.Chem.* **267**, 17040-17046.

61) Willardson,B.M., Pou,B., Yoshida,T., and Bitensky,M.W. (1993) *J Biol.Chem.* **268**, 6371-6382.

62) Skiba,N.P., Bae,H., and Hamm,H.E. (1996) *J.Biol.Chem.* **271**, 413-424.

63) Papermaster,D.S. (1982) *Methods Enzymol.* **81:48-52**, 48-52.

64) Wald G. The molecular basis of visual excitation. Nature **219**, 800-807. 8-24-1968.

65) Hofmann,K.P. (1999) *Novartis.Found.Symp.* **224**, 158-175.

66) Godchaux,W. and Zimmerman,W.F. (1979) *Exp.Eye Res.* **28**, 483-500.

67) Kwok-Keung,F.B. and Stryer,L. (1980) *Proc.Natl.Acad.Sci.U.S.A* **77**, 2500-2504.

68) Emeis,D., Kuhn,H., Reichert,J., and Hofmann,K.P. (1982) *FEBS Lett.* **143**, 29-34.

69) Kibelbek,J., Mitchell,D.C., Beach,J.M., and Litman,B.J. (1991) *Biochemistry* **30**, 6761-6768.

70) Kuhn,H., Bennett,N., Michel-Villaz,M., and Chabre,M. (1981) *Proc.Natl.Acad.Sci.U.S.A* **78**, 6873-6877.

71) Bennett,N., Michel-Villaz,M., and Kuhn,H. (1982) *Eur.J Biochem.* **127**, 97-103.

72) Phillips,W.J. and Cerione,R.A. (1988) *J Biol.Chem.* **263**, 15498-15505.

73) Guy,P.M., Koland,J.G., and Cerione,R.A. (1990) *Biochemistry* **29**, 6954-6964.

74) Parkes,J.H. and Liebman,P.A. (1984) *Biochemistry* **23**, 5054-5061.

75) Bennett,N. and Dupont,Y. (1985) *J.Biol.Chem.* **260**, 4156-4168.

76) Ferguson,K.M., Higashijima,T., Smigel,M.D., and Gilman,A.G. (1986) *J Biol.Chem.* **261**, 7393-7399.

77) Panico,J., Parkes,J.H., and Liebman,P.A. (1990) *J.Biol.Chem.* **265**, 18922-18927.

78) Lewis,J.W., Szundi,I., Fu,W.Y., Sakmar,T.P., and Kliger,D.S. (2000) *Biochemistry* **39**, 599-606.

79) Szundi,I., Mah,T.L., Lewis,J.W., Jager,S., Ernst,O.P., Hofmann,K.P., and Kliger,D.S. (1998) *Biochemistry* **37**, 14237-14244.

80) Wenzel-Seifert,K., Hurt,C.M., and Seifert,R. (1998) *J Biol.Chem.* **273**, 24181-24189.

81) Han,M., Groesbeek,M., Smith,S.O., and Sakmar,T.P. (1998) *Biochemistry* **37**, 538-545.

82) Cohen,G.B., Oprian,D.D., and Robinson,P.R. (1992) *Biochemistry* **31**, 12592-12601.

83) Zvyaga,T.A., Fahmy,K., and Sakmar,T.P. (1994) *Biochemistry* **33**, 9753-9761.

84) Han,M., Smith,S.O., and Sakmar,T.P. (1998) *Biochemistry* **37**, 8253-8261.

85) Miettinen,H.M., Mills,J.S., Gripentrog,J.M., Dratz,E.A., Granger,B.L., and Jesaitis,A.J. (1997) *J.Immunol.* **159**, 4045-4054.

86) Robinson,P.R., Cohen,G.B., Zhukovsky,E.A., and Oprian,D.D. (1992) *Neuron* **9**, 719-725.

87) Nathans,J. (1990) *Biochemistry* **29**, 9746-9752.

88) Arnis,S. and Hofmann,K.P. (1993) *Proc.Natl.Acad.Sci.U.S.A* **90**, 7849-7853.

89) Parkes,J.H., Gibson,S.K., and Liebman,P.A. (1999) *Biochemistry* **38**, 6862-6878.

90) Acharya,S., Saad,Y., and Karnik,S.S. (1997) *J.Biol.Chem.* **272**, 6519-6524.

91) Kim,J.M., Altenbach,C., Thurmond,R.L., Khorana,H.G., and Hubbell,W.L. (1997) *Proc.Natl.Acad.Sci.U.S.A* **94**, 14273-14278.

92) Fahmy,K., Sakmar,T.P., and Siebert,F. (2000) *Biochemistry* **39**, 10607-10612.

93) Yamashita,T., Terakita,A., and Shichida,Y. (2000) *J.Biol.Chem.* **275**, 34272-34279.

94) Muradov,K.G. and Artemyev,N.O. (2000) *Biochemistry* **39**, 3937-3942.

95) Posner,B.A., Mixon,M.B., Wall,M.A., Sprang,S.R., and Gilman,A.G. (1998) *J.Biol.Chem.* **273**, 21752-21758.

96) Iiri,T., Herzmark,P., Nakamoto,J.M., van Dop,C., and Bourne,H.R. (1994) *Nature* **371** , 164-168.

97) Thomas,T.C., Schmidt,C.J., and Neer,E.J. (1993) *Proc.Natl.Acad.Sci.U.S.A* **90**, 10295-10298.

98) Hamm,H.E., Deretic,D., Arendt,A., Hargrave,P.A., Koenig,B., and Hofmann,K.P. (1988) *Science* **241**, 832-835.

99) Marin,E.P., Gopala,K.A., Archambault,V., Simuni,E., Fu,W.Y., and Sakmar,T.P. (2001) *J Biol.Chem.*

100) Noel,J.P., Hamm,H.E., and Sigler,P.B. (1993) *Nature* **366**, 654-663.

101) Sprang,S.R. (1997) *Annu.Rev.Biochem.* **66:639-78.**, 639-678.

102) Han,M., Groesbeek,M., Sakmar,T.P., and Smith,S.O. (1997) *Proc.Natl.Acad.Sci.U.S.A* **94**, 13442-13447.

103) Ganter,U.M., Schmid,E.D., Perez-Sala,D., Rando,R.R., and Siebert,F. (1989) *Biochemistry* **28**, 5954-5962.

104) Nakayama,T.A. and Khorana,H.G. (1990) *J.Biol.Chem.* **265**, 15762-15769.

105) Borhan,B., Souto,M.L., Imai,H., Shichida,Y., and Nakanishi,K. (2000) *Science* **288**, 2209-2212.

106) Barnidge,D.R., Dratz,E.A., Sunner,J., and Jesaitis,A.J. (1997) *Protein Sci.* **6**, 816-824.

107) Ball,L.E., Oatis,J.E.J., Dharmasiri,K., Busman,M., Wang,J., Chowden,L.B., Galijatovic,A., Chen,N., Crouch,R.K., and Knapp,D.R. (1998) *Protein Sci.* **7**, 758-764.

108) Franke,R.R., Sakmar,T.P., Graham,R.M., and Khorana,H.G. (1992) *J.Biol.Chem.* **267**, 14767-14774.

109) Acharya,S. and Karnik,S.S. (1996) *J.Biol.Chem.* **271**, 25406-25411.

110) Rens-Domiano,S. and Hamm,H.E. (1995) *FASEB J.* **9**, 1059-1066.

111) Scheer,A., Fanelli,F., Costa,T., De Benedetti,P.G., and Cotecchia,S. (1996) *EMBO J.* **15**, 3566-3578.

112) Haskell,C.A., Cleary,M.D., and Charo,I.F. (1999) *J.Biol.Chem.* **274**, 10053-10058.

113) Zhu,S.Z., Wang,S.Z., Hu,J., and el Fakahany,E.E. (1994) *Mol.Pharmacol.* **45**, 517-523.

114) Jones,P.G., Curtis,C.A., and Hulme,E.C. (1995) *Eur.J.Pharmacol.* **288**, 251-257.

115) Seibold,A., Dagarag,M., and Birnbaumer,M. (1998) *Receptors.Channels* **5**, 375-385.

116) Perlman,J.H., Colson,A.O., Wang,W., Bence,K., Osman,R., and Gershengorn,M.C. (1997) *J.Biol.Chem.* **272**, 11937-11942.

117) Rhee,M.H., Nevo,I., Levy,R., and Vogel,Z. (2000) *FEBS Lett.* **466**, 300-304.

118) Ridge,K.D., Zhang,C., and Khorana,H.G. (1995) *Biochemistry* **34**, 8804-8811.

119) Resek,J.F., Farrens,D., and Khorana,H.G. (1994) *Proc.Natl.Acad.Sci.U.S.A* **91**, 7643-7647.

120) Yang,K., Farrens,D.L., Altenbach,C., Farahbakhsh,Z.T., Hubbell,W.L., and Khorana,H.G. (1996) *Biochemistry* **35**, 14040-14046.

121) Cai,K., Klein-Seetharaman,J., Hwa,J., Hubbell,W.L., and Khorana,H.G. (1999) *Biochemistry* **38**, 12893-12898.

122) Struthers,M., Yu,H., and Oprian,D.D. (2000) *Biochemistry* **39**, 7938-7942.

123) Farrens,D.L., Altenbach,C., Yang,K., Hubbell,W.L., and Khorana,H.G. (1996) *Science* **274**, 768-770.

124) Sheikh,S.P., Vilardarga,J.P., Baranski,T.J., Lichtarge,O., Iiri,T., Meng,E.C., Nissenson,R.A., and Bourne,H.R. (1999) *J.Biol.Chem.* **274**, 17033-17041.

125) Sheikh,S.P., Zvyaga,T.A., Lichtarge,O., Sakmar,T.P., and Bourne,H.R. (1996) *Nature* **383**, 347-350.

126) Dunham,T.D. and Farrens,D.L. (1999) *J.Biol.Chem.* **274**, 1683-1690.

127) Osawa,S. and Weiss,E.R. (1994) *Mol.Pharmacol.* **46**, 1036-1040.

128) Cai,K., Klein-Seetharaman,J., Farrens,D., Zhang,C., Altenbach,C., Hubbell,W.L., and Khorana,H.G. (1999) *Biochemistry* **38**, 7925-7930.

129) Marin,E.P., Krishna,A.G., Zvyaga,T.A., Isele,J., Siebert,F., and Sakmar,T.P. (2000) *J.Biol.Chem.* **275**, 1930-1936.

130) Ernst,O.P., Meyer,C.K., Marin,E.P., Henklein,P., Fu,W.Y., Sakmar,T.P., and Hofmann,K.P. (2000) *J.Biol.Chem.* **275**, 1937-1943.

131) Conklin,B.R., Farfel,Z., Lustig,K.D., Julius,D., and Bourne,H.R. (1993) *Nature* **363**, 274-276.

132) Osawa,S. and Weiss,E.R. (1995) *J.Biol.Chem.* **270**, 31052-31058.

133) Sunahara,R.K., Tesmer,J.J., Gilman,A.G., and Sprang,S.R. (1997) *Science* **278**, 1943-1947.

134) Tsai,S.C., Adamik,R., Kanaho,Y., Halpern,J.L., and Moss,J. (1987) *Biochemistry* **26** , 4728-4733.

135) Gilchrist,A., Mazzoni,M.R., Dineen,B., Dice,A., Linden,J., Proctor,W.R., Lupica,C.R., Dunwiddie,T.V., and Hamm,H.E. (1998) *J.Biol.Chem.* **273**, 14912-14919.

136) Mazzoni,M.R., Taddei,S., Giusti,L., Rovero,P., Galoppini,C., D'Ursi,A., Albrizio,S., Triolo,A., Novellino,E., Greco,G., Lucacchini,A., and Hamm,H.E. (2000) *Mol.Pharmacol.* **58**, 226-236.

137) Rasenick,M.M., Watanabe,M., Lazarevic,M.B., Hatta,S., and Hamm,H.E. (1994) *J.Biol.Chem.* **269**, 21519-21525.

138) Konig,B., Arendt,A., McDowell,J.H., Kahlert,M., Hargrave,P.A., and Hofmann,K.P. (1989) *Proc.Natl.Acad.Sci.U.S.A* **86**, 6878-6882.

139) Seibert,C., Harteneck,C., Ernst,O.P., Schultz,G., and Hofmann,K.P. (1999) *Eur.J.Biochem.* **266**, 911-916.

140) Meyer,C.K., Bohme,M., Ockenfels,A., Gartner,W., Hofmann,K.P., and Ernst,O.P. (2000) *J.Biol.Chem.* **275**, 19713-19718.

141) Takemoto,D.J., Morrison,D., Davis,L.C., and Takemoto,L.J. (1986) *Biochem.J.* **235**, 309-312.

142) Phillips,W.J. and Cerione,R.A. (1994) *Biochem.J.* **299**, 351-357.

143) Ruiz-Avila,L., McLaughlin,S.K., Wildman,D., McKinnon,P.J., Robichon,A., Spickofsky,N., and Margolskee,R.F. (1995) *Nature* **376**, 80-85.

144) Dratz,E.A., Furstenau,J.E., Lambert,C.G., Thireault,D.L., Rarick,H., Schepers,T., Pakhlevaniants,S., and Hamm,H.E. (1993) *Nature* **363**, 276-281.

145) Kisselev,O.G., Kao,J., Ponder,J.W., Fann,Y.C., Gautam,N., and Marshall,G.R. (1998) *Proc.Natl.Acad.Sci.U.S.A* **95**, 4270-4275.

146) Koenig, B. et al. Structure and Oreintation of a Transducin Peptide Fragment in the Rhodopsin Bound State Obtained from Residual Dipolar Couplings. Biophysical Journal 45th Annual Meeting , 181a. 1. (GENERIC) Ref Type: Generic

147) Tesmer,J.J., Berman,D.M., Gilman,A.G., and Sprang,S.R. (1997) *Cell* **89**, 251-261.

148) Martin,E.L., Rens-Domiano,S., Schatz,P.J., and Hamm,H.E. (1996) *J.Biol.Chem.* **271**, 361-366.

149) Aris,L., Gilchrist,A., Rens-Domiano,S., Meyer,C., Schatz,P.J., Dratz,E.A., and Hamm,H.E. (2001) *J.Biol.Chem.* **276**, 2333-2339.

150) Hamm,H.E. and Gilchrist,A. (1996) *Curr.Opin.Cell Biol.* **8**, 189-196.

151) Hamm,H.E. (1998) *J.Biol.Chem.* **273**, 669-672.

152) Hamm,H.E. and Rarick,H.M. (1994) *Methods Enzymol.* **237**, 423-436.

153) Scheer,A. and Gierschik,P. (1995) *Biochemistry* **34**, 4952-4961.

154) Mills,J.S., Miettinen,H.M., Barnidge,D., Vlases,M.J., Wimer-Mackin,S., Dratz,E.A., Sunner,J., and Jesaitis,A.J. (1998) *J.Biol.Chem* **273**, 10428-10435.

155) Ploug,M. (1998) *Biochemistry* **37**, 16494-16505.

156) Chaurand,P., Luetzenkirchen,F., and Spengler,B. (1999) *J.Am.Soc.Mass Spectrom.* **10** , 91-103.

157) Papermaster,D.S. (1982) *Methods Enzymol.* **81:48-52**, 48-52.

158) Jonas,R.E., Yuan,C., and Ebrey,T.G. (1994) *Prep.Biochem.* **24**, 279-288.

159) Sternweis,P.C. and Robishaw,J.D. (1984) *J.Biol.Chem.* **259**, 13806-13813.

160) Schagger,H. and von Jagow G. (1987) *Anal.Biochem.* **166**, 368-379.

161) Kahlert,M., Konig,B., and Hofmann,K.P. (1990) *J.Biol.Chem.* **265**, 18928-18932.

162) Lambright,D.G., Sondek,J., Bohm,A., Skiba,N.P., Hamm,H.E., and Sigler,P.B. (1996) *Nature* **379**, 311-319.

163) Lambright,D.G., Noel,J.P., Hamm,H.E., and Sigler,P.B. (1994) *Nature* **369**, 621-628.

164) Coleman,D.E. and Sprang,S.R. (1998) *Biochemistry* **37**, 14376-14385.

165) Natochin,M., Muradov,K.G., McEntaffer,R.L., and Artemyev,N.O. (2000) *J.Biol.Chem.* **275**, 2669-2675.

166) Bommakanti,R.K., Dratz,E.A., Siemsen,D.W., and Jesaitis,A.J. (1995) *Biochemistry* **34**, 6720-6728.

167) Bommakanti,R.K., Dratz,E.A., Siemsen,D.W., and Jesaitis,A.J. (1994) *Biochim.Biophys.Acta* **1209**, 69-76.

168) Mills,J.S., Miettinen,H.M., Barnidge,D., Vlases,M.J., Wimer-Mackin,S., Dratz,E.A., Sunner,J., and Jesaitis,A.J. (1998) *J.Biol.Chem* **273**, 10428-10435.

169) Mills,J.S., Miettinen,H.M., Cummings,D., and Jesaitis,A.J. (2000) *J.Biol.Chem.* **275**, 39012-39017.

170) Gripentrog,J.M., Jesaitis,A.J., and Miettinen,H.M. (2000) *Biochem.J.* **352 Pt 2**, 399-407.

171) Miettinen,H.M., Gripentrog,J.M., Mason,M.M., and Jesaitis,A.J. (1999) *J.Biol.Chem.* **274**, 27934-27942.

172) Marin,E.P., Gopala,K.A., Archambault,V., Simuni,E., Fu,W.Y., and Sakmar,T.P. (2001) *J.Biol.Chem.*

173) Ploug,M. (1998) *Biochemistry* **37**, 16494-16505.

174) Dorman,G. and Prestwich,G.D. (1994) *Biochemistry* **33**, 5661-5673.

175) Prestwich,G.D., Dorman,G., Elliott,J.T., Marecak,D.M., and Chaudhary,A. (1997) *Photochem.Photobiol.* **65**, 222-234.

176) Weber,P.J. and Beck-Sickinger,A.G. (1997) *J.Pept.Res.* **49**, 375-383.

177) Resek,J.F., Farrens,D., and Khorana,H.G. (1994) *Proc.Natl.Acad.Sci.U.S.A* **91**, 7643-7647.

178) kotzyba-Hibert, f, kapfer, i, and goeldner, m. Recent Trends in Photoaffinity Labeling. Angew.Chem.Int.Ed.Engl. **34**, 1297-1313. 1995. (GENERIC) Ref Type: Generic

179) Slep,K.C., Kercher,M.A., He,W., Cowan,C.W., Wensel,T.G., and Sigler,P.B. (2001) *Nature* **409**, 1071-1077.

180) Hirota,N., Mizuno,K., and Goto,Y. (1998) *J.Mol.Biol.* **275**, 365-378.

181) Bennett,N. and Dupont,Y. (1985) *J.Biol.Chem.* **260**, 4156-4168.

182) Kisselev,O.G., Meyer,C.K., Heck,M., Ernst,O.P., and Hofmann,K.P. (1999) *Proc.Natl.Acad.Sci.U.S.A* **96**, 4898-4903.

183) Kisselev,O., Pronin,A., Ermolaeva,M., and Gautam,N. (1995) *Proc.Natl.Acad.Sci.U.S.A* **92**, 9102-9106.

184) Gilchrist,A., Mazzoni,M.R., Dineen,B., Dice,A., Linden,J., Proctor,W.R., Lupica,C.R., Dunwiddie,T.V., and Hamm,H.E. (1998) *J.Biol.Chem.* **273**, 14912-14919.

185) Onrust,R., Herzmark,P., Chi,P., Garcia,P.D., Lichtarge,O., Kingsley,C., and Bourne,H.R. (1997) *Science* **275**, 381-384.

186) Ruiz-Avila,L., McLaughlin,S.K., Wildman,D., McKinnon,P.J., Robichon,A., Spickofsky,N., and Margolskee,R.F. (1995) *Nature* **376**, 80-85.

187) Hillenkamp,F., Karas,M., Beavis,R.C., and Chait,B.T. (1991) *Anal.Chem.* **63**, 1193A-1203A.

188) Fenn,J.B., Mann,M., Meng,C.K., Wong,S.F., and Whitehouse,C.M. (1989) *Science* **246**, 64-71.

189) Heitzmann,H. (1972) *Nat.New Biol.* **235**, 114

190) Papermaster,D.S. and Dreyer,W.J. (1974) *Biochemistry* **13**, 2438-2444.

191) Dratz,E.A.a.H.D.A. (1983) *Trends Biochem.Sci.* **8**, 128-131.

192) Poincelot,R.P. and Abrahamson,E.W. (1970) *Biochim.Biophys.Acta* **202**, 382-385.

193) Schey,K.L., Papac,D.I., Knapp,D.R., and Crouch,R.K. (1992) *Biophys.J.* **63**, 1240-1243.

194) Hufnagel,P., Schweiger,U., Eckerskorn,C., and Oesterhelt,D. (1996) *Anal.Biochem.* **243**, 46-54.

195) Barnidge,D.R., Dratz,E.A., Jesaitis,A.J., and Sunner,J. (1999) *Anal.Biochem.* **269**, 1-9.

196) Marchese,A., George,S.R., Kolakowski,L.F.J., Lynch,K.R., and O'Dowd,B.F. (1999) *Trends.Pharmacol.Sci.* **20**, 370-375.

197) Nakanishi,K., Zhang,H., Lerro,K.A., Takekuma,S., Yamamoto,T., Lien,T.H., Sastry,L., Baek,D.J., Moquin-Pattey,C., and Boehm,M.F. (1995) *Biophys.Chem* **56**, 13-22.

198) Mills,J.S., Miettinen,H.M., Barnidge,D., Vlases,M.J., Wimer-Mackin,S., Dratz,E.A., Sunner,J., and Jesaitis,A.J. (1998) *J.Biol.Chem* **273**, 10428-10435.

199) Borhan,B., Souto,M.L., Imai,H., Shichida,Y., and Nakanishi,K. *Science 2000.Jun.23.;288.(5474.):2209.-12.* **288**, 2209-2212.

200) Ploug,M. (1998) *Biochemistry* **37**, 16494-16505.

201) Rosinke,B., Strupat,K., Hillenkamp,F., Rosenbusch,J., Dencher,N., Kruger,U., and Galla,H.-J. (1995) *Journal of Mass Spectrometry* **30**, 1462-1468.

202) Orlando,R., Kenny,P., Moquin-Pattey,C., Lerro,K.A., and Nakanishi,K. (1993) *Org Mass Spectrom* **28**, 1395-1402.

203) le Coutre,J., Whitelegge,J.P., Gross,A., Turk,E., Wright,E.M., Kaback,H.R., and Faull,K.F. (0 AD/4/18) *Biochemistry 2000.Apr.18.;39.(15.):4237.-42.* **39**, 4237-4242.

204) Waldhoer,M., Bofill-Cardona,E., Milligan,G., Freissmuth,M., and Nanoff,C. (1998) *Mol.Pharmacol.* **53**, 808-818.

205) Larsson,T., Bergstrom,J., Nilsson,C., and Karlsson,K.A. (2000) *FEBS Lett.* **469**, 155-158.

206) Hong,K. and Hubbell,W.L. (1973) *Biochemistry* **12**, 4517-4523.

207) Ebrey,T.G. (1971) *Vision Res.* **11**, 1007-1009.

208) Chang,Y.C. (1992) *Anal.Biochem.* **205**, 22-26.

209) Schagger,H. and von,J.G. (1987) *Anal.Biochem.* **166**, 368-379.

210) Ablonczy,Z., Knapp,D.R., Darrow,R., Organisciak,D.T., and Crouch,R.K. *Mol.Vis.2000.Jun.27.;6.:109.-15.* **6:109-15**, 109-115.

211) Gross,E. (1967) *Methods in Enzymology* **11**, 238-255.

212) Kaiser,R. and Metzka,L. (1999) *Anal.Biochem.* **266**, 1-8.

213) Zhang,X., Dillen,L., Vanhoutte,K., Van,D.W., Esmans,E., and Claeys,M. (1996) *Anal.Chem* **68**, 3422-3430.

214) Kornfeld,R. and Kornfeld,S. (1985) *Annu.Rev.Biochem.* **54:631-64**, 631-664.

215) Biemann,K. (1990) *Methods Enzymol.* **193:886-7**, 886-887.

216) Burlingame,A.L., Boyd,R.K., and Gaskell,S.J. (1998) *Anal.Chem* **70**, 647R-716R.

217) Jeannot,M.A., Zheng,J., and Li,L. (1999) *J.Am.Soc.Mass Spectrom* **10**, 512-520.

218) Ogorzalek,L.R., Mitchell,C., Stevenson,T.I., Martin,S.A., Hines,W.M., Juhasz,P., Patterson,D.H., Peltier,J.M., Loo,J.A., and Andrews,P.C. (1997) *Electrophoresis* **18**, 382-390.

219) Amando,F.M.L., Santana-Marques,M.G., Ferrer-Correia,A.J., and Tomer,K.B. (97 A.D.) *Anal.Chem* **69**, 1102-1106.

220) Kraft,P., Alimpiev,S., Dratz,E., and Sunner,J. (1998) *J.Am.Soc.Mass Spectrom* **9**, 912-924.

221) Kraft, P. and Mills, J. S. Dratz E. A. Mass Spectrometric Analysis of Cyanogen Bromide Fragments of Integral Membrane Proteins at the Picomole Level: Application to Rhodopsin. Anal.Biochem. (in press). 2001.

222) Berkenkamp,S., Karas,M., and Hillenkamp,F. (1996) *Proc.Natl.Acad.Sci.U.S.A.* **93**, 7003-7007.

223) Berkenkamp,S. (1997) *Rapid Communication Mass Spectrometry* **11**, 1399-1406.

224) Cummings,J.P. and Walsh,J.T. (1992) *SPIE* **1646**, 242-253.

225) Nelson,R.C. (1989) *Science* **246**, 1585-1587.

226) Williams,P. (1994) *Int.J.Mass Spectrom.Ion Processes* **131**, 335-344.

227) Cummings,J.P. and Walsh,J.T. (1993) *Appl.Phys.Lett.* **62**, 1988-1990.

228) Staveteig,P.T. and Walsh,J.T. (1996) *Applied optics* **35**, 3392

229) Jongma,R.T., Huang,Y., and Wodtke,A.M. (1998) *The journal of physical chemistry.a.* **102**, 8847

230) Wodtke,A.M. (2001) *Unpublished Results*

231) Williams,K.P. and Shoelson,S.E. (1993) *J.Biol.Chem* **268**, 5361-5364.

232) Ploug,M., Ostergaard,S., Hansen,L.B., Holm,A., and Dano,K. (1998) *Biochemistry* **37** , 3612-3622.

MONTANA STATE UNIVERSITY - BOZEMAN
3 1762 10351173 7